



NTNU – Trondheim
Norwegian University of
Science and Technology

Hardware-in-the-Loop Testing Systems for ROV Control Systems

Martin Lauritzsen

Master of Science in Engineering and ICT

Submission date: June 2014

Supervisor: Asgeir Johan Sørensen, IMT

Co-supervisor: Mauro Candeloro, IMT

Norwegian University of Science and Technology
Department of Marine Technology



MASTER THESIS IN MARINE CYBERNETICS

SPRING 2014

FOR

STUD. TECHN. MARTIN LAURITZSEN

Hardware-in-the-Loop Testing Systems for ROV Control Systems

Work description:

The use of advanced Remotely Operated Vehicles (ROVs) are widespread and design and implementation of efficient and easy to use control systems are important in the further development of ROVs. The increasing use of computers in control applications raises the vulnerability to software errors in control systems, and new testing methods must be developed to ensure safe and reliable operations. This thesis will continue the work done by AUR-Lab/NTNU within the development of computer based control. The thesis will focus improvements and implementation of new functionality such as sensor noise and Software-in-the-Loop (SIL) capabilities on an already existing Hardware-in-the-Loop (HIL) system, as well as documenting the system design. Different models for ROVs, environments and sensors will be presented and discussed. All implementation and changes will be documented.

Scope of work:

- Review relevant literature on ROV control systems, DP systems and HIL systems
- Review documentation and previous implementations of HIL systems
- Formulate mathematical models of the ROV dynamics and sensors including implementation for the purpose of HIL simulators
- Implement communication to allow changing between HIL and SIL simulations
- Improvements on HIL simulator with interface to ROV control systems
- Perform tests on control systems and compare HIL results with sea trial
- Document each step in the process

The report shall be written in English and edited as a research report including literature survey, description of mathematical models, description of control algorithms, simulation results, model test results, discussion and a conclusion including a proposal for further work. Source code should be provided on a CD with code listing enclosed in appendix. It is supposed that Department of Marine Technology, NTNU, can use the results freely in its research work, unless otherwise agreed upon, by referring to the students work. The thesis should be submitted in two copies within June 10th.

Co-supervisor: Mauro Candeloro

Professor Asgeir J. Sørensen
Supervisor

Preface

This Master thesis was written during the spring semester of 2014 at the Department of Marine Technology of the Norwegian University of Science and Technology (NTNU). It is a continuation of a Project thesis written during fall 2013. The specialization of the thesis is Marine Cybernetics.

The motivation of the thesis is to explore the possibilities of Hardware-in-the-Loop (HIL) testing in commercial and scientific environments, and to improve an existing HIL simulator to better analyze and test control systems for Remotely Operated Vehicles (ROVs). The main focus has been on improving the usability, sensor simulations and modeling in the simulator to achieve results as close as possible to a sea trial.

Acknowledgments

I would like to thank my supervisor Professor Asgeir J. Sørensen for his guidance and help, both during this thesis and earlier. His enthusiasm and knowledge have inspired me a great deal during the years. Another huge thank you to my co-supervisor PhD candidate Mauro Candeloro. He has provided me with help and tips when I was stuck, as well as valuable information and advice on pretty much every part of my thesis. PhD candidate Daniel de Almeida Fernandes deserves mentions and thanks for his input on modeling and dynamics, as does the crew of R/V Gunnerus who have allowed me to come on cruises and enjoy first-hand experience with ROVs.

A thank you is also due to the wonderful people of room C1.058 who have provided motivation and entertainment through the last year. Lastly, I would like to thank my friends and family for their support.

Martin Lauritzsen

Trondheim, June 10th, 2014

Abstract

The use of ROVs has increased in the last decades and today advanced underwater vehicles are used in a wide array of offshore, military and scientific applications. To further improve the usefulness of ROVs modern control systems, such as DP systems, are employed to decrease the strain on the ROV operator and perform tasks faster, safer and cheaper. These control systems are implemented using computers, and as such are vulnerable to software and hardware malfunctions. To prevent these errors from occurring, and minimizing the effect of them if they do occur, thorough testing is necessary.

This thesis will address the uses of Hardware-in-the-Loop testing of Dynamic Positioning systems and other control systems found in ROVs. The different functions of HIL testing and how it can help reduce cost and development time while improving safety compared to more traditional software testing will be discussed. The thesis also gives a short introduction to relevant topics such as Dynamic Positioning systems and how modern software implementations make control systems vulnerable.

The mathematical models for ROVs, sensors and other relevant parts of a simulation system is presented, as well as the structure and characteristics of the current systems being used at NTNU.

Improvements to the existing HIL system is performed, and such features as Software-in-the-Loop testing, sensor noise, umbilical forces and model uncertainty is implemented. In addition there are several improvements the user interfaces.

A sea trial using the R/V Gunnerus and ROV Minerva were performed, and the results logged from the cruise are used to compare the results from simulations to real life data. This is done to evaluate how good results from a HIL simulator can be, and to predict weaknesses and suggest further improvements in the current HIL system.

Sammendrag

Bruken av ROV-er har økt betraktelig de siste tiårene og i dag er avanserte undervannsfartøyer i bruk innen en rekke offshore, militære og vitenskapelige formål. For å kunne videreutvikle bruksområdet til ROV-er tar man i bruk moderne kontrollsystemer, for eksempel systemer for dynamisk posisjonering, for å minske byrden på ROV-operatører, og samtidig utføre arbeidsoppgaver raskere, tryggere og billigere. Disse kontrollsystemene er implementert på datamaskiner, og er dermed sårbare for feil i programvare og maskinvare. For å forhindre at disse feilene oppstår, og å minske effekten av dem hvis de likevel inntreffer, er det nødvendig med grundig testing.

Denne oppgaven vil se på bruken av Hardware-in-the-Loop testing av systemer for dynamisk posisjonering og andre kontrollsystemer i ROV-er. De forskjellige bruksområdene til HIL-testing og hvordan det kan hjelpe til å redusere kostnader og utviklingstid mens det samtidig forbedrer sikkerhet sammenliknet med mer tradisjonell programvaretesting vil bli diskutert. Oppgaven vil også gi en kort innføring til relevante temaer som dynamiske posisjonerings-systemer og hvorfor moderne datamaskin-baserte implementasjoner gjør kontrollsystemer sårbare.

Matematiske modeller for ROV-er, sensorer og andre relevante deler av simuleringssystemet vil bli presentert, i tillegg til strukturen og egenskapene ved de nåværende systemene ved NTNU.

HIL systemet ved NTNU har gjennomgått forbedringer, og nye funksjoner for Software-in-the-Loop testing, sensorstøy, krefter på umbilical og modellusikkerheter er blitt implementert. I tillegg er brukergrensesnittene forbedret.

En sjøprøve er blitt gjennomført ved bruk av R/V Gunnerus og ROV Minerva, og resultatene ble brukt til å sammenlikne en simulering med faktiske data. Dette ble gjort for å undersøke hvor gode resultater man kan få fra en HIL simulator, og for å forutse eventuelle svakheter og foreslå videre forbedringer i HIL systemet.

Contents

Scope of Work	i
Preface	iii
Abstract	v
Sammendrag	vii
Table of Contents	ix
List of Figures	xiii
Nomenclature	xv
1 Introduction	1
1.1 Unmanned Underwater Vehicles	1
1.1.1 Remotely Operated Vehicles	1
1.1.2 Autonomous Underwater Vehicles	2
1.1.3 NTNU's ROVs	3
1.2 Control Systems	3
1.2.1 Dynamic Positioning Systems	3
1.2.2 Computer-Based Control Systems	4
1.2.3 Current Control Systems at NTNU	4
1.3 Hardware-in-the-Loop	4
1.3.1 Current HIL Simulator at NTNU	5
1.4 Contributions	5
1.5 Outline of Thesis	6
2 Hardware-in-the-Loop Systems	7
2.1 DP Software Challenges	7
2.2 The Concept of HIL Testing	8
2.3 HIL in Different Industries	9
2.4 The Cost of Testing	10
2.5 Difference Between HIL and Regular Software Testing	10

2.6	Test Design	11
2.7	Independence in Testing	12
2.8	Class Notations and Regulations	12
2.9	HIL at NTNU	12
3	Modeling	15
3.1	ROV Plant Model	15
3.1.1	General Nonlinear Equations	15
3.1.2	Reference Systems	16
3.1.3	System Inertia Matrix	16
3.1.4	Coriolis and Centripetal Matrix	17
3.1.5	Damping Matrix	17
3.1.6	Rigid Body and Hydrodynamic Forces	17
3.1.7	Hydrostatic and Restoring Forces	18
3.1.8	Forces on Umbilical	19
3.1.9	Control Forces	20
3.1.10	Final ROV Plant	20
3.2	HIL Modeling	20
3.2.1	The Vessel Model	21
3.2.2	Propulsion	22
3.2.3	Power Management System	22
3.2.4	Sensors	23
3.2.5	Current Loads	23
3.2.6	FMEA Simulations	25
3.2.7	Interface Between DP and HIL System and Real-Time Simulations	25
4	Current Systems at NTNU	27
4.1	Model Parameters	27
4.2	General Observations	28
4.3	Damping	28
4.3.1	Damping Plots	29
4.4	HIL system	33
4.4.1	Communication	33
4.4.2	Software-in-the-Loop System	35
4.5	ROV Sensors	35
4.5.1	Sensors in Use	36
4.5.2	Position: HiPAP, GPS and Navipac	36
4.5.3	Depth: Pressure Gauge	40
4.5.4	Heading and Yaw Rate: Inertial Measurement Unit	40
4.5.5	Velocities: Doppler Velocity Log	41
4.6	Control System	41
4.7	Changes and Contributions	42
5	Simulations and Results	45
5.1	Sea Trials	45

5.1.1	Conditions	45
5.1.2	Positions	46
5.1.3	Velocities	50
5.1.4	Thrust Forces	54
5.2	SIL Simulation	55
5.2.1	Test Setup	55
5.2.2	Positions	56
5.2.3	Velocities	60
5.2.4	Thrust Forces	64
5.2.5	Forces on ROV and Umbilical	65
5.3	Comparison and Discussion	70
5.4	Additional Simulations	71
6	Conclusions and Further Work	77
6.1	Conclusions	77
6.2	Recommendations for Further Work	78
	Bibliography	81
A	Parameters for NTNU's ROVs	I
A.1	Minerva: Kirkeby	I
A.1.1	Master model	I
A.1.2	Project model	III
A.2	Minerva: Daniel de Almeida Fernandes	IV
A.2.1	Data set 1	V
A.2.2	Data set 2	V
A.3	SF 30k: Berg	VI
B	System Changes	IX
B.1	Control System Njord	IX
B.1.1	Opening and Closing connection	IX
B.1.2	Private Data	IX
B.1.3	Getters and Setters Blocks	X
B.1.4	Read and Write Communication Blocks	X
B.2	HIL System	XI
B.2.1	Communication	XI
B.2.2	Sensors	XI
B.2.3	Umbilical Forces and Plots	XII
B.2.4	Models and User Interface	XII
C	Code Listing	XIII
C.1	LabVIEW	XIII
C.2	MATLAB	XIV

List of Figures

1.1	NTNU's two ROVs (both connected to R/V Gunnerus)	2
1.2	A simple DP feedback system	3
2.1	Comparison of a control system connected to a real vessel and a HIL simulator (Based on [1])	9
3.1	Diagram showing the connections and operations between the HIL and DP system in a test. Based on figures from [1].	21
3.2	Thrusters of both NTNU's ROVs. The forward x-direction is to the right.	22
3.3	The front of ROV Minerva showing some of its sensors, as well as cameras and lights	24
4.1	The damping for ROV Minerva based on (A.15) and (A.16).	29
4.2	The damping for ROV Minerva based on (A.3) and (A.4).	30
4.3	The damping in surge, sway and heave for ROV Minerva comparing numbers from (A.3), (A.4) and (A.15), (A.16).	31
4.4	The damping for ROV SF 30k based on (A.23) and (A.24).	32
4.5	The damping for Minerva in surge based on (A.3), (A.4) with exponential decay from (A.5). Surge speed given as v .	32
4.6	The structure of the HIL system shown.	34
4.7	The ROV and Ship trajectory shown in the North-East plane. Based on raw HiPAP and GPS data.	37
4.8	The ROV (HiPAP) and Ship (GPS) North positions shown.	38
4.9	The ROV (HiPAP) and Ship (GPS) East positions shown.	38
4.10	Zoomed in signal from Figure 4.9.	39
4.11	Measurements for the pressure sensor as the ROV is stationary and descending to approx 270 meters with zoomed in area. (From cruise 2014-04-10)	40
4.12	The heading and yaw rate given from the IMU. (From cruise 2014-04-10)	41
4.13	The bottom fixed velocities of the ROV in surge and sway given by the DVL. (From cruise 2014-04-10)	42

5.1	The desired path for the ROV in the sea trials.	46
5.2	The north positions of the ROV in the sea trials.	47
5.3	The east positions the ROV in the sea trials.	48
5.4	The positions the ROV in the north-east plane (from sea trials). . .	48
5.5	The depth of the ROV in the sea trials.	49
5.6	The heading of the ROV in the sea trials.	49
5.7	The desired velocities in surge and sway in the sea trial.	51
5.8	The Surge velocities of the ROV in sea trials.	51
5.9	The Sway velocities at the sea trials.	52
5.10	Heave velocities at the sea trials.	52
5.11	Yaw rate in the sea trials.	53
5.12	Thruster/control forces at the sea trials.	54
5.13	The desired path in the North-East plane for the SIL simulation. . .	55
5.14	The north positions of the ROV in the simulations.	57
5.15	The east positions the ROV in the simulations.	57
5.16	The positions the ROV in the north-east plane (from simulations). .	58
5.17	The depth of the ROV in the simulations.	58
5.18	The heading of the ROV in the simulations.	59
5.19	The desired velocities in surge and sway in the simulations.	61
5.20	The Surge velocities of the ROV in ssimulations.	61
5.21	The Sway velocities at the simulations.	62
5.22	Heave velocities at the simulations.	62
5.23	Yaw rate from the simulations.	63
5.24	Thruster/control forces from the simulations.	64
5.25	Linear damping forces acting on the ROV during simulations. All Amplitudes are forces in Newtons [N].	66
5.26	Nonlinear damping forces acting on the ROV during simulations. All Amplitudes are forces in Newtons [N].	67
5.27	Forces acting on the ROV due to the umbilical during simulations. All Amplitudes are forces in Newtons [N] or moments in Newton meters [Nm].	68
5.28	Total environmental forces acting on the ROV during simulations. All Amplitudes are forces in Newtons [N].	69
5.29	North position in a simulated DP and path following operation. . . .	73
5.30	East position in a simulated DP and path following operation. . . .	73
5.31	Position in the North-East plane in a simulated DP and path fol- lowing operation.	74
5.32	Heading in a simulated DP and path following operation.	74
5.33	Surge velocity in a simulated DP and path following operation. . . .	75
5.34	Sway velocity in a simulated DP and path following operation. . . .	75
5.35	Yaw rate in a simulated DP and path following operation.	76
5.36	Thrust forces in a simulated DP and path following operation. . . .	76

Nomenclature

Latin Letters

C	Coriolis and Centripetal matrix
C_A	Hydrodynamic Coriolis and Centripetal matrix
C_d	Drag coefficient
C_{RB}	Rigid Body Coriolis and Centripetal matrix
D	Damping matrix
D_L	Linear Damping matrix
D_{NL}	Nonlinear Damping matrix
d	Down position/depth
e	East position
g	Restoring vector
n	North position
M	Mass matrix
M_A	Hydrodynamic and Added Mass matrix
M_{RB}	Rigid Body Mass matrix
l	Length of ROV
m	Mass of ROV
p	Roll rate
q	Pitch rate
r	Yaw rate
r_B	Placement of Center of Buoyancy
r_G	Placement of Center of Gravity
U	Velocity of surface current
u	Surge speed
$V_{r,hor}$	Relative horizontal velocity
v	Sway speed
w	Heave speed
x	x-direction in a coordinate system
y	y-direction in a coordinate system
z	z-direction in a coordinate system

Greek Letters

η	Position vector
η_d	Desired position vector
$\hat{\eta}$	Estimated position vector
θ	Pitch angle
ν	Velocity vector
ν_r	Relative Velocity vector
ν_c	Current Velocity vector
ρ	Density of water
τ	Thrust forces vector
τ_{wave}	Wave force vector
$\tau_{\text{umbilical}}$	Forces on umbilical
ϕ	Roll angle
ψ	Yaw angle

List of Abbreviations

ABS	American Bureau of Shipping
AUR-Lab	Applied Underwater Robotics Laboratory
AUV	Autonomous Underwater Vehicle
BODY	Body-fixed reference frame
CAD	Computer Aided Design
CAE	Computer Aided Engineering
cRIO	Compact RIO
CS	Control System
CoB	Center of Buoyancy
CoG	Center of Gravity
DNV	Det Norske Veritas
DOF	Degree of Freedom
DP	Dynamic Positioning
DVL	Doppler Velocity Log
FMEA	Failure Modes and Effect Analysis
FPGA	Field-Programmable Gate Array
GPS	Global Positioning System
GUI	Graphical User Interface
HIL	Hardware-in-the-Loop
HiPAP	High Precision Acoustic Positioning
IMO	International Maritime Organization
IMU	Inertial Measurement Unit
I/O	Input/Output
LR	Lloyd's Register
NED	North-East-Down reference frame
NI	National Instruments
NTNU	Norwegian University of Science and Technology
PG	Pressure Gauge
PMS	Power Management System
ROV	Remotely Operated Vehicle
SIL	Software-in-the-Loop
TCP	Transmission Control Protocol
UDP	User Datagram Protocol
UUV	Unmanned Underwater Vehicle

Chapter 1

Introduction

Every year a number of changes and new additions to the control system of NTNU's Remotely Operated Vehicles (ROV) are done, and the need of proper and easily available testing is always present. In order to achieve this a Hardware-in-the-Loop system has been developed, but this system is quite basic and lack a lot of features to accurately simulate the conditions an ROV will face in real life operations. The current HIL system also lacks documentation of the current implementations.

While HIL-testing is preferable due to results being closer to the actual applications it does limit the uses of the systems as an expensive connection is required, which makes the simulator less available to most students who want a simple and fast way to test code.

1.1 Unmanned Underwater Vehicles

Surface vessels has been used by humans for thousands of years, and by comparison manned and unmanned underwater vehicles are newer inventions. Unmanned underwater vehicles (UUVs) is a generic term for all vessels capable of operating under water and without a human operator on board. These vessels can be used for a wide variety of tasks and are often specialized to perform specific operations.

1.1.1 Remotely Operated Vehicles

The use of Remotely Operated Vehicles (ROVs) have increased rapidly in the last decade due to widespread demand in the offshore oil and gas industries. An ROV typically has a low velocity, but is very maneuverable and well fit to solve complex tasks in deep water. ROVs are connected to, and controlled from, a surface vessel

through an umbilical providing power and communications. Most ROV have a box-shaped frame, mostly because the slow operating speed and nearly unlimited power from the umbilical removes the need for hydrodynamic design and maneuverability and compactness is instead prioritized. Most ROVs will have thrusters in several directions to allow high precision control.

ROVs are typically divided into several categories depending on their size, power and abilities. The smallest and weakest ROVs are in the micro and mini classes, and typically weighs between 3 kg (micro) and 15 kg (mini). These ROVs usually have very little payload and are mostly used for exploration and surveying. The general class ROVs are larger and can usually carry a small manipulator, have less than 5 hp propulsion and can reach depths of 1000 meters. The two work classes are the most common in the subsea oil and gas industry and can carry two or more manipulators and usually have significant payload; the light work class typically has less than 50 hp propulsion and can dive to 2000 meters, while the heavy work class can have as much as 220 hp propulsion and a maximum depth of 3500 meters. A special class is the trenching/burial ROVs which are designed to carry a cable laying sledge and can operate down to 6000 meters with more than 200 hp propulsion.

1.1.2 Autonomous Underwater Vehicles

Autonomous Underwater Vehicles (AUVs) are usually torpedo shaped and as the name suggests not reliant on a connection to a surface vessel, and can operate for a prolonged period of time on their own. They are much more focused on speed, energy conservation and hydrodynamic properties than the ROVs, and usually has only one main thruster. AUVs are generally used for data collection such as acoustic surveying of a seabed or monitoring of the ocean space in military operations.



(a) The ROV Minerva being launched.

(b) The ROV SF 30k on deck

Figure 1.1: NTNU's two ROVs (both connected to R/V Gunnerus)

1.1.3 NTNU's ROVs

NTNU is currently in possession of several ROVs used for scientific research and testing of new control systems, most notably the Minerva and SF 30k (can be seen in Figure 1.1), both designed by Sperre A/S and acquired by NTNU in 2003 and 2010, respectively.

Minerva is a SUB-Fighter 7500, and can be categorized as a General Class ROV with a total of five thrusters providing 2 hp each, and a maximum depth of 700 meters. The SF 30k is, as the name suggests, a SUB-Fighter 30k. It has six thrusters with 4 hp each, and as such can be categorized as a very Light Work Class or a heavy General Class ROV. It is attached to a 1100 meters long umbilical, limiting it's maximum depth.

1.2 Control Systems

Modern vessels usually have a number of different, often automatic, control systems that help the personnel perform different operations. Examples of such control systems are Dynamic Positioning, Autopilots, Thrust and Propulsion control systems and Power Management systems. Nearly all these systems are implemented using a computer in modern design, and as such the software of the system is of great importance.

1.2.1 Dynamic Positioning Systems

A Dynamic Positioning (DP) system is occupied with keeping a vessel in a given position, and thus having to counter forces from wind, waves, currents and other environmental forces with the available thrusters. This is usually done with a control system implementing feedback control with sensors providing information about the current state of the system (usually position and velocities), an observer estimating any missing states and filtering noise from the sensors, a controller estimating the forces needed to move the vessel to the desired position and thrust allocation to distribute the computed control forces to the thrusters of the vessel. Figure 1.2 contains a simple block diagram of the closed feedback loop.

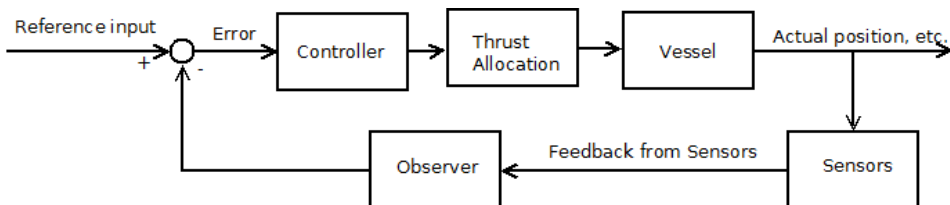


Figure 1.2: A simple DP feedback system

1.2.2 Computer-Based Control Systems

All DP and most other control systems designed today run on computers. This introduces a new source of errors from software implementation, which might lead to relatively small mistakes in implementation or use having large effects on the overall system, for example program crashes. To avoid such failures it is important to thoroughly test all code, both stand alone and as part of the complete system.

The advantages of using computers are huge as they allow for complex computations and large systems being implemented both faster and cheaper than what would be the case for mechanical systems based on hardware and electric circuits. Making changes to software control systems is also simple, but to ensure quality rigid testing and documentation is required.

1.2.3 Current Control Systems at NTNU

The current control systems running on Minerva and SF 30k are developed by students over the past years and are still being developed and improved. Most notably is the work in [2] and [3] where the full control system currently controlling the ROVs (called Njord) and the user interface for control (called Frigg) are designed and implemented. Tolpinrud [2] is mainly responsible for the programming and design of the computer based control system, while Berg [3] focuses on development of the DP algorithms, thrust allocation, etc., especially for the ROV SF 30k. The control systems allows for basic operations such as tracking, path following and DP with several different controllers.

The Frigg and Njord systems are implemented in National Instrument's (NI) LabVIEW and the documentation of both systems is good, although some modifications have been made to them. Njord and Frigg have also proved their worth in sea trials and during many cruises with the ROVs since their implementation. Communication between the ROVs and control computer is set up through NI's compact RIO (cRIO) and real time feedback from the sensors through the surface vessel's network.

1.3 Hardware-in-the-Loop

The use of ROVs in the offshore oil and gas industry has increased rapidly during the last decade. The development seems to be fewer manned surface structures and more subsea installations, installed and maintained by the use of advanced ROVs. The number of control systems in such an ROV is growing, and the industry relies more on automated systems such as Dynamic Positioning, even though DP is not a common feature on many ROVs today. As the control systems in the ROVs get more advances, the need for proper testing and verification of the systems arises.

Many systems are also updated and changed during their life time, and relevant documentation and update logs are not always updated as they should. This leads to an increased risk of critical failure in vital components, and such failures might cause delays and down-time in subsea installations costing companies money, or even worse they might cause accidents harming the environment, equipment and endangering humans.

Hardware-in-the-Loop (HIL) testing allows developers and customers to test software systems in a virtual environment, on the hardware it is supposed to run in actual operations. Testing both the hardware and software together increases the quality of the test as the behavior and performance of software will change depending on the hardware it is installed on. This can help uncover errors otherwise overlooked by conventional software testing and not discovered before the system is installed and in operation, in worst case not before it encounters a critical failure. HIL simulations is also capable of testing a system in extreme conditions it is otherwise impossible to test due to the consequences should the test fail, such as a ship in extremely rough sea and an aircraft in a dive.

The ROVs at NTNU go through continuous updates and are used for research on control systems, most notably different observers and controllers for DP systems. As the update frequency is high and time-frames tight when testing the ROVs in the ocean, it is important to get good test data as quickly as possible. When proper HIL testing is not performed before the sea trials it can easily results in over half of a 12 hour test cruise being used fixing bugs and getting the system to work properly, rather than testing the desired additions to the control systems. If the systems could be run through an extensive HIL-simulation before the tests begin most of the problems might be caught and the time spent trouble shooting at sea might be significantly reduces, thus resulting in better scientific output.

1.3.1 Current HIL Simulator at NTNU

The current HIL simulator at NTNU is designed and implemented in LabVIEW and consists of contributions from several PhD and MSc students, it is not well documented. The current implementation is quite simple and does not feature the object oriented design found in the Njord and Frigg systems. In addition it lacks proper modeling of the sensors, thrusters, umbilical, and errors/changes in the ROV model.

1.4 Contributions

The contributions of this thesis are within improvements of a basic HIL testing system, as well as mapping the structure and functionality. The contributions can be divided into four main areas:

- Software-in-the-Loop simulations allowing students and other users of the system to perform tests on the same control system that are used for HIL tests and sea trials without needing a cRIO.
- Improved sensor modeling in the HIL simulator to provide better simulations closer to the real sensors. The behavior of the different sensors is also discussed.
- ROV model parameters have been moved for easier access. The possibility to add modeling noise to the models have been added. In addition different sets of parameters have been reviewed.
- Forces on the umbilical have been included in the HIL simulator.
- Some user interface features such as graphing the forces acting on the ROV and easier access to parameters for sensors and models have been implemented for easier access.

1.5 Outline of Thesis

Chapter 2

Focuses on the advantages of HIL testing and how it is used in different industries today. The concept of HIL testing is also presented.

Chapter 3

Presents the mathematical background of modeling an ROV, sensors and HIL system. A more detailed description of the different components, design and structure of a HIL system is given.

Chapter 4

Contains an overview of the systems being used at NTNU and a discussion of the different ROV model parameters and how they will affect the system. Also includes a detailed description of the current HIL system at NTNU and sensor pack of the ROVs.

Chapter 5

Contains results from a sea trial and simulation to see if the responses are comparable.

In addition appendices containing ROV model parameters, change logs and a description of the code are included.

Chapter 2

Hardware-in-the-Loop Systems

This chapter contains more detailed information about HIL systems, why they are important, how and where they can be used as well as comparison to other test methods.

One of the main reasons HIL testing is becoming popular is the ever growing complexity software-based control systems, and the fragility of software systems is also addressed.

2.1 DP Software Challenges

As with most other advanced control systems virtually all DP systems today are designed and run on a computer, and such parts as the controller and thrust allocation are implemented as advanced algorithms. This leads to large and complex computer programs that can be hard to interpret and understand without proper documentation. A complete control system on-board a vessel will usually incorporate software from a wide range of different vendors, each designed to support a specific component, but not necessarily made with thought of optimal interaction with the other components in the system. Faulty communications between different software and hardware might lead to safety- and operation critical situations, and the risk of getting such errors rise as the software grows more complex and are subject to frequent updates, often performed by the individual vendors without much knowledge of the other parts of the system.

Software is extremely vulnerable to faults. In a mechanical system small variations might occur without degrading the performance of the system in a noticeable degree, but this is not the case with software, where even the slightest error might

cause entire systems to crash. Making a software system reliable and knowing how it will interact with other software and hardware is always difficult. In [1] there are listed several reasons why software failure occurs:

- Logical/semantic errors in the code;
- Tailor made systems, not a clear standard;
- Configured on tight time schedule late in the projects;
- Complex control systems;
- Problems with integration of systems from different vendors;
- Frequent updates;
- Unaccounted for scenarios;

Redundancy in software is also a challenge. According to [4] DP vessels can be divided into three equipment classes depending on the consequence of failures in the system. Equipment class 2 and 3 demands redundancy in a variety of mechanical systems, and such features as fire insulation between control stations and different engine compartments might be necessary. As most new supply ships and rigs today strive for at least the equivalent of IMO DP class 2 there are physical redundancy in all hardware necessary for the DP operation. The software running on the hardware will usually be the same on all the redundant systems, and this makes them susceptible to the same faults. If one specific bug makes the main system crash, it is thus likely the same bug will be present in the backup system and could make it crash as well. As mentioned in [5] and [6] some advances systems employ several computers with different software in failure-critical operations (in this case Space Shuttles), but this is extremely costly and complicated and not a solution used in modern DP vessels.

It seems quite clear that as an increasing number of critical systems rely on non-redundant software, the quality of this software becomes exceedingly important. The best way to prevent any potentially harmful failures in the software is to test it thoroughly in it's supposed environment; as an embedded part of the DP system. This is what HIL testing is striving to achieve with a simulated environment providing full feedback and environmental forces to test the software on it's designated hardware.

2.2 The Concept of HIL Testing

The idea behind Hardware-in-the-Loop testing is to simulate a control system in use as close as possible to it's natural environment without actually installing it on a vessel. To achieve such results, a simulator must be developed to replicate the signals the control system would otherwise get from the sensors and position reference systems. For the ROVs, this is done by connecting the control system to

a real-time simulations program representing the ROV, the surface vessel and the environment.

In a successful HIL test, the control system will not register any difference between the HIL simulation and an actual sea trial. This gives opportunities to test functionality, performance, robustness and other important features in the system and allows to check for software errors, bad configurations and other problems with the code. To uncover any such faults is the main goal of the HIL system.

Figure 2.1 show the conceptual difference between a control system on a real vessel and in a HIL-simulation.

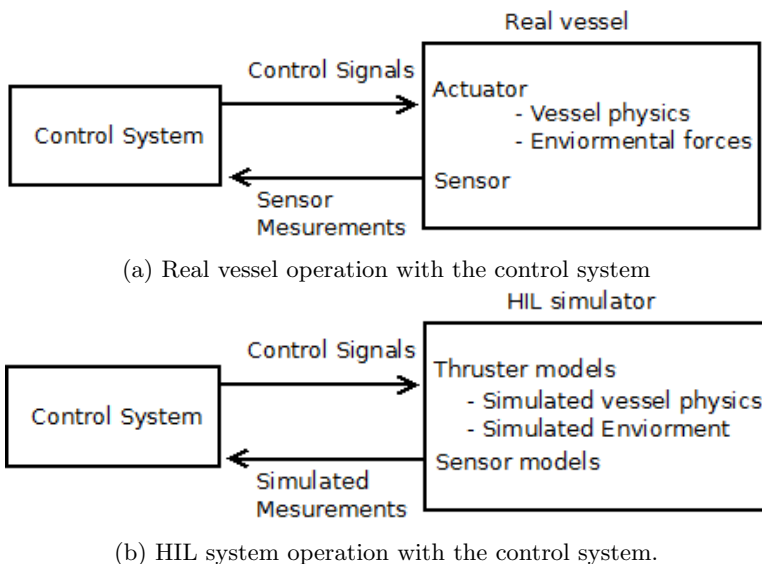


Figure 2.1: Comparison of a control system connected to a real vessel and a HIL simulator (Based on [1])

2.3 HIL in Different Industries

HIL testing is in use in a wide array of industries today, such as avionics, aerospace, automotive and nuclear, and with increasing interests it is finding new uses. The aerospace industry was the first to introduce HIL testing of safety critical software systems, motivated by the rising pressure to develop safer systems in a shorter time span while at the same time reducing costs, this is noted in [7]. According to [8], in the automotive industry as much as 90% of all faults found using a traditional test drive were also found using HIL-simulations while spending much less time and money than the physical tests.

One of the advantages with HIL testing is its usability in all stages of a system's life-cycle. Many other testing techniques are suitable for specific time, while HIL tests easily can be performed to test new functionality and diagnose problems in an aging system.

2.4 The Cost of Testing

In industries such as automotive and large scale production of aircrafts it has been common to build prototypes to fully test functionality, also in critical conditions (such as a crash test for a car). Even so, manufacturers are looking for new ways to improve their profit, with design and testing being areas where many see possibilities to cut expenses. Thus the use of Computer Aided Design (CAD) and Computer Aided Engineering (CAE) design tools and simulators for testing are becoming more frequent. In the marine industry this is much less common as each vessel is unique and custom made, and even newly built sister ships will usually have some differences. This also makes it difficult to transfer knowledge from previous projects and use it directly in new designs.

In addition the cost of a ship, a platform or an ROV is usually much higher than the cost of a car. For an automobile manufacturer, making a prototype to test is a relatively small investment related to the number of vehicles they hope to sell, but for a yard destructive testing is not an option on a billion USD semi-submersible. Replicating the right environments for testing a ship in extreme conditions is also nearly impossible and dangerous. Because of this use of HIL in marine systems has a large potential to uncover errors that otherwise might be ignored until the vessel was in a critical operation and failed, which again might lead to large economical and human losses.

The development or acquisition of a HIL system is comparatively much cheaper, and in [9] it is stated that an investment in a HIL system in the automotive industry from experience pays off within three to six months.

2.5 Difference Between HIL and Regular Software Testing

Testing is one of the foundations in modern software development, and such programming methods as Test Driven Development (TDD) and Extreme Programming (XP) rely on writing test before writing the actual code to emphasize the importance of testing the code's compliance with the desired results. This kind of testing only concerns the functionality of the isolated code, and even large system tests will usually only consist of the code from one vendor, meaning there will usually still be trouble analyzing relevant failure modes in more complex systems with several different vendors and no single company responsible for the functionality of the

complete system. Testing the code of several different vendors together in traditional white-box testing will be difficult as most of the source code is closed source and secret. This problem is not present when testing the software for NTNU's ROVs as the control system is student made and all the code readily available, although not always well documented and easy to understand.

HIL testing relies on black-box testing, meaning the tester knows nothing about the internal states of the system, but is only concerned with the inputs and generated outputs. This means it is extremely important for the tester to do a thorough job feeding the test system all possible input values as this is the only way to know the response from the control system. As virtually no knowledge of the inside system is required to perform black-box testing it is ideal for checking the functionality of a complex system from different vendors.

Another problem with general software testing and code review only uncovers errors in the topmost application layer of the software, while HIL also tests compliance with other aspects of the software such as I/O, drivers, memory and CPU management and hardware compatibility.

2.6 Test Design

When preparing to run HIL simulations several considerations must be made, and setting up a test plan will help checking the system in a thorough and efficient manner. The most important parts to define is the test scope and test different cases to make sure the scope is fulfilled.

The test scope defines the desired functionality in the system to be tested. These tests might be necessary to achieve certain criteria from given rules and regulations, to meet demands for functional performance or other specifications.

The test cases are given in order to make sure the functionality described in the scope is satisfactorily tested. According to [1] the tests can often be categorized as:

- Functional tests: verifying the control system functions in normal operation;
- Failure testing: testing the handling of different failure modes;
- Performance tests: to make sure the DP system behaves as predicted in different operational and environmental conditions;
- Integration tests: testing the integration of different control systems to make sure they are compatible;

A well performed HIL test can be part of such important events in a system's life cycle as Factory Acceptance Test (FAT) and Customer Acceptance Test (CAT). Thus they will often need to be properly executed and documented to meet strict requirements from shipowners and classification societies.

2.7 Independence in Testing

One of the foundations in software testing is independence; the person testing the code should always be another person than the one writing it. Preferably tests should be run by a third party who has no interest in the outcome of the test, and thus are completely unbiased. The importance of this independence has been appreciated for a long time, and it can be argued that such classification societies as Lloyd's Register (LR) and Det Norske Veritas (DNV) were founded to conduct third party testing of ships to clarify their condition. According to [10] the forms of independence in a typical DP system can be defined by three parameters; technical independence, managerial independence, and financial independence. The highest form, Classical, is achieved when the test personnel, technical solutions, test organization and test finances all are separate from the developers of the program.

In a complex software based DP system with parts from many vendors, third party testing is necessary to make sure the final integration is working, and that the testing is performed on "equal ground", and not leaving any suppliers feeling badly treated or allowing anyone to skip important testing to make deadlines. To achieve this desirable independence in HIL testing, an industry of independent testers are required, which can be combined with the already existing classification societies in the marine industry.

2.8 Class Notations and Regulations

Large class societies and regulations from flag states and international organizations have a large impact on the development of technology in the marine industry. According to [11] currently there are two class societies with notations concerning HIL testing; American Bureau of Shipping (ABS) and DNV. ABS has included rules relating to HIL testing in [12] and DNV has published it as a Standard of Certification in [13] and as an optional additional class in [14]. DNV demands a high level of independence in testing, while ABS allows the owner of the vessel to select a lower level of independence.

The first ship to get awarded DNV's HIL test certificate was the Acergy Osprey in June 2006, this event is documented in [15].

Other large classification societies such as LR and Bureau Veritas (BV) have no specific mention of HIL testing in any of their rules or standards.

2.9 HIL at NTNU

The current system in use in the Department of Marine Technology at NTNU is less advanced than the full systems described in this chapter, and is mostly fit for func-

tional testing and to some degree performance testing and failure testing.

Testing is usually performed in a much less rigorous manner than described in Sections 2.6 and 2.7. This works fine as the control systems at NTNU are also generally much smaller and well known to the tester, unlike a typical system found in the industry. No class rules applies to the ROVs usually used for testing of control systems, and much of the work is of academical interest rather than for profit.

Independence in testing is a problem as most people testing the control systems will know the HIL system well and even change it to fit their case, and as such the testing is more of a white box approach where all internal and external states in both the control system and HIL simulator can be monitored, which is of course an advantage when trouble shooting, but allows for hidden faults the developer/tester regard as not significant.

Chapter 3

Modeling

In this chapter the mathematical models for a Plant of a DP system and a HIL simulator design for ROVs will be discussed. The DP system will not be described in great detail, but as the plant of the DP system and HIL system will be essentially the same it is included. The HIL simulator has to both calculate forces working on the ROV given certain operational conditions and provide a reasonable response to the forces provided from the ROV's thrusters due to commands from the control/DP system.

The models will be prepared in 6 degrees of freedom (DOFs), even though NTNU's ROVs are not controllable in roll and pitch.

3.1 ROV Plant Model

The models and equations here are mostly based on [16], [17] and [18].

The plant model used in design and implementation of DP systems are usually a simplified version of the model presented here. In HIL simulations it is desirable for the model to be as realistic as possible, and the full model is desirable.

3.1.1 General Nonlinear Equations

According to [16], the nonlinear equations of motion adapted for an ROV with 6 degrees of freedom (DOF) can be given in a body-fixed reference system as:

$$\dot{\boldsymbol{\eta}} = \mathbf{J}(\boldsymbol{\eta})\boldsymbol{\nu} \quad (3.1)$$

$$\mathbf{M}\dot{\boldsymbol{\nu}} + \mathbf{C}(\boldsymbol{\nu})\boldsymbol{\nu} + \mathbf{D}(\boldsymbol{\nu})\boldsymbol{\nu} + \mathbf{g}(\boldsymbol{\eta}) + \mathbf{g}_0 = \boldsymbol{\tau} + \boldsymbol{\tau}_{\text{wave}} + \boldsymbol{\tau}_{\text{umbilical}} \quad (3.2)$$

Where

$$\begin{aligned}\boldsymbol{\eta} &= [x \ y \ z \ \phi \ \theta \ \psi]^\top \\ \boldsymbol{\nu} &= [u \ v \ w \ p \ q \ r]^\top\end{aligned}$$

are the positions (surge, sway, heave, roll, pitch and yaw) and velocity of the vessel.

The forces from waves might be excluded from this model if the ROV is assumed to work well below the wave zone, which is often the case.

3.1.2 Reference Systems

To simplify equations (3.1) and (3.2) two different reference frames are used:

- The position vector $\boldsymbol{\eta}$ is given in an Earth fixed reference frame with the x-axis in pointing North, y East and z Down (NED).
- The velocities $\boldsymbol{\nu}$ are given relative to the body in a body fixed reference system (BODY) moving with the ROV. In BODY the x-axis is given straight forward, y is given starboard and z is given downwards.

The two reference frames are connected by the transformation matrix $\mathbf{J}(\boldsymbol{\eta})$:

$$\mathbf{J}(\boldsymbol{\eta}) = \begin{bmatrix} c\psi c\theta & -s\psi c\phi + c\psi s\theta s\phi & s\psi s\phi + c\psi c\phi s\theta & 0 & 0 & 0 \\ s\psi c\theta & c\psi c\phi + s\phi s\theta s\psi & -c\psi s\phi + s\theta s\psi c\phi & 0 & 0 & 0 \\ -s\theta & c\theta s\phi & c\theta c\phi & 0 & 0 & 0 \\ 0 & 0 & 0 & 1 & s\phi t\theta & c\phi t\theta \\ 0 & 0 & 0 & 0 & c\phi & -s\phi \\ 0 & 0 & 0 & 0 & \frac{s\phi}{c\theta} & \frac{c\phi}{c\theta} \end{bmatrix} \quad (3.3)$$

where $c(\cdot) = \cos(\cdot)$, $s(\cdot) = \sin(\cdot)$ and $t(\cdot) = \tan(\cdot)$, and depending on the angles in $\boldsymbol{\eta}$.

3.1.3 System Inertia Matrix

The system inertia matrix \mathbf{M} contains all mass and inertia components of the systems, and can be divided into two parts, one describing the rigid body dynamics and one related to the hydrodynamic forces:

$$\mathbf{M} = \mathbf{M}_{RB} + \mathbf{M}_A \quad (3.4)$$

For a rigid body system such as an ROV it can be assumed that \mathbf{M} is symmetric, constant and positive definite:

$$\mathbf{M} = \mathbf{M}^\top > 0, \quad \dot{\mathbf{M}} = \mathbf{0}$$

3.1.4 Coriolis and Centripetal Matrix

The system Coriolis and centripetal matrix \mathbf{C} can also be split into a rigid body and hydrodynamic force, note that both parts depend on the velocity $\boldsymbol{\nu}$:

$$\mathbf{C}(\boldsymbol{\nu}) = \mathbf{C}_{RB}(\boldsymbol{\nu}) + \mathbf{C}_A(\boldsymbol{\nu}) \quad (3.5)$$

For a rigid body system the Coriolis and centripetal matrix can be shown to be skew-symmetric:

$$\mathbf{C}(\boldsymbol{\nu}) = -\mathbf{C}^\top(\boldsymbol{\nu})$$

The Coriolis-Centripetal Matrix can be found from \mathbf{M} and $\boldsymbol{\nu}$ (given in [16]):

$$\mathbf{C}(\boldsymbol{\nu}) = \begin{bmatrix} \mathbf{0} & -\mathbf{S}(\mathbf{M}_{11}\boldsymbol{\nu}_1 + \mathbf{M}_{12}\boldsymbol{\nu}_2) \\ -\mathbf{S}(\mathbf{M}_{11}\boldsymbol{\nu}_1 + \mathbf{M}_{12}\boldsymbol{\nu}_2) & -\mathbf{S}(\mathbf{M}_{21}\boldsymbol{\nu}_1 + \mathbf{M}_{22}\boldsymbol{\nu}_2) \end{bmatrix} \quad (3.6)$$

with $\boldsymbol{\nu}_1 = [u, v, w]^\top$, $\boldsymbol{\nu}_2 = [p, q, r]^\top$, $\mathbf{M} = \begin{bmatrix} \mathbf{M}_{11} & \mathbf{M}_{12} \\ \mathbf{M}_{21} & \mathbf{M}_{22} \end{bmatrix}$, and \mathbf{S} being the

cross-product operator: $\mathbf{S}(\mathbf{k}) = \begin{bmatrix} 0 & -k_3 & k_2 \\ k_3 & 0 & -k_1 \\ -k_2 & k_1 & 0 \end{bmatrix}$ for $\mathbf{k} = [k_1, k_2, k_3]^\top$.

3.1.5 Damping Matrix

The damping matrix \mathbf{D} contains the hydrodynamical damping in the system, and as such gives no contribution to the rigid body equations. It can be separated into a linear and non-linear part:

$$\mathbf{D}(\boldsymbol{\nu}) = \mathbf{D}_{\text{linear}} + \mathbf{D}_{\text{nonlinear}}(\boldsymbol{\nu}) \quad (3.7)$$

All damping matrices can be assumed symmetric:

$$\mathbf{D}(\boldsymbol{\nu}) = \mathbf{D}^\top(\boldsymbol{\nu})$$

3.1.6 Rigid Body and Hydrodynamic Forces

There are both rigid body forces and hydrodynamic forces acting on the body, but they depend on different velocities. The rigid body forces are only dependent on the actual velocity of the ROV ($\boldsymbol{\nu}$) and can be expressed as:

$$\mathbf{M}_{RB}\dot{\boldsymbol{\nu}} + \mathbf{C}_{RB}(\boldsymbol{\nu})\boldsymbol{\nu} = \boldsymbol{\tau}_{RB} \quad (3.8)$$

The rigid body forces can usually be computed from knowledge of the mass and shape of the ROV, with the rigid body mass and inertia matrix given as;

$$\mathbf{M}_{RB} = \begin{bmatrix} m\mathbf{I}_{3 \times 3} & -m\mathbf{S}(\mathbf{r}_g^b) \\ m\mathbf{S}(\mathbf{r}_g^b) & \mathbf{I}_b \end{bmatrix} \quad (3.9)$$

where m is the total mass of the ROV, $\mathbf{I}_{3 \times 3}$ is the identity matrix, \mathbf{I}_b is the inertia matrix, \mathbf{S} is the cross-product operator and \mathbf{r}_g^b contains the relative centers of gravity with respect to an arbitrary center. \mathbf{C}_{RB} can be found from (3.6).

The hydrodynamic forces arise from such phenomena as added mass, skin friction, vortex shedding etc. due to the ROV moving through the water. Because of this the relative velocity $\boldsymbol{\nu}_r$, including current, is needed:

$$\boldsymbol{\nu}_r = \boldsymbol{\nu} - \boldsymbol{\nu}_c \quad (3.10)$$

where $\boldsymbol{\nu}_c$ is the velocity of the current expressed in BODY.

The hydrodynamic forces can then be written:

$$\mathbf{M}_A \dot{\boldsymbol{\nu}}_r + \mathbf{C}_A(\boldsymbol{\nu}_r)\boldsymbol{\nu}_r + \mathbf{D}_L\boldsymbol{\nu}_r + \mathbf{D}_{NL}(\boldsymbol{\nu}_r)\boldsymbol{\nu}_r = \boldsymbol{\tau}_{\text{hydrodyn}} \quad (3.11)$$

Unlike the rigid body forces the hydrodynamic forces must be found through tests and model trials, except \mathbf{C}_A that can be computed from \mathbf{M}_A .

3.1.7 Hydrostatic and Restoring Forces

The hydrostatic terms in 3.1 is the restoring forces/moments in $\mathbf{g}(\boldsymbol{\eta})$ and pre-trimming of ballast in \mathbf{g}_0 . As ROVs generally don't use ballast tanks $\mathbf{g}_0 = \mathbf{0}$. The restoring vector $\mathbf{g}(\boldsymbol{\eta})$ is dependent on the weight, buoyancy and the relative placements of the center of gravity (CoG) and center of buoyancy (CoB) of the ROV, and if it is assumed that CoG and CoB are located vertically on the z-axis it is given in [16] as:

$$\mathbf{g}(\boldsymbol{\eta}) = \begin{bmatrix} (W - B) \sin(\theta) \\ -(W - B) \cos(\theta) \sin(\phi) \\ -(W - B) \cos(\theta) \cos(\phi) \\ (z_g W - z_b B) \cos(\theta) \sin(\phi) \\ (z_g W - z_b B) \sin(\theta) \\ 0 \end{bmatrix} \quad (3.12)$$

where W is the total weight of the ROV in air and B is the total buoyancy. It might be assumed that weight equals displacement: $W = B$. This is not completely true as most ROVs has a slightly positive buoyancy.

3.1.8 Forces on Umbilical

The umbilical connecting the ROV to the surface vessel can be modeled as a long slender pipe, and it will experience forces from drag on the cable from the relative velocity of the ROV. Forces on the umbilical will also affect the ROV, so they must be included in the equations of motion through the force vector $\tau_{\text{umbilical}}$.

As the umbilical is comparatively thin compared to the wavelength and amplitude Morison's equation for drag force might be used to calculate the forces acting on it. It is assumed the current has no vertical component, and the force depending on the relative velocity in the horizontal plane $V_{r,hor}$:

$$f_d(V_{r,hor}) = \frac{1}{2} \rho d C_d |V_{r,hor}| V_{r,hor} \quad (3.13)$$

where d is the diameter of the umbilical, C_d is the drag coefficient and ρ is the density of water. Equation (3.13) gives the force acting on a thin horizontal strip, and integrating the cable along it's length will provide the full force. As the vertical velocities is ignored the length of the cable can be approximated as the depth of the ROV, in other words the distance from the surface vessel to the ROV.

$$F_d = \int_0^h f_d(V_{r,hor}) dz \quad (3.14)$$

Some of the forces from the umbilical will go to the surface vessel, and the ROV will get approximately half of F_d .

The vertical component of $\tau_{\text{umbilical}}$ is related to the weight of the umbilical, but as it is designed for underwater use most umbilicals are close to weightless in water ([3]).

The forces from the umbilical in surge and sway will also give moments in pitch and roll. The size of the moments will depend on r_z , which is the distance from the connection of the umbilical to the ROV and the CoG.

The total forces and moments on the ROV from the umbilical can thus be written:

$$\boldsymbol{\tau}_{\text{umbilical}} = \begin{bmatrix} -\frac{1}{4}\rho d C_d \int_0^h |u_r| u_r \\ -\frac{1}{4}\rho d C_d \int_0^h |v_r| v_r \\ 0 \\ -r_z \frac{1}{4}\rho d C_d \int_0^h |u_r| u_r \\ -r_z \frac{1}{4}\rho d C_d \int_0^h |v_r| v_r \\ 0 \end{bmatrix} \quad (3.15)$$

3.1.9 Control Forces

The control forces are provided by the fixed thrusters on the ROV. Both of NTNU's ROVs are underactuated and cannot be controlled in roll and pitch. This results in the control vector

$$\boldsymbol{\tau} = [\tau_1 \ \tau_2 \ \tau_3 \ 0 \ 0 \ \tau_6]^\top \quad (3.16)$$

3.1.10 Final ROV Plant

The equations of motion to be used as the plant in further calculations and simulations are given as:

$$\dot{\boldsymbol{\eta}} = \mathbf{J}(\boldsymbol{\eta})\boldsymbol{\nu} \quad (3.17)$$

$$\mathbf{M}_{RB}\dot{\boldsymbol{\nu}} + \mathbf{C}_{RB}(\boldsymbol{\nu})\boldsymbol{\nu} + \mathbf{M}_A\dot{\boldsymbol{\nu}}_r + \mathbf{C}_A(\boldsymbol{\nu}_r)\boldsymbol{\nu}_r + \mathbf{D}_L\boldsymbol{\nu}_r + \mathbf{D}_{NL}(\boldsymbol{\nu}_r)\boldsymbol{\nu}_r + \mathbf{g}(\boldsymbol{\eta}) = \boldsymbol{\tau} + \boldsymbol{\tau}_{\text{umbilical}} \quad (3.18)$$

3.2 HIL Modeling

There are several subsystems in a HIL testing system that should be modeled individually to get a good simulator, as mentioned in [1] and [19]. The full simulator has to both provide environmental data and how these act upon the ship to the DP system, and then take the control outputs back into the simulator and predict how the applicable control forces will affect the vessel before feeding the new position and sensor outputs back to the control system in an infinite loop. The different parts of a HIL system can thus be divided into three categories depending on their role; environmental models, vehicle models and communication models including output from sensors and input from thrusters.

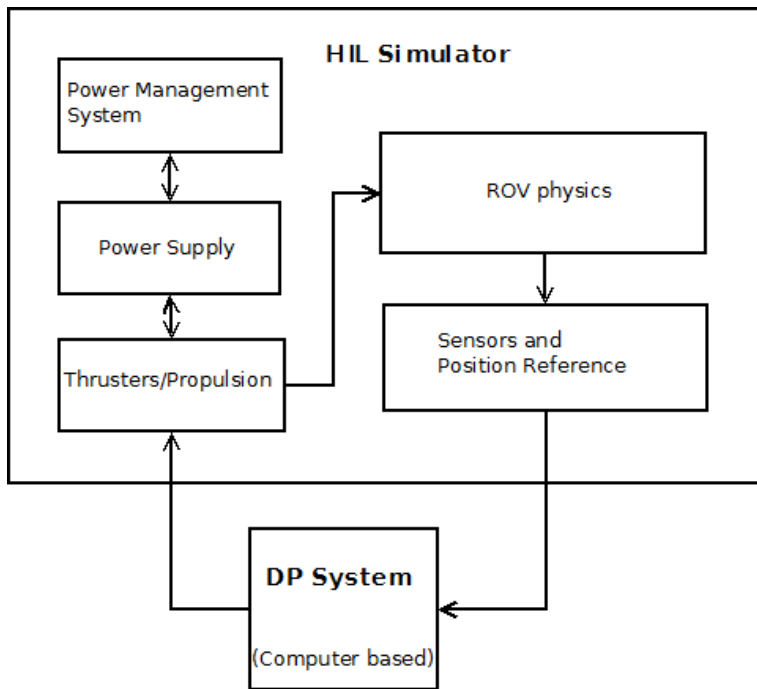


Figure 3.1: Diagram showing the connections and operations between the HIL and DP system in a test. Based on figures from [1].

3.2.1 The Vessel Model

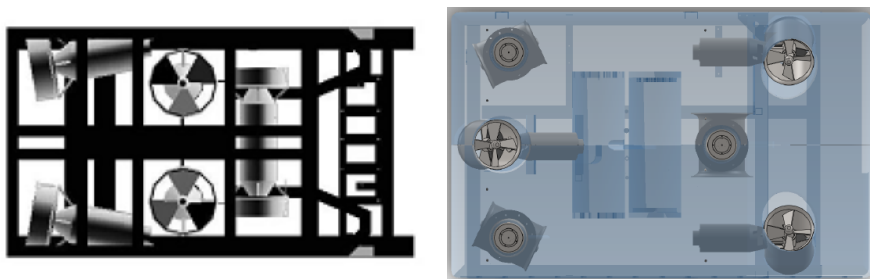
The vessel model contains all information about the vessel's size, geometry, and other factors contributing to the dynamics of the ROV, and account for the different environmental forces working on the ship. For an ROV it is necessary with six degrees of freedom: surge, sway, heave, roll, pitch and yaw to model the movements correctly. The main forces working on a surface vessel are waves, current, and wind. For an ROV the forces from waves and wind will usually be negligible as the ROV usually works in deep waters well out of the wave zone. Waves might still be accounted for as some operations, such as inspecting the legs of a platform, might be performed near the surface. ROVs generally also move slowly compared to a surface vessel, even though they have much shorter response times and can achieve higher accelerations, for example NTNU's Minerva has a top speed of 2 knots, but in working condition it is often either stationary or moving at less than 0.5 knots. Due to this slow movement it the second order forces working on the ROV are usually dominated by the first order forces. There are several models used for computing current loads, e.g. skin friction formulations, cross flow drag or experimental results. The model for the umbilical should also be included as part of the vessel or as independent forces acting on it.

The equations of motions given in (3.17) and (3.18) given for the DP system can be used to describe the motions of the vessel in a HIL simulator, although without any simplifications as is common when designing control systems. This also applies for the forces working on the umbilical in (3.15).

Many of the variables of the ROV is often unknown, such as the weight and buoyancy that rely on the current configuration of sensors, cameras, lights etc. on the ROV, and in addition has shown to change during a day of operations as the ROV will often absorb some water.

3.2.2 Propulsion

The control system in the ROV will typically output different thrust required by the thrusters of the ROV to achieve desired control forces. ROVs are optimized for maneuverability with a relatively large number of, usually fixed, thrusters. This is the case for both Minerva and SF 30k, and their thrusters configuration from above can be viewed in Figure 3.2. The propulsion models will provide the thrust production and power consumption of each thruster, as well as thrust loss and other relevant phenomena to accurately predict the thruster's effect on the entire ROV system. Relevant constraints due to shaft speed, motor torque and maximum available power also be included. The placement and constraint on each thruster is an important factor when considering the limits of the entire vessel.



(a) Thruster configuration of ROV Minerva viewed from above. Figure from [20] (b) Thruster configuration of ROV SF 30k viewed from above. Figure from [3]

Figure 3.2: Thrusters of both NTNU's ROVs. The forward x-direction is to the right.

3.2.3 Power Management System

The power management system (PMS) distributes and monitors the power consumption of the different thrusters and other consumers in the system, such as sensors, lights and any manipulators. As the ROVs get their power from the surface vessel through the umbilical the PMS has no need to model such features as

generators and fuel consumption. However, the total power consumption of the ROV with its control systems and operational stations are of interests as it is possible to blow a fuse on the surface vessel. The amount of power consumed might also be of interest if there is a desire to minimize it, for example if the HIL system should be used to test the control system of an AUV.

If the DP system requires information such as status signals and power consumption in the individual thrusters, this will generally be provided by the PMS.

3.2.4 Sensors

Marine vessels have a number of sensors, as well as position reference systems, to help the DP system determine the location, velocities, accelerations and other relevant factors. The signals from these sensors must be simulated to give the control system requested positions for feedback, and environmental data for any feedforward, to let the system know how the vessel is responding to the control thrust. The simulated sensor signals should also reflect the actual performance of the physical sensors, such as time lags, freezes, noise and jumps, etc.

The standard sensors used in control applications on NTNU's ROVs are:

- Horizontal position from acoustic positioning systems (high precision acoustic positioning (HiPAP)) connected to a surface vessel (which gets the measurements from GPS) and ROV;
- Depth/vertical position from pressure gauge;
- Horizontal and vertical speeds from Doppler velocity log;
- Heading and turning rate from inertial measurement unit (IMU);

Other sensors, and equipment such as lights and cameras, are often equipped to the ROV if they are needed for certain tasks, but are rarely used for control purposes.

Sensors signals generally contain a bit of noise following a statistical pattern, as well as random jumps and, in case of sensor failure, a drifting signal. This is useful to include in a sensor model for HIL testing purposes in order to make sure the control system is robust enough to handle small variations and filter unwanted noise.

3.2.5 Current Loads

In most cases the only significant environmental forces acting on an ROV in submerged condition is the ocean current. The current is composed of many components, and the velocity U of a surface current can be given as (from [21]):

$$U = U_t + U_w + U_s + U_m + U_{\text{set-up}} + U_d \quad (3.19)$$

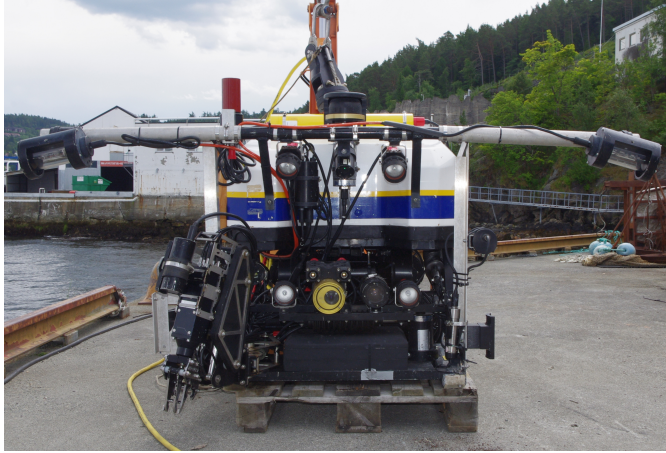


Figure 3.3: The front of ROV Minerva showing some of its sensors, as well as cameras and lights

where

U_t is the tidal component;

U_w is the wind component, set to 0 for an ROV;

U_s is the Stokes drift component which can also be set to 0;

U_m is from the major ocean circulations;

$U_{\text{set-up}}$ from set-up phenomena and storm surges;

U_d is the local density-driven current dependent on density-jumps in the ocean;

The current will affect the hydrodynamic terms and drag force on the umbilical in (3.18), where the relative velocity is given as $\boldsymbol{\nu}_r = \boldsymbol{\nu} - \boldsymbol{\nu}_c$. The total current velocity is given as U , and is used to determine the velocity components in an irrotational current using different methods mentioned in [17]. A typical velocity for design of structures in the North Sea is 1 m/s.

For a computer implemented simulation system the 1st-order Gauss-Markov Process is recommended:

$$\dot{U} + \mu U = w \quad (3.20)$$

where w is Gaussian white noise and $\mu \geq 0$ is a constant. This method is usually implemented with a saturation element to keep the simulated current within given limits. A transformation between the direction of the flow and the NED and BODY-frames of the ROV is also needed.

3.2.6 FMEA Simulations

An important part of vessel testing is the Failure Modes and Effect Analysis (FMEA), and in [22] DNV lists a series of demands for an FMEA for redundant systems, such as a DP system with IMO redundancy class 2 or 3. An FMEA document will specify a large amount of possible failures in a system, the probability and severity of a failure and the response from the system. Including FMEA simulations to the HIL system will help thoroughly testing the control system's ability to deal with unexpected errors.

Examples of common failure modes easy to simulate would be random or constant signals from sensors, different kinds of power failures causing the loss of a thruster, and communication errors resulting in lost signals in the feedback. The reaction of the control system will then be observed to determine the fault tolerance of the system.

3.2.7 Interface Between DP and HIL System and Real-Time Simulations

To connect the control system and HIL simulator together NTNU uses National Instrument's CompactRIO which works as an advanced I/O module and translates signals coming from and going to the ROV. The cRIO consists of a real-time controller, reconfigurable IO modules, field-programmable gate array (FPGA) module and an Ethernet connection [23]. LabVIEW is used to program the cRIO to perform the desired tasks. When the ROV is used at sea the cRIO will transfer control commands from the DP system computer to the ROV's thrusters. The sensor data from the ROV is then fed back up through the umbilical and through the cRIO who then feeds them back to the control computer. This process is exactly the same in a HIL simulation except the ROV is replaced by a computer running the simulation software to receive the control commands and provide appropriate sensor feedback.

As the DP system is running in real time and the ROV will provide continuous feedback in regular operation it is important to have a HIL system that can handle real time communications, and this is taken care of by the real-time controller in the cRIO.

Chapter 4

Current Systems at NTNU

This chapter contains a description of the current systems used in this thesis, as well as changes and improvements conducted.

4.1 Model Parameters

Chapter 3 covers the mathematical models of the ROVs, but finding the parameters for the mass M and damping D is often a problem, especially for the hydrodynamic forces in (3.11) that usually require a series of tests.

In 2003 ROV Minerva went through a series of tests at Marintek to determine the drag coefficients as well as thrust capacities, this is documented in [24]. These are the only test aimed at determining the ROV model parameters ever performed on either Minerva and SF 30k, and as the sensor outfitting etc. have changed repeatedly this poses a large uncertainty in the models.

In [20] and [25] Kirkeby proposes model parameters for Minerva based on the tests and earlier experience with the mathematical models. These parameters are still used as a basis today, even though they are often changed and adapted to fit the need of the user. As no tests have ever been performed on the SF 30k, all hydrodynamic parameters used for it are based on work done by Berg in [3] and are scaled from the values used on Minerva.

A selection of commonly used parameters for ROVs Minerva and SF 30k can be found in Appendix A.

4.2 General Observations

The different linear and nonlinear damping in a ROV is the factor that varies the most in the different data sets. In the models used for both Minerva and SF 30k this is natural as the mass matrices to some degree can be based on CAD and mathematical computations. Some CAD models can be provided by Sperre AS, which is the manufacturer of the ROVs. These models and computations are done on a stripped ROV as delivered, and thus does not include any sensors and extra equipment added to the ROV by NTNU at a later stage and water penetration, making the accuracy of the models low. The weight of the ROVs are probably higher now than when they were last weighted, and installation of equipment might have changed the damping and centers of gravity and buoyancy.

The damping needs to be determined through either model of full scale tests, and thus has a much larger uncertainty such tests have not been performed since 2003, as documented in [26] and [27]. Even though many of the parameters can be assumed to include an error, the models give a reasonable approximate representation of the reality and for practical control purposes they have proven to work well.

Most, if not all, ROV control systems at the Department of Marine Technology at NTNU today are based on the same basic models and parameters, but with slight variations depending on the specific task the model is intended for and any preferences of the user/designer of the system.

4.3 Damping

As discussed in Chapter 3 there are two damping elements; linear and non-linear. All tests performed and described in [26] and [27] are done for velocities over 0.3 m/s, and as such the non-linear damping will be dominating.

Linear damping is dominating for lower velocities (less than ca. 0.1 m/s), while the nonlinear damping will govern the damping for higher speeds. To make this effect more pronounced an exponentially decaying function might be used on the linear part to remove it and have a purely nonlinear damping for higher velocities (as can be seen in the models from Kirkeby in section A.1).

The damping in the different directions are noteworthy as it varies in the different data sets given in Appendix A. If the ROV is regarded as a rectangular box where the height and width are nearly even (Minerva: $h = 0.80\text{m}$, $w = 0.82\text{m}$; SF 30k: $h = 1.60\text{m}$, $w = 1.50\text{m}$) it is fair to assume the damping in sway and heave should be close to identical. However, this is a simplification as the ROV contains lots of hollow space and additional equipment etc. At the top of both of NTNU's ROVs are buoyancy tanks that cover nearly the entire top of the vehicle (some holes are of course present for the thrusters), and thus little water can pass through in the vertical direction (heave). In sway there are several gaps that will allow water to

flow much more freely than in heave. Thus the damping force should be larger in heave than in sway, and this is not reflected in all the models. In surge the ROV will naturally have a much smaller surface area and thus smaller damping than in sway and heave, and it will also allow some water flow.

The moments caused in roll, pitch and yaw are not usually a priority in the modeling, and thus they might suffer from even larger uncertainties. In Kirkeby's models (section A.1), for example, the damping in yaw has been deemed uninteresting and thus is simply set to 1. Some of the same arguments used for surge, heave and sway might be used for roll, pitch and yaw, as the water will be able to flow more freely through gaps in the structure in yaw than in roll, and nearly no flow will be allowed in pitch.

To determine the damping and water flow through the vehicle in different directions as well as more accurate damping a full scale test or accurate model test is needed, and at the current time qualified guesses and small adaptations to fit the intended purpose of the model are the best way to modify the models.

4.3.1 Damping Plots

The damping of the different models and directions can be plotted and visualized in Matlab to help see the differences.

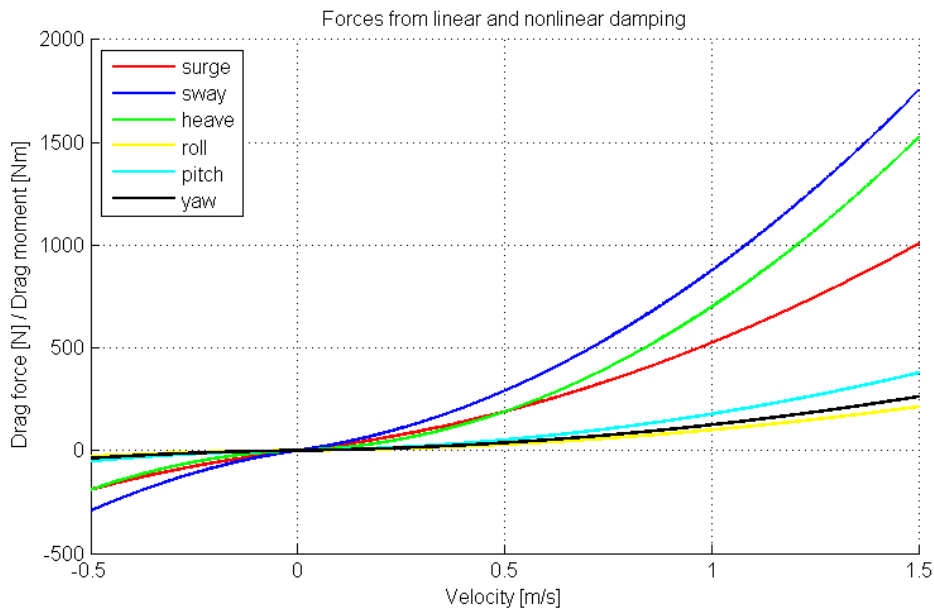


Figure 4.1: The damping for ROV Minerva based on (A.15) and (A.16).

Figure 4.1 shows the damping of Minerva in different directions based on parameters used by Daniel de Almeida Fernandes. The most noticeable result here is the damping in sway being considerably larger than in heave. As discussed above this is probably incorrect as the water flow through Minerva is significantly larger in sway than heave, and a large surface breaking the water should provide a higher damping making heave larger than sway. The linear damping in (A.16) contains larger numbers in surge and sway than any of the other data sets. The model is symmetric for negative velocities, and the ROV will seldom reach speeds over 1.5 m/s.

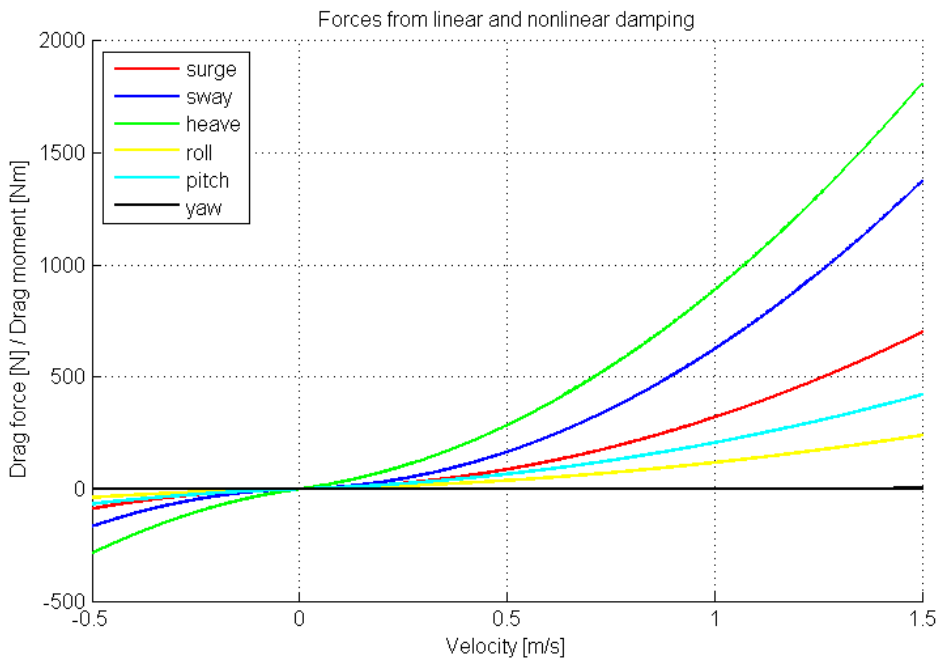


Figure 4.2: The damping for ROV Minerva based on (A.3) and (A.4).

Figure 4.2 is based on the Master thesis of Kirkeby [20] and is used as a foundation for many other models. It has the same non-linear damping as Fernandes' in Figure 4.1, but the linear damping in heave is larger and thus we get a more expected result with damping in heave being greater than in sway.

To compare the numbers shown in Figures 4.1 and 4.2 the surge, sway and yaw for both cases are plotted in Figure 4.3. The most striking difference is the difference between the sway and heave components. They nearly seem to have switched places in the two models. In Fernandes' models surge and sway have a higher linear damping while the heave is much lower. Kirkeby has the opposite with relatively low values for surge and sway but high in heave.

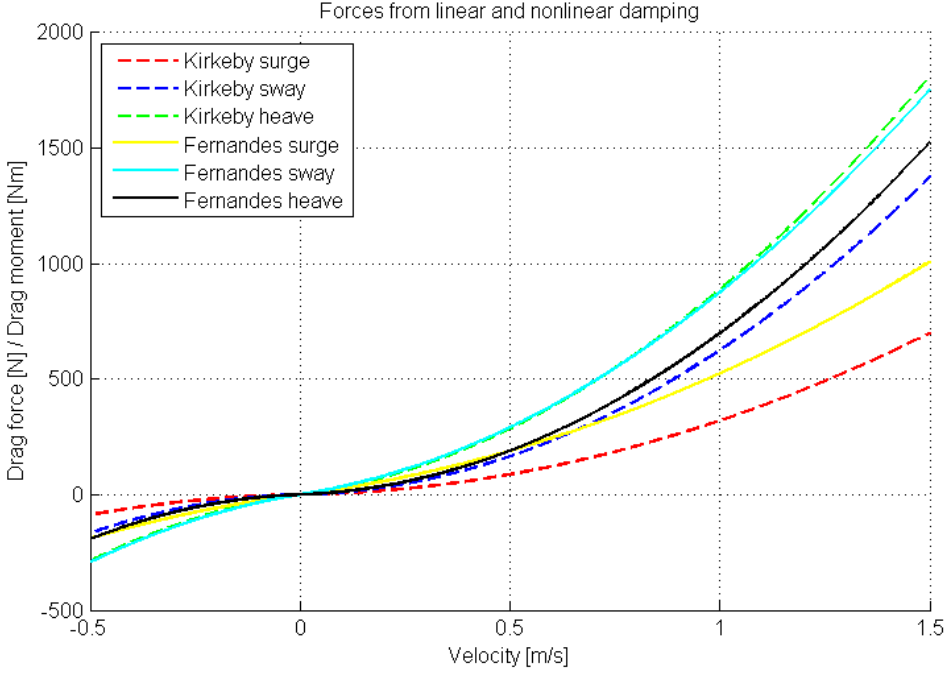


Figure 4.3: The damping in surge, sway and heave for ROV Minerva comparing numbers from (A.3), (A.4) and (A.15), (A.16).

The damping in different directions of the SF 30k is shown in Figure 4.4. As the SF 30k is a much larger ROV than Minerva the damping effects will of course be larger. The nonlinear heave force is especially dominant, which also logically means high drag moment in pitch. These numbers are based on Bergs Master [3] and are a combination of simulations and CAD models and scaling of numbers from the Minerva.

Based on the results from [26] and as discussed in [20] it is natural to assume the linear damping should only be present in the low velocity segment, and should be very small at high speed. Thus assuming the linear damping follows $\tau_{DL} = \mathbf{D}_L \mathbf{v}_r$ is inaccurate, and an exponentially decaying linear damping, as seen in (A.5), can be used. This is shown in Figure 4.5 where the exponentially decaying curve follows the linear curve to a much larger extend than the nonlinear curve for low speeds.

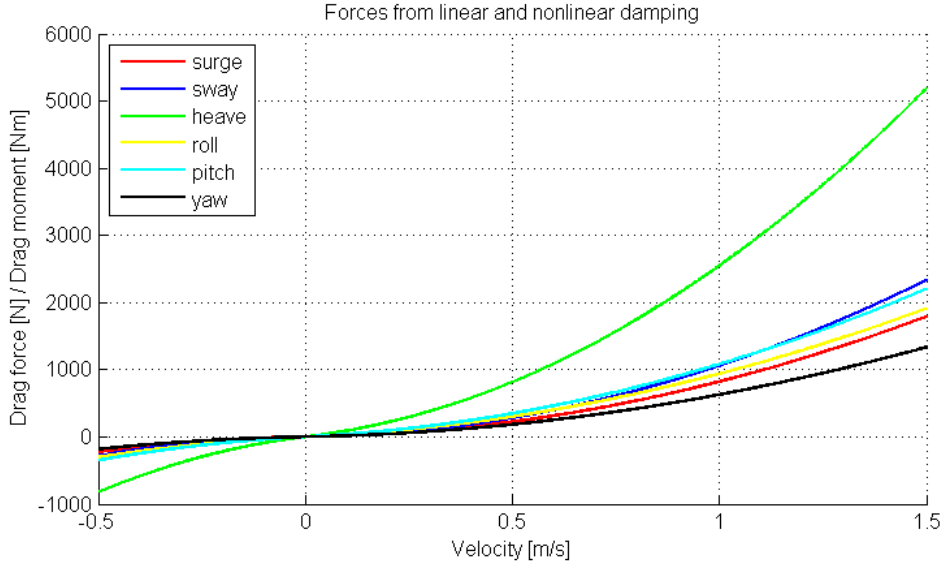


Figure 4.4: The damping for ROV SF 30k based on (A.23) and (A.24).

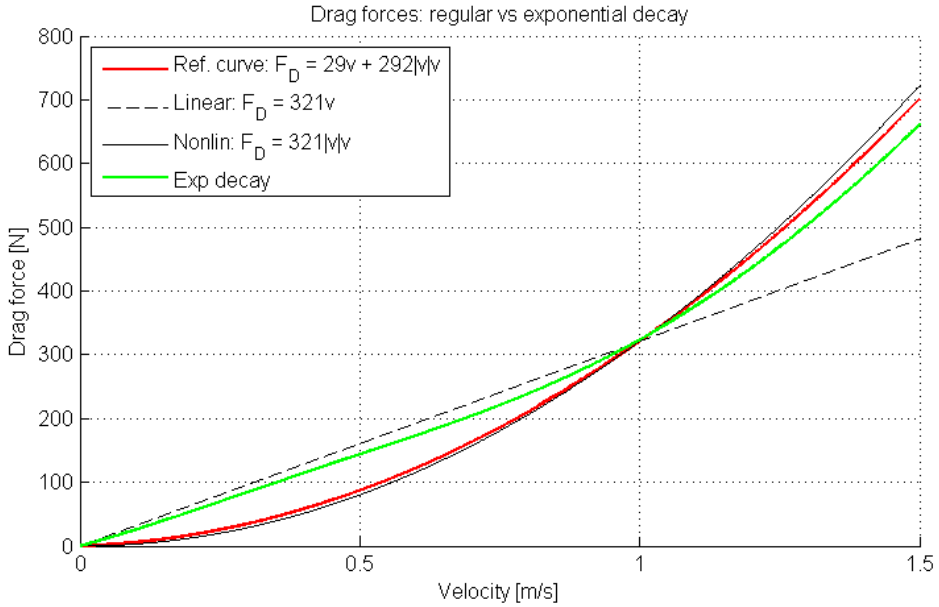


Figure 4.5: The damping for Minerva in surge based on (A.3), (A.4) with exponential decay from (A.5). Surge speed given as v .

4.4 HIL system

The HIL system currently in use at NTNU is implemented in National Instrument's LabVIEW, which is a visual programming language. In real life application the ROV is connected to the control computer through a compactRIO and the internal network on NTNU's research vessel R/V Gunnerus. When the HIL simulator is used it will communicate with the control system (ideally running on another computer) through a cRIO connection.

The basic flow of signals in the HIL system when it is run is as follows; the communication and ROV parameters are set and configured and queues for handling the information flow are established. The system then runs its two loops. The simulation loop contains all models of the ROV, sensors etc and will get the commanded thrust in propeller speed from the control system, as well as information about waves, currents and additional forces action on the ROV to compute the changes in position and velocities using (3.17) and (3.18).

The outputs from these calculations are then fed through the sensor-models to add appropriate delay, noise and signal behavior. It is also possible to log the data before it enters the sensor models if the non-disturbed states are desired. After the sensors the signals are sent to the relevant queues as numerical vectors. The queues are sent to the communication loop of the system. This loop handles all inputs and outputs between the HIL system and the connected control system. The values in the queues from the simulation loop are written into strings in the appropriate format to be read by the control system and are sent using a communication protocol.

The communication loop also receives a string from the control system containing the desired thrust forces given in shaft speed (RPM). These values are converted from bit-values into a matrix giving the commanded thrust for each engine, and are fed to a queue. These values are then read and transformed into thrust forces in the different direction, $\boldsymbol{\tau}$, in the simulation loop and used to compute another set of new values for positions $\boldsymbol{\eta}$ and velocities $\boldsymbol{\nu}$.

The simulation and communication loops are run continuously at a selectable period (usually 0.150 seconds for the simulation loop and 0.010 seconds for the communication loop) as long as the system is running. When the system is stopped the loops will stop running and the communication ports will be closed.

The structure of the entire HIL system is shown in Figure 4.6.

4.4.1 Communication

The HIL system communicates with the control system by sending and receiving strings. The HIL system is set up to send two strings; the Navipac string and the ROV string. The Navipac string contains more info than it needs as the current

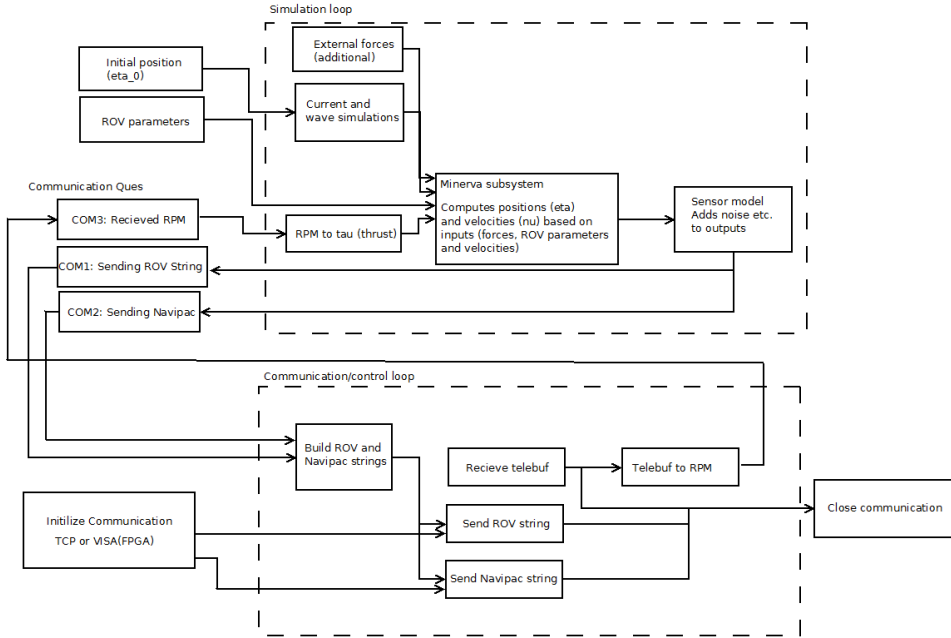


Figure 4.6: The structure of the HIL system shown.

control system relies less on it than it used to. The structure of the Navipac string:

$$[!init; N; E; Z; u_b; v_b; w_b; u_w; v_w; w_w; a_1; a_2; a_3; a_4; N_s; E_s; \psi_s]$$

where N , E and Z are the global positions of the ROV from HiPAP and GPS, u_b , v_b and w_b are the bottom fixed velocities from the Doppler velocity log (DVL), u_w , v_w and w_w are the water fixed (relative) velocities from the DVL, a_1 , a_2 , a_3 and a_4 are values from the altimeter of the DVL (which has four beams), and N_s , E_s and ψ_s are the surface vessel position and heading. The only information currently used by the control system from the Navipac string is the three positions of the ROV, and thus the other information sent from the HIL system is not relevant and sometimes not updated. The “!init” at the start of the string is included to simulate the output of the actual Navipac software.

The ROV string consists of:

$$[d, alt, n_{\text{turns}}, \phi_C, r, , , ,]$$

where d is the depth from the pressure gauge, alt is the altitude from the DVL, n_{turns} and ϕ_C are the number of complete turns and angle from the compass, and r is the yaw rate from the IMU. The end of the string includes some commas at the end to match with values expected in the control system.

From the control system the HIL system receives a single string containing the data from a telebuf of 28 bytes controlling the desired control forces to the thrusters. These bytes contain all the signals possible to send to NTNU's ROVs and the bits in each byte holds a specific meaning. In the HIL simulator only the thrust forces are relevant and the other information is not used.

4.4.2 Software-in-the-Loop System

While HIL-testing is preferable due to the test environment being closer to the actual applications, it does limit the use of the testing systems as an expensive connection is required. This makes the simulator less available to most students who want a simple and fast way to test code. To make the system more available to the general student population a Software-in-the-Loop (SIL) solution will provide the most important aspects of testing for most student-developed systems.

The chosen communication platform is the Transmission Control Protocol (TCP) as it provides reasonably fast, reliable, ordered and error-checked communication [28]. This communication can be conducted on a single computer, between different computers on a local area network, or through the Internet. Thus the SIL and control systems can be run on a single computer or two different computers if this is desirable, even though the gain of testing the cRIO communication is removed.

The SIL system is made to be as similar to the HIL system as possible, and only the communication is changed. Some changes are also necessary in the control system, such as creating new blocks to handle sending and receiving communication on the new form. The strings sent are still the same as discussed in section 4.4.1. The communication parts depending on either TCP or cRIO communication are wrapped in if-structures and wired so it is possible to choose between cRIO communication for real operations with an ROV or HIL and TCP communication for SIL. This means all future implementations of controller, observers and other control structures in the control system can be implemented one place and then tested in both HIL and SIL with a simple switch.

4.5 ROV Sensors

The sensors mentioned in section 3.2.4 all have different characteristics and provide different outputs. This section will focus on the signal characteristic of each sensor and how it should be modeled.

The primary information needed in the feedback control of an ROV is the positions, meaning the north, east and down coordinates, as well as the yaw to keep track of the heading. However, in order to improve the performance of the system the following measurements are available with the current sensor pack:

- The positions in north and east (x and y)
- The depth
- The heading and yaw rate
- The velocities u in surge and v in sway

Other measurements can also be made if desired, such as the salinity in the water, the accelerations of the ROV, the velocity of the currents, etc., but these are not usually used in the feedback control.

4.5.1 Sensors in Use

The current sensors and software for measurements in use on NTNU's ROV Minerva are:

- Ship GPS
- Kongsberg HiPAP 500 (High Precision Acoustic Positioning System)
- EIVA NaviPac software
- Valeport miniIPS Intelligent Pressure Sensor
- Xsens MTi-100 series IMU (Inertial Measurement Unit)
- RD Instruments Workhorse Navigator DVL (Doppler Velocity Log)

4.5.2 Position: HiPAP, GPS and Navipac

The Kongsberg HiPAP 500 is a high precision acoustic positioning system using super short baseline principle to get relative positions underwater. The R/V Gunnerus is fitted with a transducer and ROV Minerva has a transponder, and thus the relative positions can always be measured. It is capable of providing north, east and downwards positions relative to the surface vessel, but due to signal quality only north and east are used for control purposes.

In [29] Kongsberg gives the range detection accuracy as less than 20 cm, but this is under optimal conditions. Cruises performed with NTNU's ROVs suggests this error might be larger and dependent on several different factors such as salinity and depth. The refresh rate of the signal is usually approximately 1 Hz, but this can also drop under bad conditions. As the signal has to travel from the ROV to the Ship and then fed through software before being given to the control system.

The main faults in the HiPAP signal are wild points and areas with high variance, as well as some smaller signal freezes. This can be seen in Figures 4.7, 4.8 and 4.9 where the wild points are large and easily visible. In Figure 4.10 a zoomed in version of the east position shows an area of high variance, a wild point disappearing from

the graph, and some minor signal freezes which lead to high derivatives when the signal is regained.

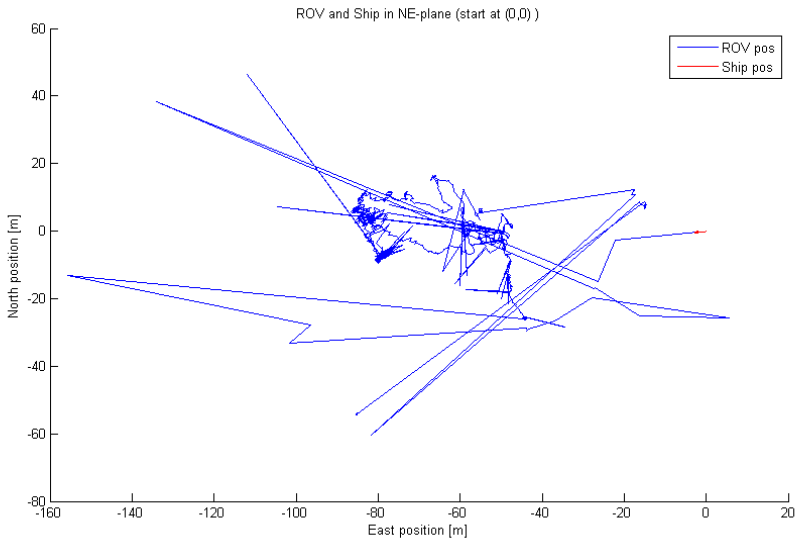


Figure 4.7: The ROV and Ship trajectory shown in the North-East plane. Based on raw HiPAP and GPS data.

All the signals shown in Figures 4.7, 4.8, 4.9 and 4.10 are based on raw data from HiPAP and GPS collected on a cruise with NTNU's Applied Underwater Robotics Laboratory (AUR-Lab) on 24 April 2014. The GPS outputs data in the \$GPGGA [30] format while the HiPAP uses the \$PSIMSSB [31] format.

The GPS signal is shown in the Ship position in Figures 4.7, 4.8 and 4.9. This signal is far less affected by sensor noise than the HiPAP and it is updated each second. The surface vessel will also generally move much less than the ROV in most operations.

The HiPAP system is run from the Acoustic Positioning Operating Station (APOS) software pack, also delivered by Kongsberg Maritime.

Connecting the GPS and HiPAP and making sure the updates match each other and providing options for signal processing and filtering. This functionality is provided by Navipac, a software that specializes in creating the desired outputs from a series of raw data from GPS and HiPAP or other positioning methods. It is speculated that the Navipac creates some delays in the system and if desired it should be possible to implement code to bypass it completely.

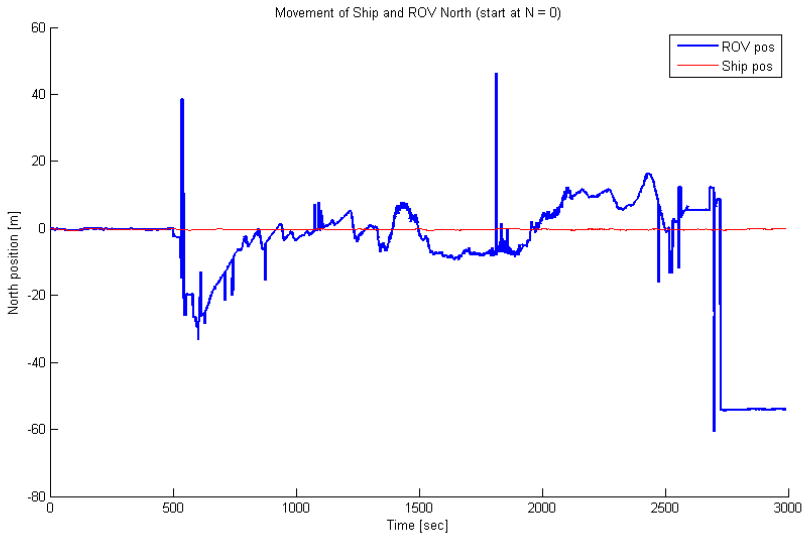


Figure 4.8: The ROV (HiPAP) and Ship (GPS) North positions shown.

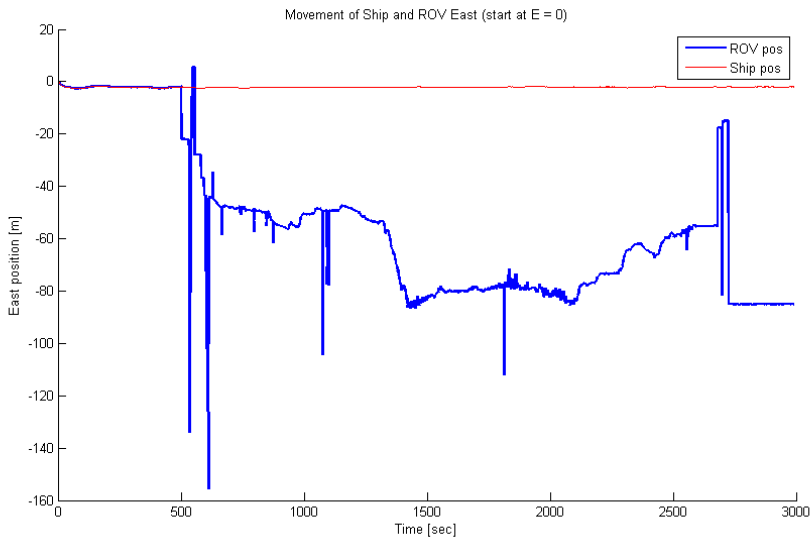


Figure 4.9: The ROV (HiPAP) and Ship (GPS) East positions shown.

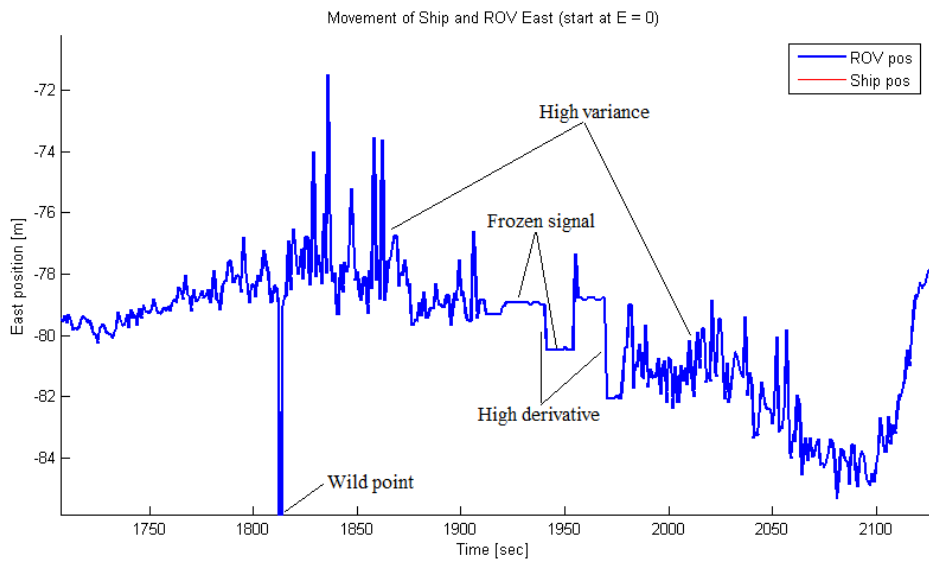


Figure 4.10: Zoomed in signal from Figure 4.9.

4.5.3 Depth: Pressure Gauge

The Valeport miniIPS Intelligent Pressure Sensor [32] has a accuracy of 0.01% of its current value. This is far better than the HiPAP and thus all depth measurements used for control purposes are from the pressure gauge (PG). Some noise is present, but it is generally less than 10 cm. In Figure 4.11 the measurements from the pressure gauge can be seen as the ROV is descending. The zoomed in areas are included to show the signal performance. It is reasonable to assume the ROV is oscillating a bit as the depth controller is not usually prioritized and the movements are quite slow.

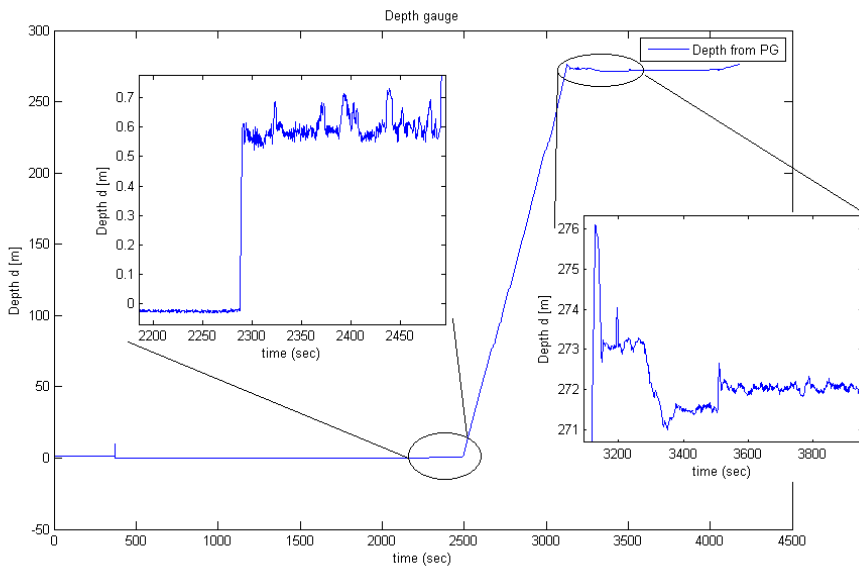


Figure 4.11: Measurements for the pressure sensor as the ROV is stationary and descending to approx 270 meters with zoomed in area. (From cruise 2014-04-10)

4.5.4 Heading and Yaw Rate: Inertial Measurement Unit

The IMU is used to get the heading and yaw rate for the vessel using accelerometers, gyroscopes and magnetometer. The Xsens MTi-100 IMU [33] is used on Minerva with a presumed accuracy of 0.4 degrees. It experiences quite a bit of noise with a relatively low amplitude but high frequency, especially in the yaw rate r . Figure 4.12 shows the behavior of the signals from the IMU during a regular operation, with heading angle between -180° and 180° .

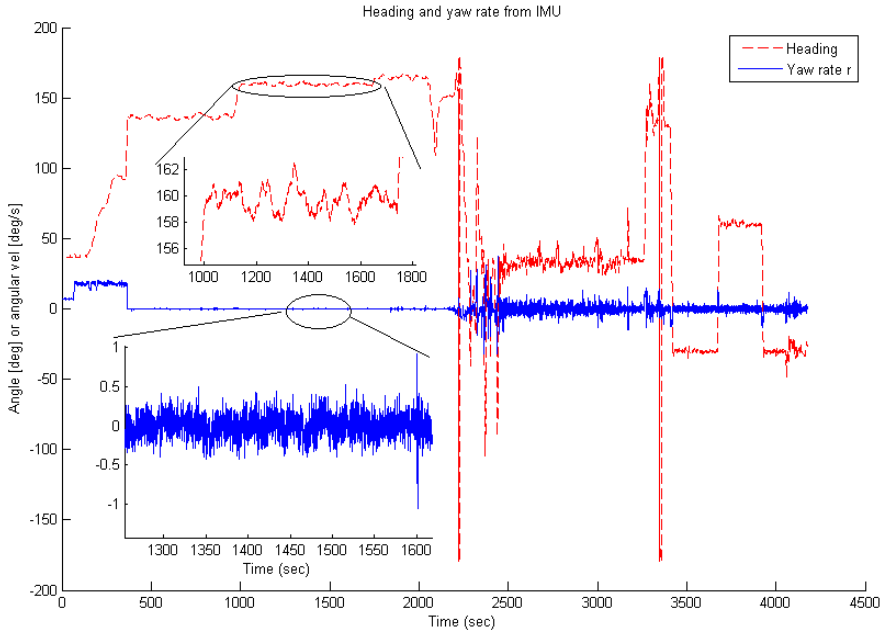


Figure 4.12: The heading and yaw rate given from the IMU. (From cruise 2014-04-10)

4.5.5 Velocities: Doppler Velocity Log

The velocity components in surge and sway are measured by the Doppler Velocity Log (DVL). For velocities of 1 m/s or less (the typical operating velocities for an ROV) the standard deviation is given as less than 0.4 cm/s [34]. As the velocities of the ROV naturally varies during controlled operations, especially when the ROV is trying to remain at the same spot, the output will look noisy even though the performance of the sensor is satisfactory. However, the sensor itself also adds noise to the measurement. This can be seen in Figure 4.13.

4.6 Control System

The current Njord control system (CS) are designed with a flat sequence structure making sure all communication is established before the main parts of the system started, and closed after use. The system contains five loops running continually at different frequencies and provide all the main functionality of the system;

- The IMU/MTi loop included if control using IMU inputs is desirable

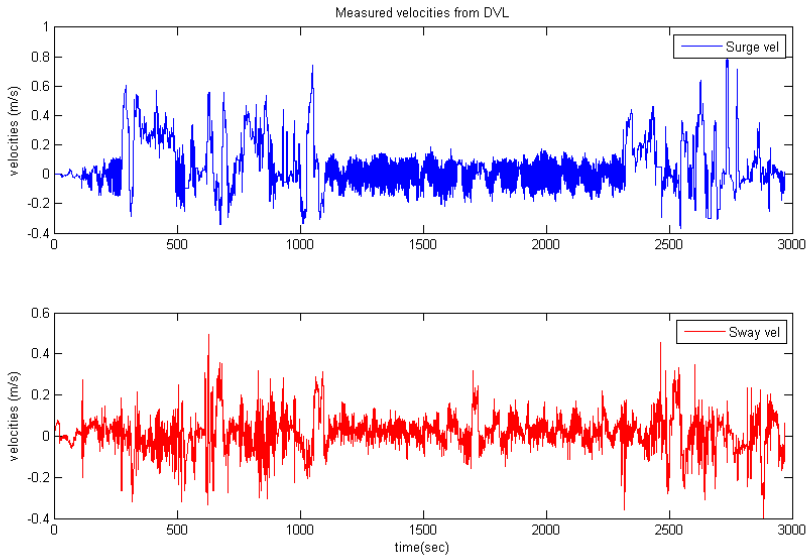


Figure 4.13: The bottom fixed velocities of the ROV in surge and sway given by the DVL. (From cruise 2014-04-10)

- The Main Thread contains all communication between the CS and ROV, signal processing, observer and control structure, etc.
- The Joystick loop receives commands from a joystick and transform
- TCP send loop sending information to the Graphical Used Interface (GUI)
- TCP receive loop receives information form the GUI

It is worth noting that the TCP communication used between the CS Njord and GUI Frigg is not connected to the TCP communication used in the SIL system described in Section 4.4.2.

4.7 Changes and Contributions

The only changes made to the control system Njord is in it's communication to allow for SIL operation as described in Section 4.4.2. These changes have not influenced the structure of the system or the control functionality in it.

Compared to the CS there are more changes in the HIL system. These changes can relate to four main areas;

- Communication: Allowing SIL through TCP

- Sensors: Better simulations of signals
- Model Parameters: Easier to change, possible to add error if desired
- Umbilical: Added forces and moments due to the umbilical

The communication mostly consists of changing already existing blocks using cRIO and FPGA communication into the corresponding blocks using TCP, but as the communication protocols behave differently some adjustments are necessary.

Sensor signals in the original system are just the states with some added Gaussian white noise. Getting better simulations of signals closer to the real life sensors improves the quality of the HIL and SIL systems as error checking and signal filtering are important parts of a robust control system. In addition to simulating the signals better there are also added a new communication stream creating and sending the raw \$GPGGA and \$PSIMSSB strings based on the states in the HIL system to the CS through UDP communication.

In the original implementation the parameters of the ROV were put in a MathScript node inside the system and not easily accessible for the user of the HIL system without extensive knowledge of the system. The new implementation includes a tab in the main interface where important ROV parameters such as length, breadth, weight and mass and damping matrices can be defined. Other values, such as the rigid body mass matrix and weight, is computed from the given parameters. Adding multiplicative errors in the damping and mass matrices is possible, and this utilizes a random function returning a matrix value between 0.7 and 1.3 times the original value. This can be used to test the robustness of systems when changes are made to the ROV, but not included in the control system.

The umbilical is subject to hydrodynamic forces calculated using the Morison equation (shown in (3.15)) in both sway and surge due to ROV movement and current. This adds new forces and moments on the ROV, but these are generally much smaller than the forces acting on the vessel directly. Moments in roll and pitch are added due to the placement of the umbilical attachment, and these have to be countered by the restoring forces as these DOFs are not controllable.

A more detailed description of changes are given in Appendix B.

Chapter 5

Simulations and Results

This chapter contains results from a HIL/SIL simulation as well as a sea trial. The HIL tests has been performed to replicate the real life test as closely as possible in order to compare the results and determine if the simulation systems is capable of providing reasonable results which can be used to improve the control system.

5.1 Sea Trials

The sea trials were conducted by NTNU's AUR-Lab with the ROV Minerva on April 11 2014 in the Trondheimsfjord. The data included here shows a small sample of the ROV moving in a lawn-mower pattern often used to test the functions and performance of an observer, controller or other part of a control system. The movements of the ROV is very slow as part of the test were taking pictures underwater.

The path set for the ROV can be seen in Figure 5.1. The entire run as shown in this section takes approximately 27 minutes (1600 seconds) due to the low velocity.

5.1.1 Conditions

The conditions are good for ROV operations with small waves and very little current in the water, which is good considering the slow desired velocities.

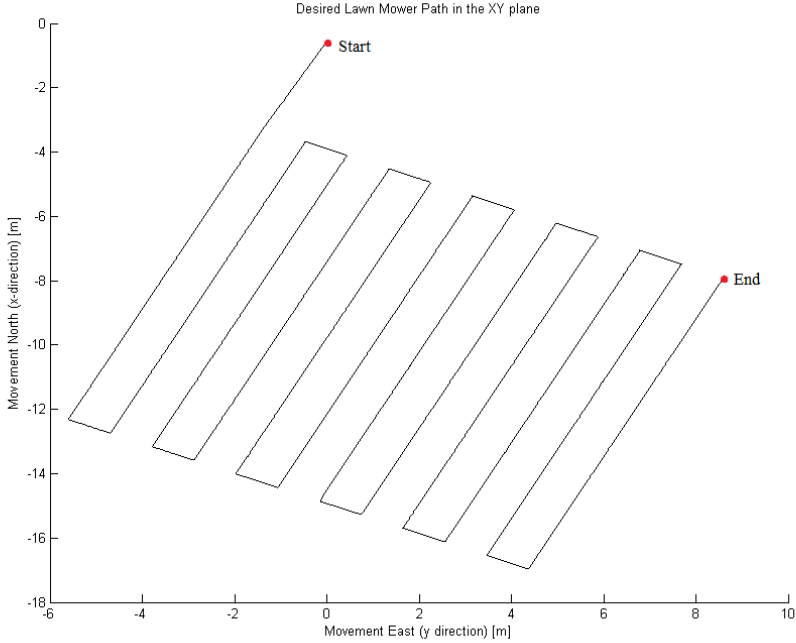


Figure 5.1: The desired path for the ROV in the sea trials.

5.1.2 Positions

Several different positions are logged in the system. The ones presented below are the raw HiPAP data for the north and east positions, as well as the raw pressure gauge for the depth. In addition the measured states after the Navipac is included, this is what is used as η in the control system, as well as the desired positions η_d and estimated positions $\hat{\eta}$ from the observer.

As can be seen in Figures 5.2, 5.3 and 5.4 the HiPAP provides noisy measurements with randomly placed wild points. The measured states are slightly filtered and most of the wild points are removed together with areas of high variance, but much of the original signal from the HiPAP is still present. Most of the filtering is done by the observer and the estimated positions follow the desired path much more closely than the two measured positions. The largest errors between the estimated and desired positions typically appears in the corners when the ROV is supposed to make a sharp turn, this is expected.

The movements in the vertical direction are smaller than in the horizontal plane and then pressure sensor provides much less noise and wild points than the HiPAP. Thus the raw data and measured states are very close, and the estimated values seem to follow measured states closely, as can be seen in Figure 5.5.

Figure 5.6 shows the heading of the Minerva during the trials, given in degrees and values between 0 deg and 360 deg. The values follow the expected pattern and the angle is nearly constant when the ROV is moving along the edges, with a rapid change in the corners. After the heading has changed it stabilizes for a short while while the vessel travels along the short edge, before changes to a heading 180 degrees different from its original course.

The raw IMU provides a bit of noise and values that are too large due to the sensor's placement on the ROV. This is corrected in the measured signals, and the estimated values follows the the measured closely, with very little error from the desired.

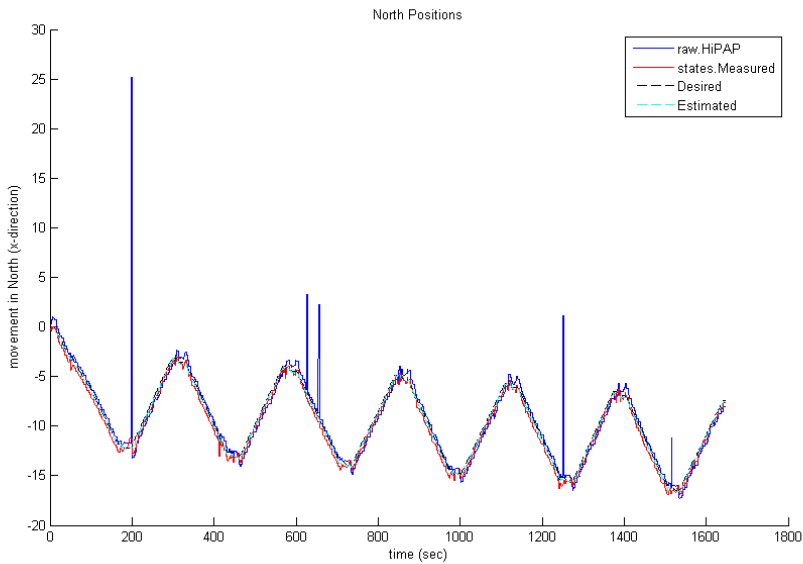


Figure 5.2: The north positions of the ROV in the sea trials.

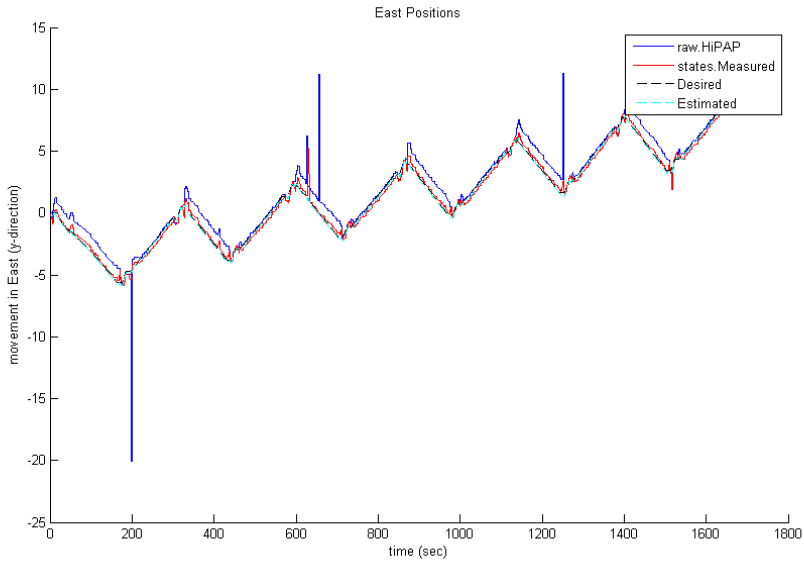


Figure 5.3: The east positions the ROV in the sea trials.

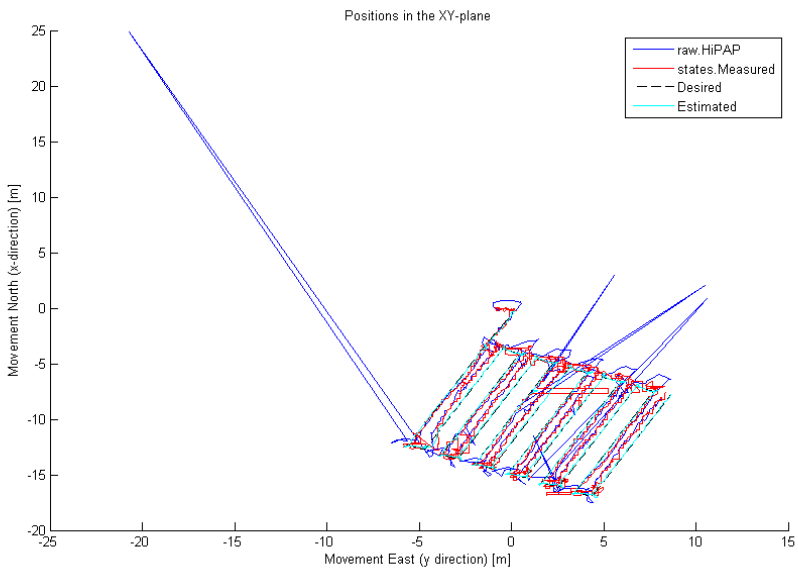


Figure 5.4: The positions the ROV in the north-east plane (from sea trials).

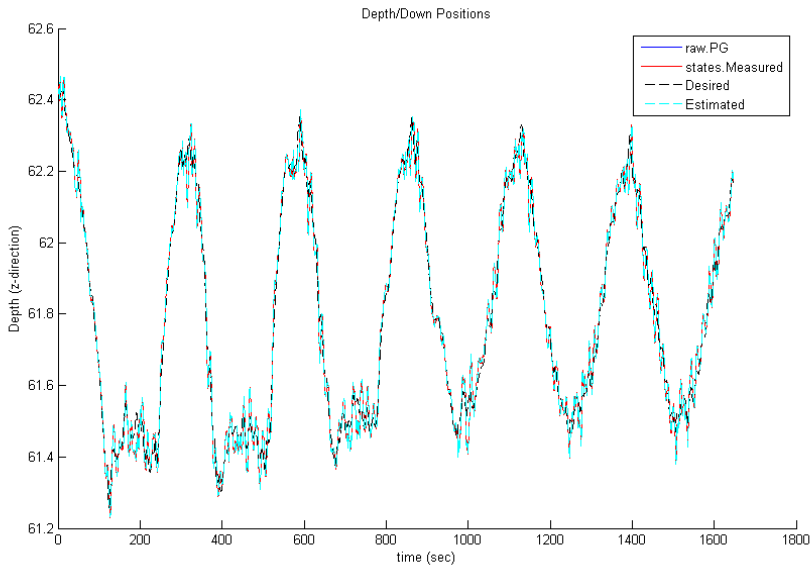


Figure 5.5: The depth of the ROV in the sea trials.

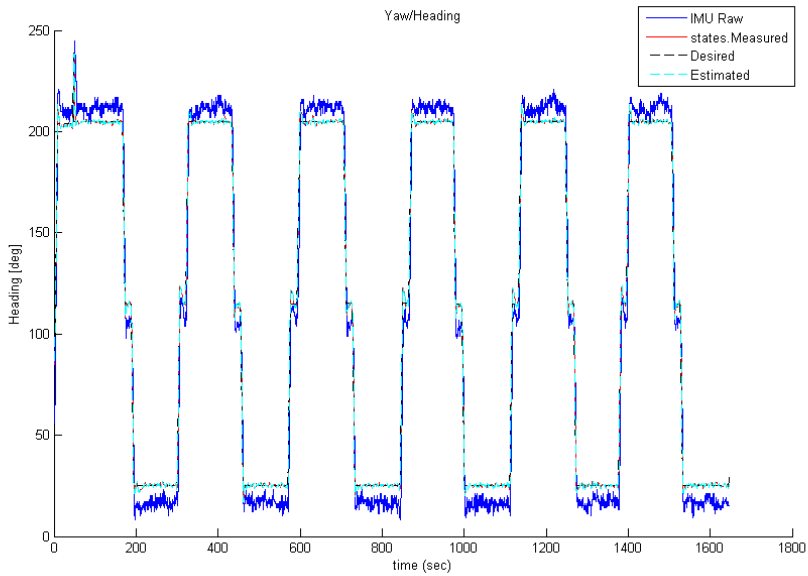


Figure 5.6: The heading of the ROV in the sea trials.

5.1.3 Velocities

Due to the test run being designed to take pictures more than testing the functionality of the control system the velocities are smaller than usual, and thus some oscillations occur.

The graphs in Figure 5.7 shows the desired velocities in the horizontal plane and how the surge velocity will drop whenever there is a turn in the pattern.

The raw data from the DVL is included to show the sensor noise and much more extreme values than in the measured states used in the control system. The estimated state seems to follow the measured pretty closely in surge and sway, with some variation in heave.

Figure 5.8 shows the surge velocities with the desired velocity constant at approximately 0.1 m/s for large parts of the graph. This corresponds to the straight parts of the pattern where the ROV is moving more or less straight ahead at low velocity. The turn are clearly visible as the values increase dramatically for a relatively short period of time. These extreme values are also seen in the sway velocities in Figure 5.9. The movement in Sway is desired to be as close to 0 m/s as possible as the ROV is ideally moving straight ahead with no sideways movements except when it turns.

The most notable in Figure 5.9, which is also somewhat present in figure Figure 5.8, is the offset between the measurements of the DVL and the measured state. In sway it can be seen as a nearly constant error of approximately -0.1 m/s and somewhat smaller in surge. This offset is due to the actual placement of the DVL on the ROV - it is placed at an angle, so that straight ahead (surge) for the DVL is not the same direction as straight ahead for the ROV. This means that the velocities from the DVL must be transformed before they are used in the control system, and this is done for the measured ν signal, but the error in the original DVL signal is still present in the plots. The placement of the DVL is also responsible for the large peaks in sway as it is mounted far away from the center and will register sway motions when the ROV is turning.

Figure 5.10 shows the velocities in heave which are generally smaller than the two other directions and concerned with keeping the ROV at the desired depth seen in Figure 5.5. The most notable feature is the very high estimated states, often higher than the measured states. This is unusual and probably connected to the design of the vertical guidance system, which is separate from the horizontal system in Njord.

The yaw rate is shown in Figure 5.11. As with the other plots it clearly displays how the ROV mostly just keeps its course with some minor oscillations, and major peaks in the velocity at the corners then the vessel turns 90 degrees twice in a relatively short period of time.

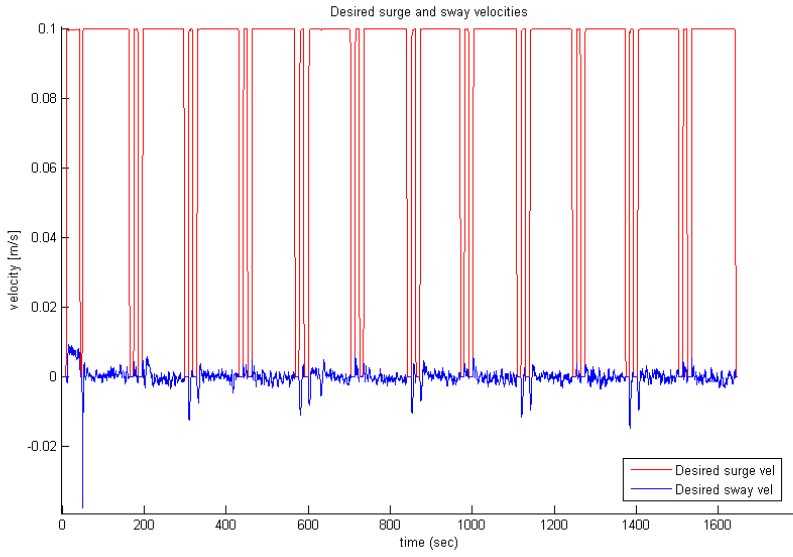


Figure 5.7: The desired velocities in surge and sway in the sea trial.

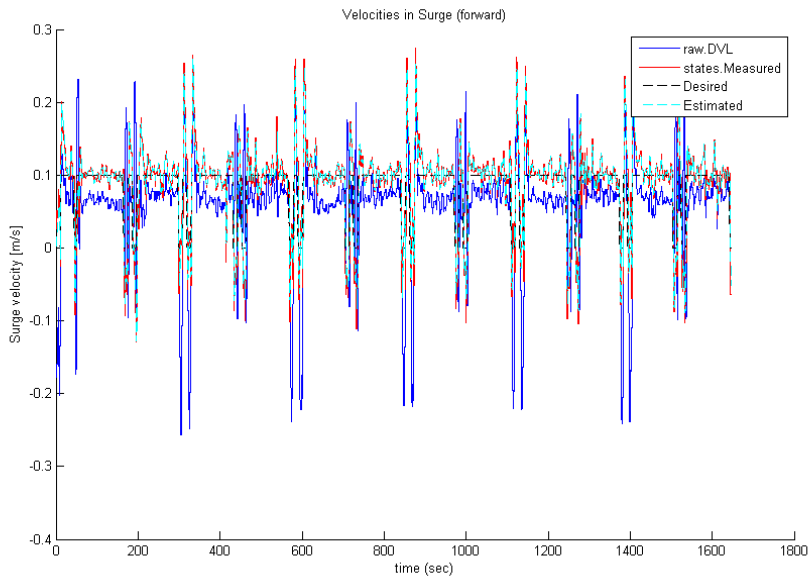


Figure 5.8: The Surge velocities of the ROV in sea trials.

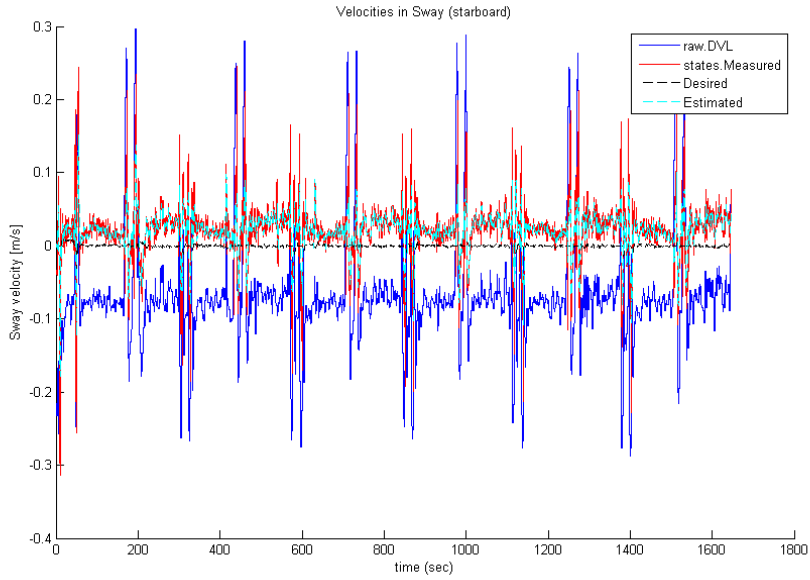


Figure 5.9: The Sway velocities at the sea trials.

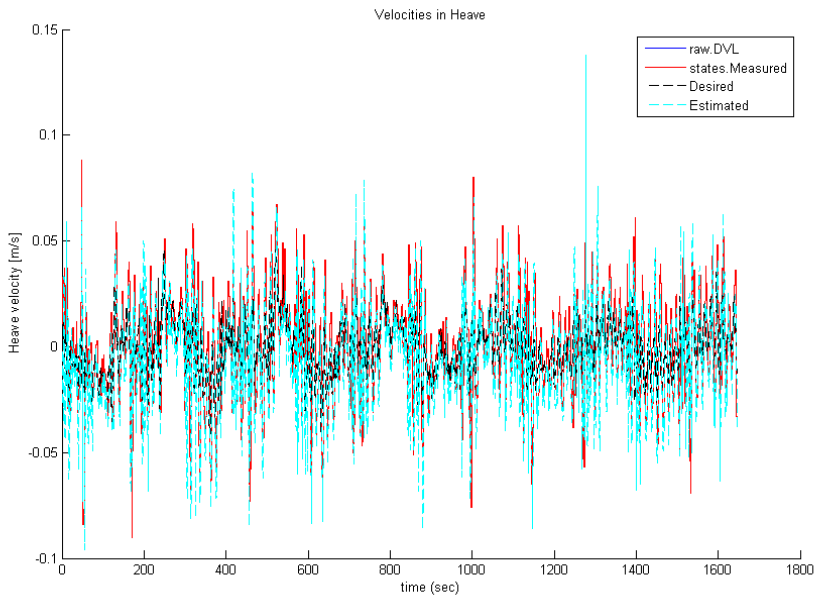


Figure 5.10: Heave velocities at the sea trials.

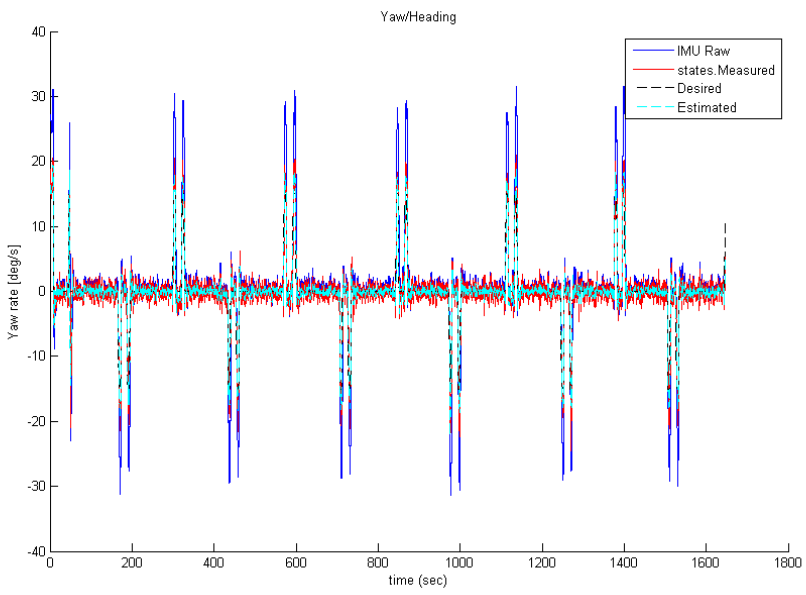


Figure 5.11: Yaw rate in the sea trials.

5.1.4 Thrust Forces

To counter any currents and moving the ROV along the desired path the thrust vector τ is computed. The ROV is controllable in surge, sway, heave and yaw and the thrust forces for these four directions are plotted.

Figure 5.12 shows the thrust forces in the controllable DOFs, and compared to the plots in Figures 5.8 and 5.9 the values seem reasonable. The ROV maintains a a slow surge velocity with little force and some small variations for most the of the run, while during turns surge and sway velocities and forces rise to peaks.

The heave force and velocity in Figures 5.12 and 5.10 have no clear pattern, but they seem to match each other. As the ROV has positive buoyancy a constant heave force is also necessary to keep it submerged.

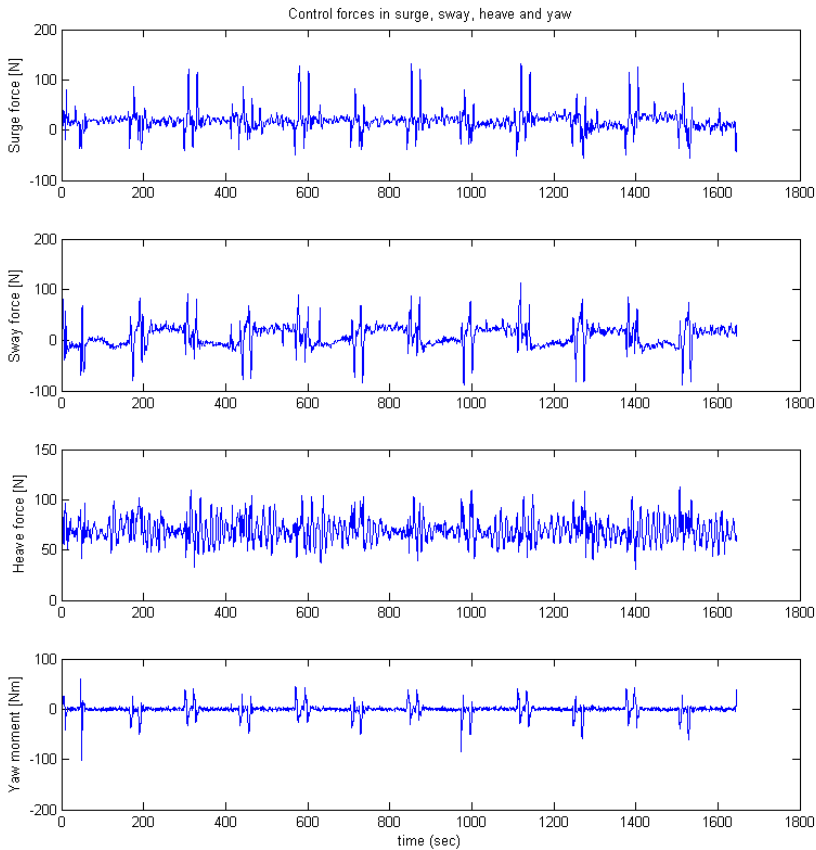


Figure 5.12: Thruster/control forces at the sea trials.

5.2 SIL Simulation

Due to time constraints and availability of the HIL hardware the test is performed on the SIL simulator system. The results are predicted to be exactly the same, but the effect of testing the communication is lost. The current HIL and control system have also been tested with a cRIO connection and the behavior is the same as in SIL simulations.

The simulation is set up to closely resemble the sea trial presented in Section 5.1, but with a larger velocity to show a more common ROV operation. The way points used to generate the desired path in Figure 5.1 were saved and used to generate the desired path for the simulations seen in Figure 5.13.

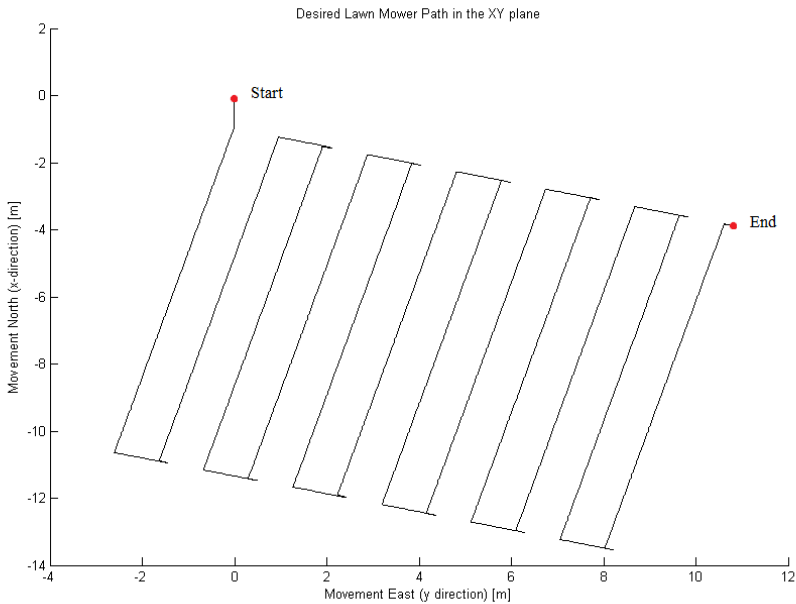


Figure 5.13: The desired path in the North-East plane for the SIL simulation.

As can be seen in Figures 5.1 and 5.13 the paths are very similar although they are at slightly different angles and the desired SIL path have some overshoot in some of the corners where the ROV is supposed to do a 90 degree turn.

5.2.1 Test Setup

The test is set up as a SIL simulations running on a single computer.

ROV parameters are based on Kirkeby's Master Model for Minerva given in Section

A.1. No error in the damping or mass matrices is included, even though many of the values are probably outdated.

As the sea trials were carried out in a calm sea state with very little waves and current no forces from these are included in the simulation, and the only forces working on the ROV are from its movement.

The control system being tested is the standard Njord CS used for most of AUR-lab's operations and is fitted with a Kalman-filter based observer as well as a PID controller. This is the same system as being used in the sea trial and as it contains a logging function the same states will be logged for the simulations and sea trials.

The desired velocities are increased compared to the sea trial to show a more typical ROV movement. This leads to a shorter time span, and the entire test run is approximately 13 minutes (800 seconds).

5.2.2 Positions

The simulator will provide measurements from the HiPAP and PG to the control system. These are presented as the raw data, while the measured data are given for a slightly filtered state from the control system's signal processing removing all extreme wild points.

Figures 5.14, 5.15 and 5.16 show the raw measured positions, the measured states after the signal processing, the desired path, and the estimated states from the observer. The noisy signal of the HiPAP is simulated to include delays and wild points to replicate the real sensor, as can be seen in the plots. The measured state is less noisy and the wild points and high variance-areas have been removed.

The raw HiPAP signal seems to have problems at the corners when the ROV is supposed to turn 90 degrees. This is related to the fact that the transponder is placed in the rear of the vessel, and thus will be moved out of line when the ROV turns around its center. The desired path is computed for the center of the ROV and the measured states are calculated so they are in the center and not rear, and thus these errors are unique to the HiPAP.

As expected to largest errors appear for all states in the corners when a sharp turn is commanded.

The depth is shown in Figure 5.17 and shows how the vessel settles at a desired depth of 60 meters after some small oscillations due to a too deep initial condition. The filtered measured state follow the raw pressure gauge very closely.

Figure 5.18 shows the simulated heading/yaw angles in degrees. The heading is constant at approximately 200 degrees when the ROV is moving along the path southwards, and it changes rapidly when the vessel makes a turn. The raw IMU values, measured and estimated states all follow the desired values closely and the performance seems satisfactory.

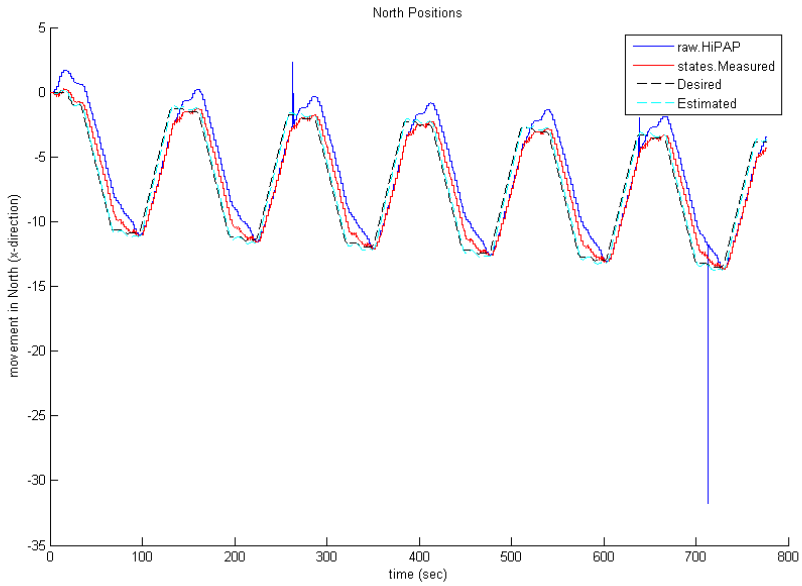


Figure 5.14: The north positions of the ROV in the simulations.

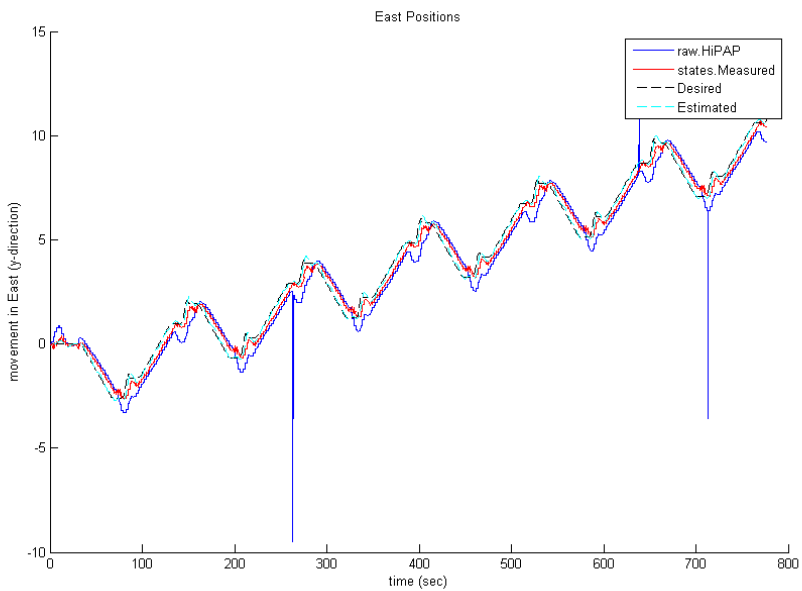


Figure 5.15: The east positions the ROV in the simulations.

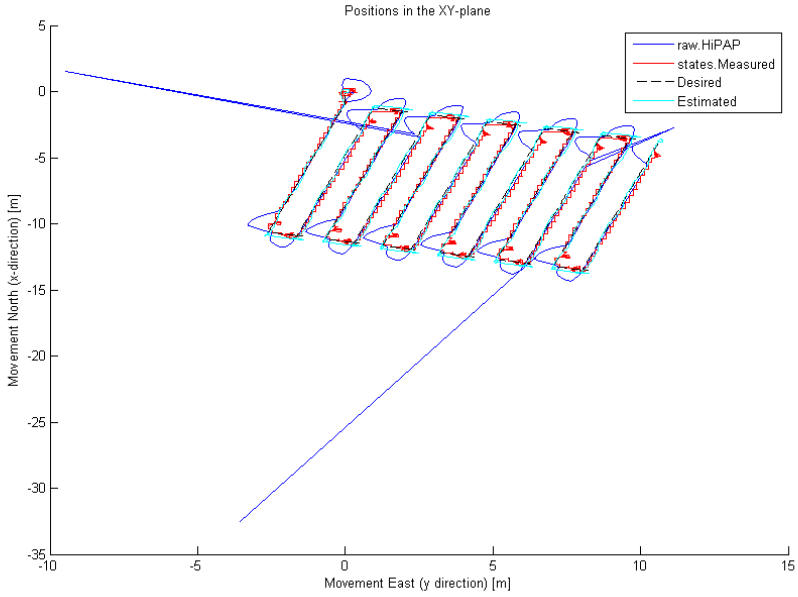


Figure 5.16: The positions the ROV in the north-east plane (from simulations).

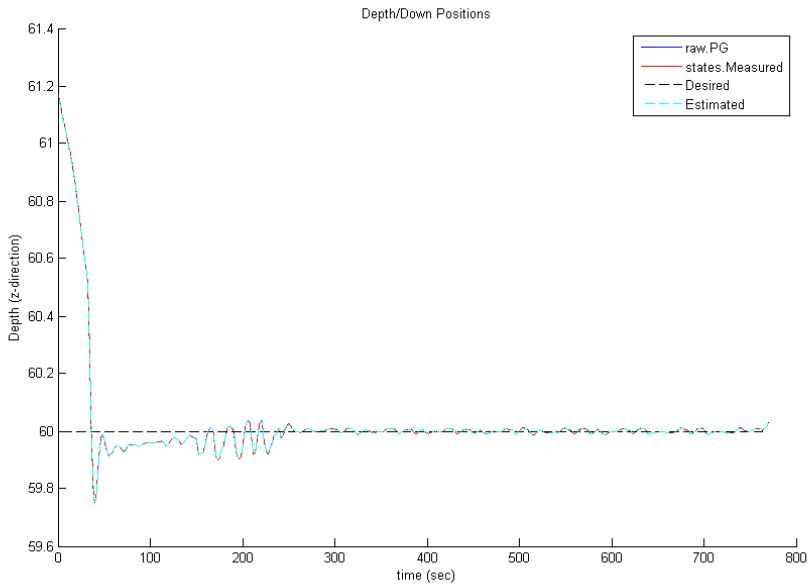


Figure 5.17: The depth of the ROV in the simulations.

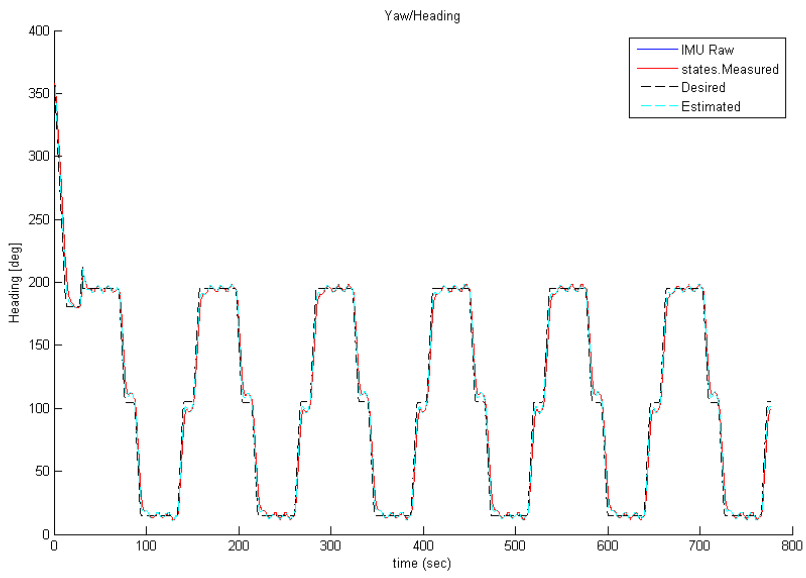


Figure 5.18: The heading of the ROV in the simulations.

5.2.3 Velocities

The velocities in the test run are higher than in the sea trial, and surge velocities will reach values as high as 0.5 m/s. This is still well within the capacities of the ROV, but will lead to larger accelerations and some overshoot.

Figure 5.19 shows the desired velocities in surge and sway. The surge velocity is naturally much larger than in sway as the ROV will try to head in the direction it is moving. The desired velocities clearly show how the speed is supposed to increase to maximum on the stretches, and then will fall to zero when the ROV reaches a corner and prepares to turn.

In Figures 5.20 and 5.21 a noticeable offset between between the raw DVL and measured and estimated states. This is due to the placement of the DVL on the ROV as explained in Section 5.1.3, and is also simulated in the HIL system. The placement of the DVL are also accountable for some of the very large peaks in the sway raw data, as the ROV turning will lead to larger sway velocities in the rear of the vessel.

Surge velocities are seen in Figure 5.20 and it should be noted that the actual velocities are as high as 0.5 m/s, even though the desired values are 0.3 m/s. The peaks in the velocity is the straight parts of the pattern where the ROV can reach high speeds, which then dramatically drops when it needs to do a turn.

The sway velocities in Figure 5.21 are much smaller than in heave, as is to be expected as the ROV is mostly moving forwards and turning. The sway speed is mostly close to the desired values around zero with peaks when the ROV makes a turn, especially in the DVL as mentioned above. Small oscillations below 0.05 m/s occur nearly constantly as the vessel struggles to keep on the desired trajectory.

Figure 5.22 displays the heave velocities of the ROV. The raw DVL-values seem to have been logged wrongly as they do not correspond to the measured or estimated errors. The measured heave velocity is also much higher than the estimated state and changing quickly. As can be seen in Figure 5.17 the position in heave only changes in the early stages of the run, before it stabilizes around 60 meters depth.

The yaw rate shown in Figure 5.23. As with the other yaw plots it shows the ROV having relatively small changes in yaw when following the long straight paths, with relatively quick changes when it reaches a corner.

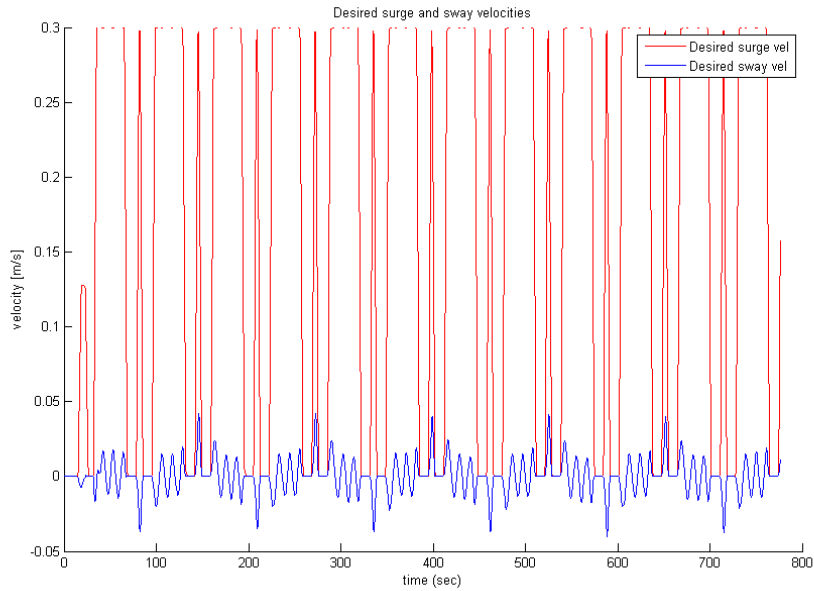


Figure 5.19: The desired velocities in surge and sway in the simulations.

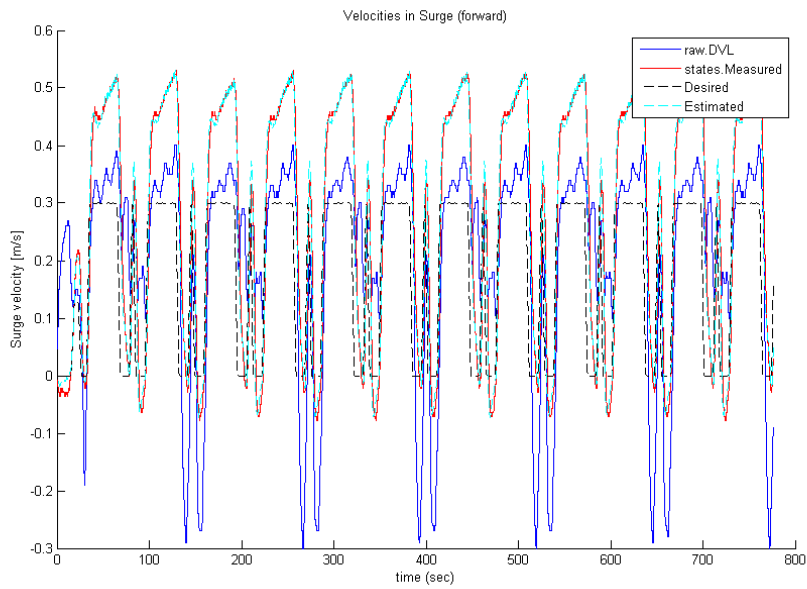


Figure 5.20: The Surge velocities of the ROV in ssimulations.

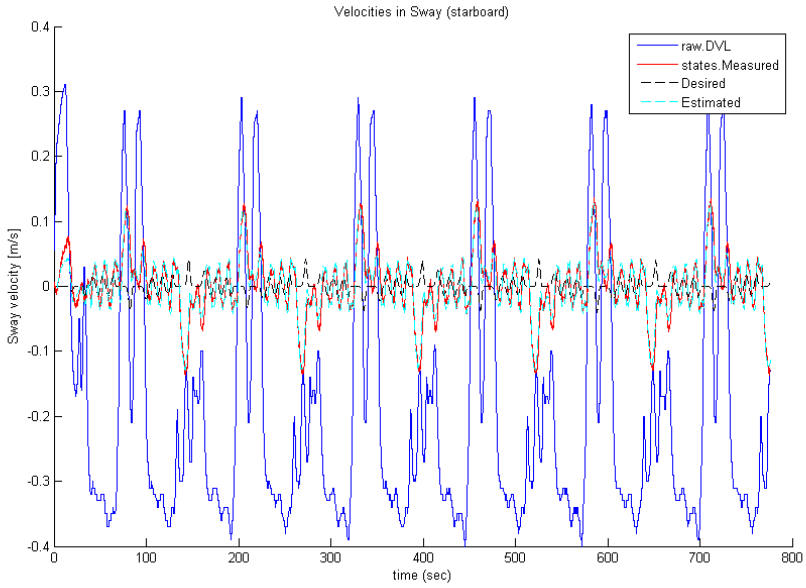


Figure 5.21: The Sway velocities at the simulations.

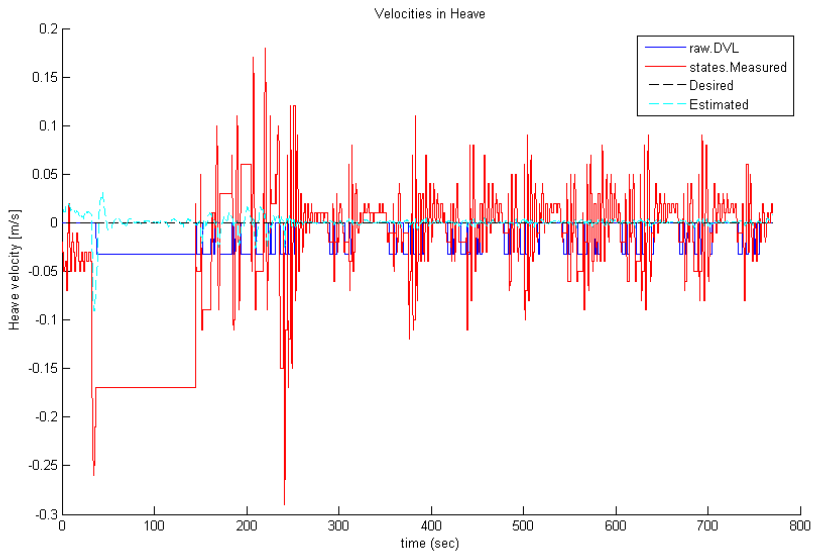


Figure 5.22: Heave velocities at the simulations.

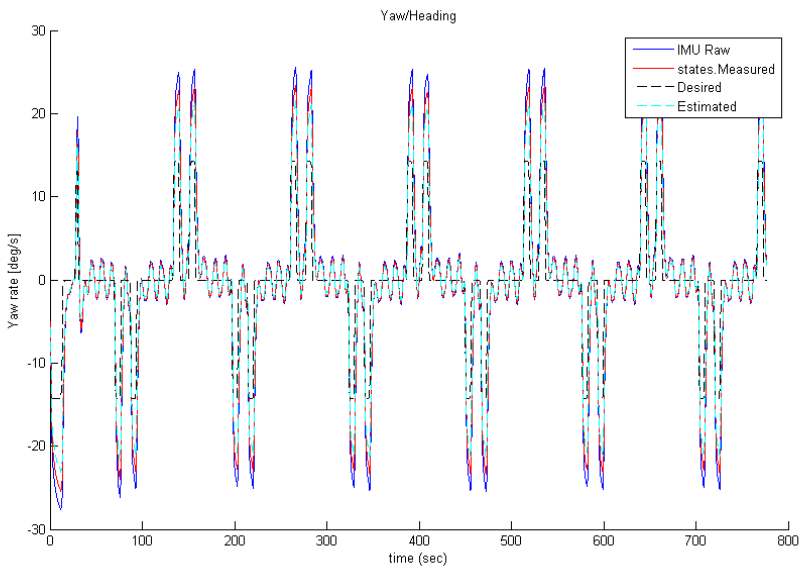


Figure 5.23: Yaw rate from the simulations.

5.2.4 Thrust Forces

The demanded thrust forces from the control system are given in Figure 5.24. The thrust commands in surge and sway seem to correspond well to the velocities given in Figures 5.20 and 5.21, and follows the pattern where forces in surge are large when the ROV is moving along the straight sides of the path, and drops when it needs to make a turn. The surge forces are more oscillatory and smaller than in surge, with some peaks where the ROV makes a turn.

The heave forces are large at first as the ROV needs to be controlled to the correct location, and compared to 5.17 it seems reasonable.

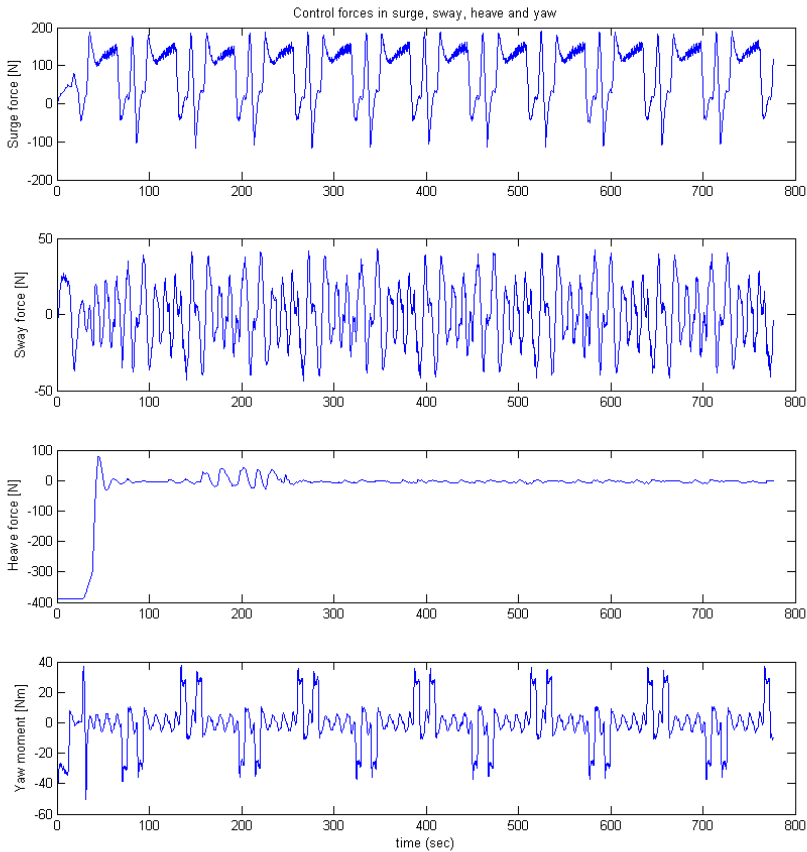


Figure 5.24: Thruster/control forces from the simulations.

5.2.5 Forces on ROV and Umbilical

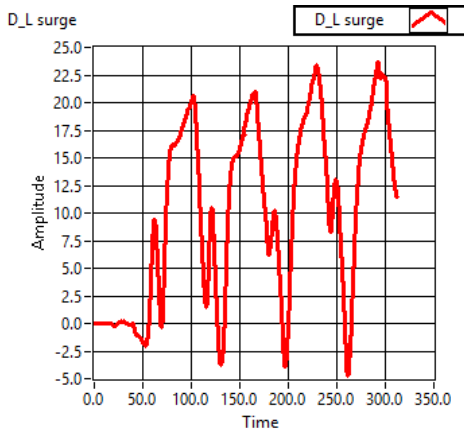
The HIL/SIL simulator allows for graphing the different forces from the environment on the ROV and umbilical. The graphs presented here show the forces from the linear and nonlinear damping as well as forces from the umbilical and the total forces on the ROV. Unfortunately the measurements were cut short and only approximately 5 minutes (300 seconds) were captured.

Figure 5.25 shows the linear damping forces on the ROV given as $\mathbf{D}_L \boldsymbol{\nu}_r$. As expected these results will look very much like the simulated velocities seen in Figures 5.20 and 5.21 in surge and sway directions. This should also apply in heave, but as the heave velocity is uncertain the correlation in Figures 5.22 and 5.25c is difficult to see.

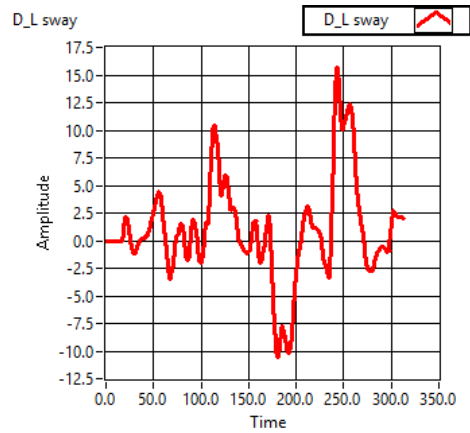
The Nonlinear damping forces given in Figure 5.26 are given as $\mathbf{D}_{NL} |\boldsymbol{\nu}_r| \boldsymbol{\nu}_r$, and also relate closely to the velocities, but the forces are nonlinear and changes much faster, with larger peaks for high speeds and smaller variations for lower speeds. This can be seen easily if the nonlinear damping is compared to the linear damping forces in Figure 5.25.

Umbilical forces ($\boldsymbol{\tau}_{\text{umbilical}}$) are given in Figure 5.27, and are computed using the Morrison equation and rely on the square of the velocity, just like the nonlinear damping. Due to this the forces in surge and sway from the umbilical have the same shape, but different amplitudes than the nonlinear damping forces. The forces on the umbilical are transferred to the ROV, and the connection does not allow transferring forces in yaw and it is assumed the umbilical is slack with no forces in heave. Roll and pitch moments are due to the placement of the umbilical connection on the top of the ROV. Overall it can be seen that the forces from the umbilical are very small compared to the linear and nonlinear damping forces.

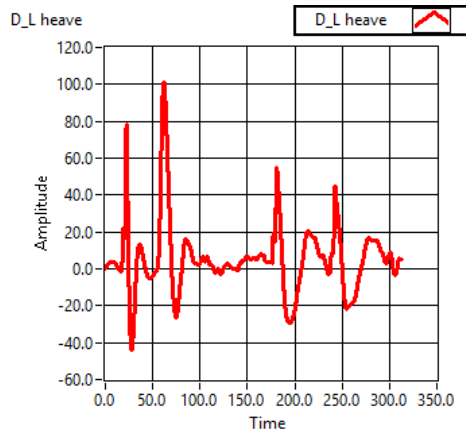
Figure 5.28 shows the total environmental forces working on the ROV in surge, sway and heave, given as $\mathbf{C}_{RB}(\boldsymbol{\nu})\boldsymbol{\nu} + \mathbf{C}_A(\boldsymbol{\nu}_r)\boldsymbol{\nu}_r + \mathbf{D}_L \boldsymbol{\nu}_r + \mathbf{D}_{NL}(\boldsymbol{\nu}_r)\boldsymbol{\nu}_r + \mathbf{g}(\boldsymbol{\eta}) + \boldsymbol{\tau}_{\text{umbilical}}$. If the graphs are compared to the linear damping in Figure 5.25 and nonlinear damping forces in Figure 5.26 it is clear that the damping, especially the nonlinear damping, provide most of the forces acting on the ROV at relatively high velocities.



(a) Linear surge forces on the ROV

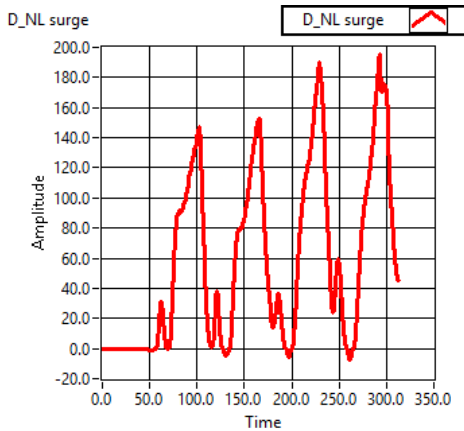


(b) Linear sway forces on the ROV

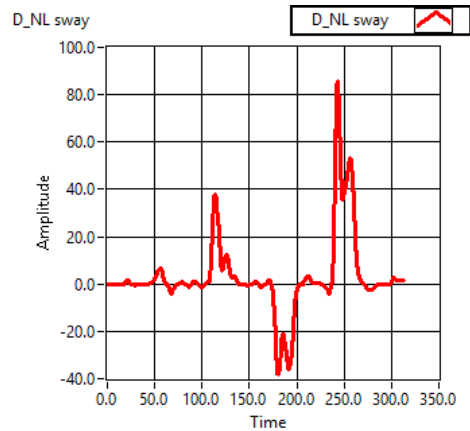


(c) Linear heave forces on the ROV

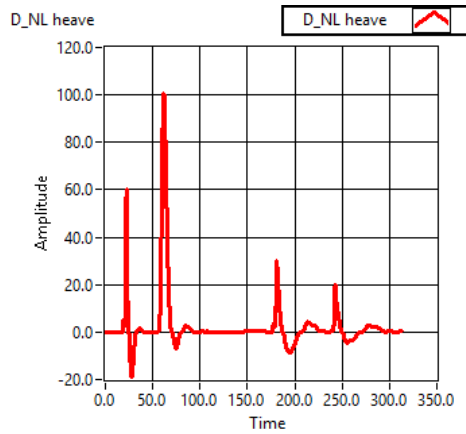
Figure 5.25: Linear damping forces acting on the ROV during simulations. All Amplitudes are forces in Newtons [N].



(a) Nonlinear surge forces on the ROV

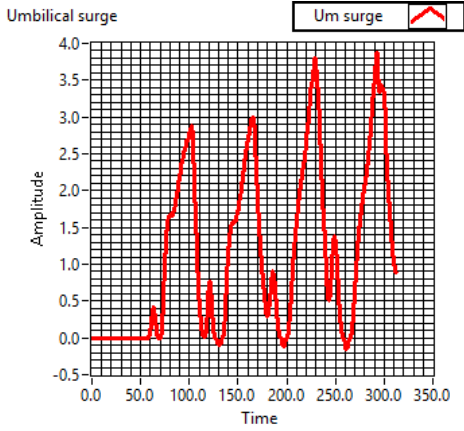


(b) Nonlinear sway forces on the ROV

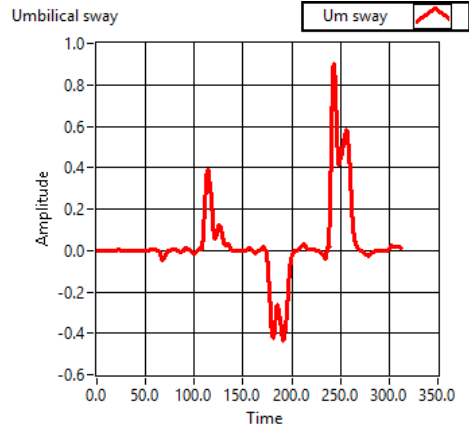


(c) Nonlinear heave forces on the ROV

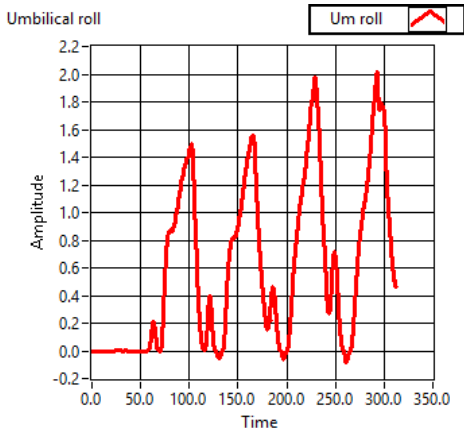
Figure 5.26: Nonlinear damping forces acting on the ROV during simulations. All Amplitudes are forces in Newtons [N].



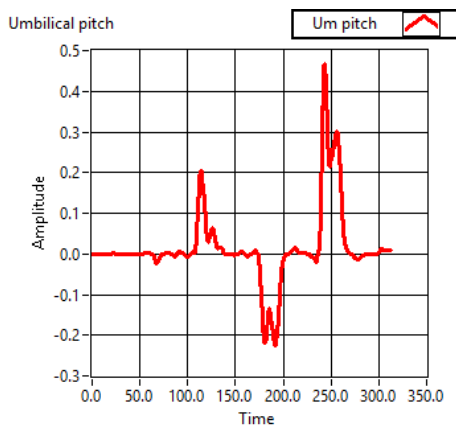
(a) Surge forces on the ROV due to the umbilical



(b) Sway forces on the ROV due to the umbilical

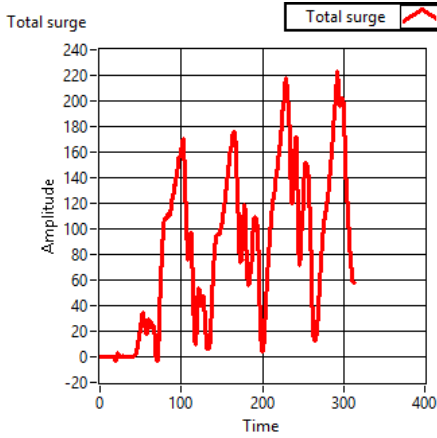


(c) Roll moments on the ROV due to the umbilical

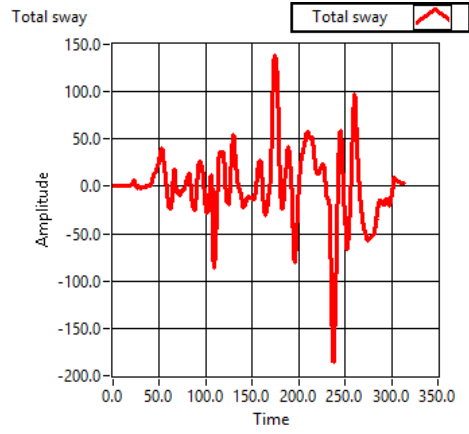


(d) Pitch moments on the ROV due to the umbilical

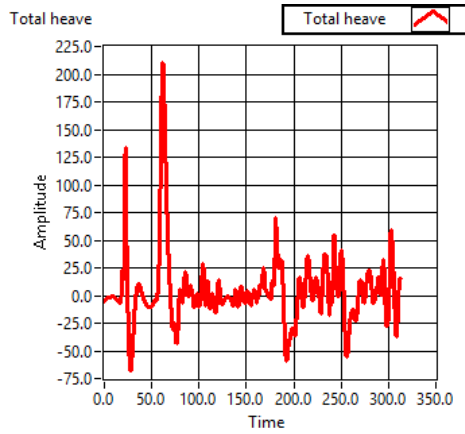
Figure 5.27: Forces acting on the ROV due to the umbilical during simulations. All Amplitudes are forces in Newtons [N] or moments in Newton meters [Nm].



(a) Total surge force on the ROV from the environment



(b) Total sway force on the ROV from the environment



(c) Total heave forces on the ROV from the environment

Figure 5.28: Total environmental forces acting on the ROV during simulations. All Amplitudes are forces in Newtons [N].

5.3 Comparison and Discussion

The simulations in Section 5.2 are based on the real sea trials documented in Section 5.1 to allow for comparisons of the two sets of results. This will be the basis of a discussion of the effectiveness of HIL and SIL testing of control systems.

Desired paths in the sea trial and simulations are very similar. This is due to the original way points being saved when the sea trial were carried out, and the SIL test being based on these data. Thus it is fair to assume the path of the two tests should be very similar. The environmental forces might be a source to errors as no currents were measured or logged during the sea trial, and the assumption that there were nearly no current are based on ROV behavior.

The simulations were run at significantly higher velocities than the sea trials, and this will of course affect the results. The expected behavior of the simulations will include more overshoot and faster accelerations than the sea trials, but all values should be well within what the ROV can handle. The difference in velocity will regardless be a source of differences between the two tests.

The ROV's positions in the two cases are seen in Figures 5.2, 5.3, 5.14 and 5.15. The results from the SIL simulations show that the HiPAP in surge and sway register higher overshoot than the measured states. This is somewhat present in the sea trial results as well, but less visible as the axis in the graph is longer and the overshoot smaller. Some of the overshoot in the simulated results are due to an inaccuracy in the desired path which can be seen in the corners in the path of Figure 5.13, and some of it might be related to the simulated placement of the HiPAP in the rear of the vessel. The path of the ROV in the north-east plane seen in Figures 5.4 and 5.16 shows that the path following of both sea trials and simulations seem to be quite good, and the wild points in both results are clearly visible.

The results in Figure 5.5 and 5.17 show the heave position and reveal a large difference between the sea trial and simulations. This is due to the sea trial being conducted over a wreck and changing the desired depth during the run to keep a constant altitude, something not captured in the SIL simulation.

Heading/yaw angle in the two runs are found in Figures 5.6 and 5.18 and corresponds very well with each other, as well as following the given references closely.

As mentioned the velocities in the two runs are different, and this can be seen in Figures 5.7 and 5.19, where the desired surge velocity of the sea trial has a maximum value of 0.1 m/s while the simulation goes all the way to 0.3 m/s. Due to this difference in values it is difficult to compare the values of the velocity graphs, but the shape should be the same.

The velocity plots for surge are given in Figures 5.8 and 5.20. The most notable thing is that both plots contain higher surge values than is desired, often as much as 0.2 m/s more. Thus it can be assumed that the fault might be in the control system rather than the HIL system as the faults appears in both sea trials and

simulations. The general shape of the surge speeds are also similar, even though the simulation speed does not settle in turns as it does in the sea trial. The HiPAP signal behaves the same way in both cases, with much larger values than the measured and estimated signals.

Sway velocities in Figures 5.9 and 5.21 also show the same behavior with similar shapes but different values. Both figures clearly show the sudden rise of velocities due to the turns and a constant offset of the HiPAP due to its placement on the ROV. The heave has not been given much attention in this simulation, and the heave velocities are nearly impossible to compare as they behave completely differently.

The yaw rates, like the yaw angles, behave in the same way as can be seen in Figures 5.11 and 5.23. The velocities are small when the ROV is moving forward with some small disturbances to keep the right heading, and rise to peaks in the corners when the vessel has to turn 90 degrees.

Control forces for sea trials and simulations are presented in Figures 5.12 and 5.24. The thrusts are of course influenced by the velocity of the ROV as some of the environmental forces are relative to the squared velocity (nonlinear damping etc.). Thus the forces in surge have larger values for a longer period of time in the simulated results than in the sea trial. Otherwise the forces in surge, sway and yaw moment seem to follow approximately the same pattern, but as with the other results the heave forces are quite different in the two cases.

5.4 Additional Simulations

To test the HIL simulator with added forces from current and waves additional simulations are run. These tests have no saved data from sea trials to compare with, but should provide some information about the usefulness of the HIL system when more noise and environmental forces are included.

During the following tests both high currents in the water and waves are used. The ROV is positioned close to the surface to be affected by the waves, which have an amplitude of 1 meter and a 5 second period, and thus affecting the ROV. The currents are set as 0.3 m/s northwards, and 0.2 m/s westwards. The sensor noise and update rate of the HiPAP is made significantly worse than in the previous simulation run to see the system's behavior during bad conditions.

The first part of the test lasts for 140 seconds and is focused on the ROV keeping a steady position in DP mode. After 140 second the ROV is given a new desired position approximately 11 meters north and 0.3 meter west. After reaching this point the ROV returns to station keeping and tries to hold the new position. Only the horizontal movement is logged and given here.

Positions are seen in Figures 5.29 and 5.30. Due to small movements early in the run the positions in the north-east plane given in Figure 5.31 are not reliable, as the

time-scale is not shown. As can be seen from the plots of the north and east position the ROV struggles to keep the desired positions and there are small oscillations in both north and east directions. Both the raw HiPAP signal and measured positions show a larger sampling period than in the previous test, and in surge it can be seen that the vessel is having a hard time following the desired position when moving. No wild points were recorded during this simulation, which is probably related to the test spanning a relatively short period of time (just over 4 minutes, 250 seconds) and probability (the wild points will on average appear approximately every 4th minute). The observer seems aware of the bad sensor performance and decide to rely more on the mathematical model than the sensors, meaning the estimated states are closer to the desired than the measured states when the ROV is moving. When the ROV reaches the new desired position after the move a quite larger overshoot is apparent, possibly due to the strong current.

Oscillations is also present in the velocities shown in Figures 5.33 and 5.34 where the velocities are changing as well as being affected by noise from the sensors. The thrust forces found in Figure 5.36 corresponds well to the velocities, but it is worth noting the large amount of thrust used at approximately 210 seconds when the ROV has reached it's new desired position and needs to slow down. This is complicated by the relatively large current northwards and all available thrust backwards is used to slow the vessel down. This is not completely successful, as can be seen in the surge velocities in Figure 5.33 that never settles at zero. The ROV overshoots the target and has to fight to come back to the right positions.

The heading angle is 45 degrees during the first DP operation, and then turns to approximately 0 degrees to face north during the moving operation. As can be seen in Figures 5.32, 5.35 and 5.36 the heading is subject to constant oscillations and large changes in yaw rate, and the control system is constantly fighting using commanded thrust forces to keep the desired angle. The plot of the heading looks worse than it is as the vessel heading oscillated around 0 deg and all values are given from 0 to 360 degrees, thus provoking sudden jumps in the plots.

The overall performance of the control system can still be considered to be quite good, but it is obvious it is struggling more to keep the constant positions with large environmental forces as well as more sensor noise. This simulation also seems to have more in common with the behavior of the signals from the sea trial in Section 5.1 and it is fair to assume the simulation in Section 5.2 were too kind with too little sensor noise and other disturbances.

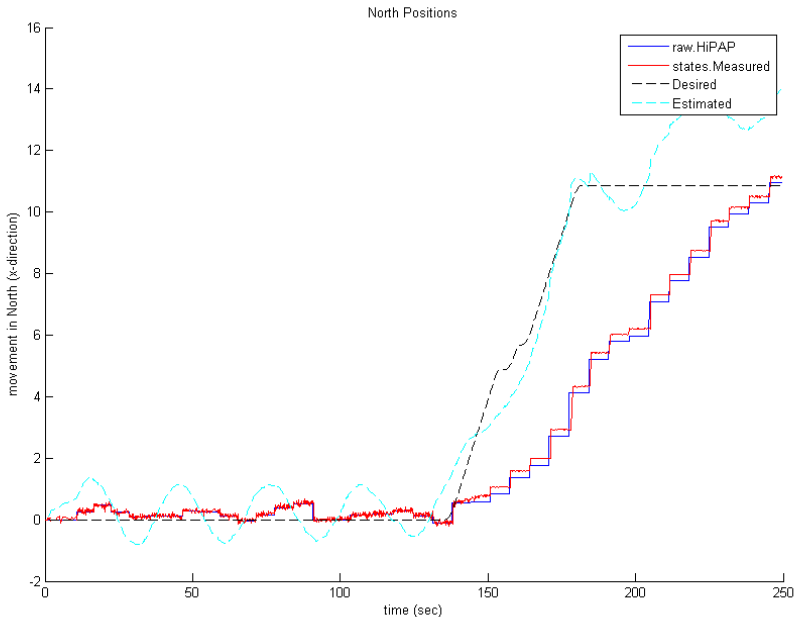


Figure 5.29: North position in a simulated DP and path following operation.

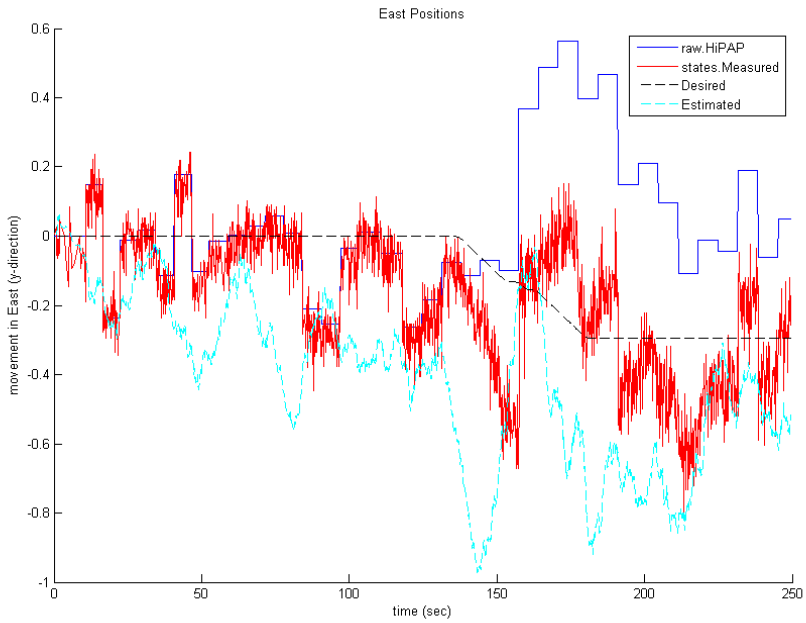


Figure 5.30: East position in a simulated DP and path following operation.

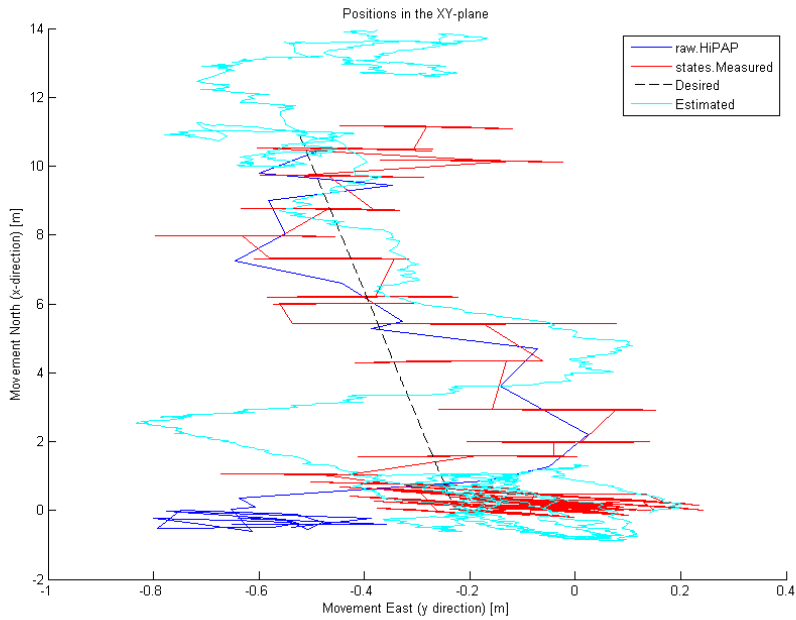


Figure 5.31: Position in the North-East plane in a simulated DP and path following operation.

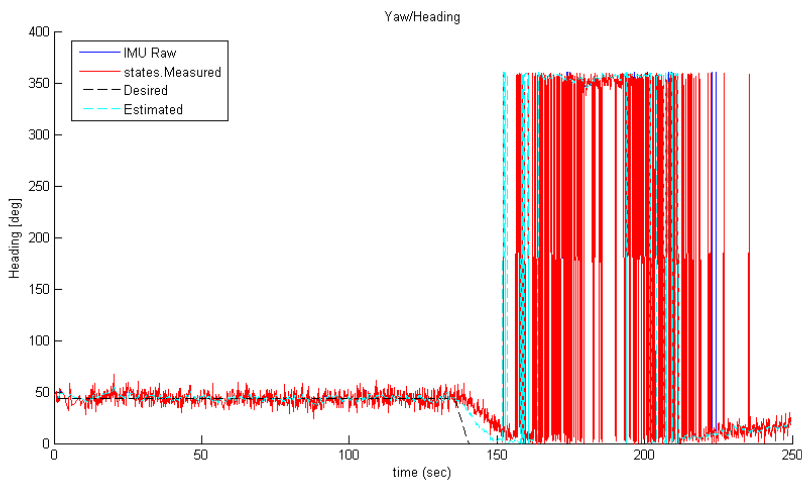


Figure 5.32: Heading in a simulated DP and path following operation.

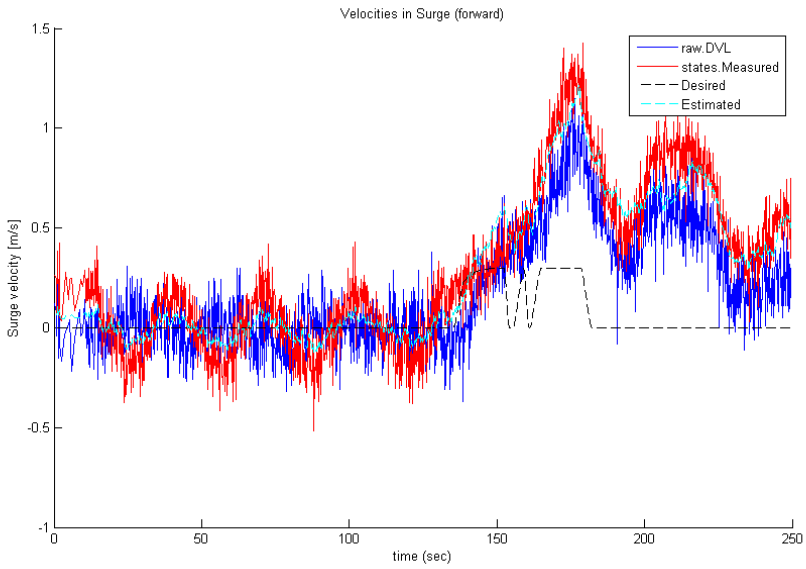


Figure 5.33: Surge velocity in a simulated DP and path following operation.

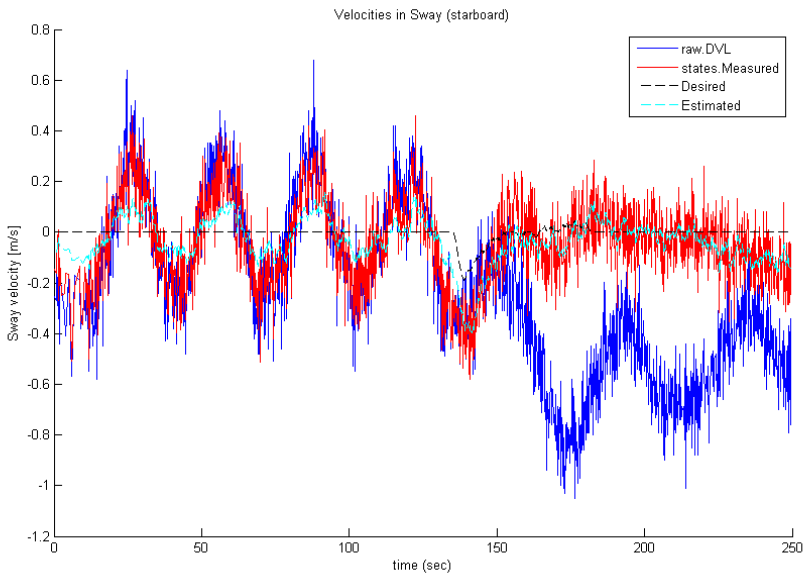


Figure 5.34: Sway velocity in a simulated DP and path following operation.

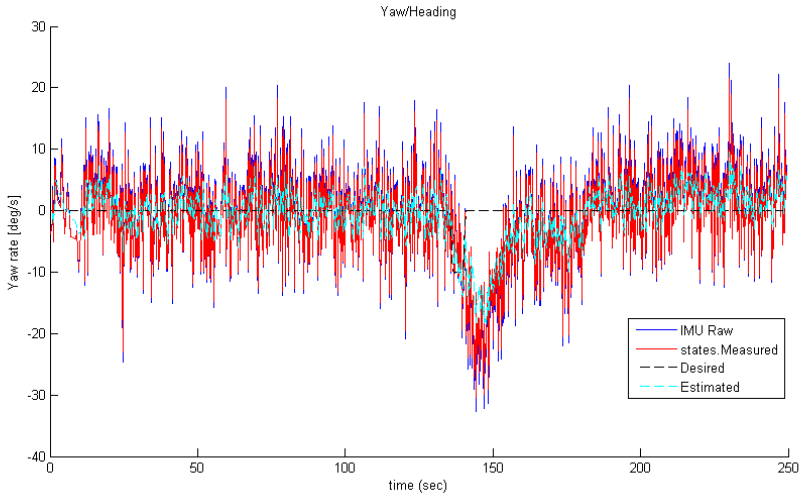


Figure 5.35: Yaw rate in a simulated DP and path following operation.

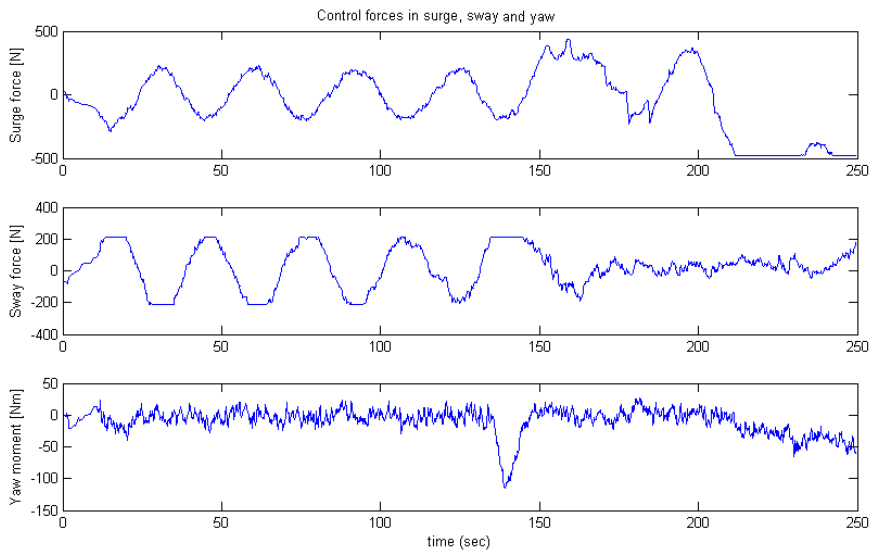


Figure 5.36: Thrust forces in a simulated DP and path following operation.

Chapter 6

Conclusions and Further Work

This chapter contains a brief conclusion based on the work done in this thesis. Suggestions for further work to improve the HIL and control systems will also be included.

6.1 Conclusions

The main goal of this thesis was to improve the functionality and usability of a HIL system and to describe the different areas of use and theoretical structure of a HIL system.

The first largest change to the system consists of the addition of SIL functionality. This saves time for students and other users of the system, and have increased the number of people capable of using the simulation system at the same time. This will hopefully prove beneficial to the future use and development of ROV control systems at NTNU as readily available testing is an important part of software development.

Sensors are an important part of the feedback control of an ROV, and the HIL simulator therefore needs to replicate the signals as closely as possible to create a realistic simulation environment. The implementation of sensor models capable of generating signals have thus improved the quality of the overall HIL system and made it more suited for testing robustness in a control system.

Model parameters determine the ROV's reaction to the different forces acting on it, and thus accurate and updated models are an essential part of a good simulator system. The different modeling parameters discussed are examples of data sets used for control purposes today. To be able to easily change the input parameters

of the ROV model in a HIL system will make it more suitable for different vessels, as well as allowing for small changes in the values for a single vessel, for example after installations of a new sensor that affects the mass. To further enable testing of control system robustness a modeling error is introduced, allowing users to add a random multiplicative error to their models. The addition of the vessel model in the main user interface has made the changing of modeling parameters much easier, and the user needs less knowledge of the system structure.

Umbilical forces are introduced to better simulate the actual forces working on the ROV in submerged operations. These forces act in surge and sway, and introduce moments in pitch and roll. Simulation results show these forces to be much smaller than the actual environmental forces and restoring forces acting on the ROV directly.

Both sea trials and simulations were performed on the ROV Minerva to verify the similarities and differences between real measured and simulated testing. The results show that the HIL simulator is capable of producing results close to that of a real sea trial if the conditions are correct. To provide simulations close to the real life tests both sensor noise and some environmental forces from waves and current should be included. When this is done the output from the simulator should be enough to accurately test the functionality and performance of a control system.

6.2 Recommendations for Further Work

The HIL system still lacks functionality to be complete, and many parts of the simulator are still missing. Implementing features to allow failure testing should be carried out. This includes making an FMEA for the control system and trying to implement the most common and critical errors in the HIL system to be able to test these.

Several new modules could be added to the HIL system to improve testing. These include a power management system and power supply. These are generally supplied from the surface vessel and power consumption is generally not a large problem in an ROV, but to make the testing system complete these features should be implemented. This will also make the testing system more versatile and suitable for e.g. AUVs.

A complete modeling of the thrusters and propellers should also be done. Today this is carried out by a simple mapping from shaft speed given from the control system to forces in the different degrees of freedom. Including models for important phenomena such as rise time and thrust loss will improve the realism of the HIL simulations.

The structure and design of the HIL system does not follow any strict conventions such as object orientation, and this is something that might be considered

a weakness. To improve this a complete rework of the system might be required, but the individual components should be reusable in a new implementation. A full documentation of the system is also lacking.

The control system Njord also contains areas which might be improved. An example of this is functions to receive raw data from the GPS and HiPAP systems and process these to get the needed positions, a task that is performed by the Navipac today. The HIL system is already set up to send these strings.

To improve the model parameters and get more realistic models for use in both simulations and control systems tests needs to be performed on the ROVs to determine their current hydrodynamic properties. They should also be weighed to determine the correct mass both before and after a sea trial.

Bibliography

- [1] Ø. Smogeli. Third party hil testing of control system software. Guest Lecture at NTNU, September 2013.
- [2] E. Tolpinrud. Development and implementation of computer-based control system for rovs with experimental results. Master's thesis, NTNU, 2012.
- [3] V. Berg. Development and commissioning of a dp system for rovs sf 30k. Master's thesis, NTNU, 2012.
- [4] International Maritime Organization. Guidelines for vessels with dynamic positioning systems. Standard IMO MSC Circular 645, 1994.
- [5] J. R. Sklaroff. Redundancy management technique for space shuttle computers. *IBM Journal of Research and Development*, 20:20–28, 1976.
- [6] A. L. Hopkins, Jr. Software issues in redundant sequential control. *IEEE Transaction on Industrial Electronics*, 29:273–278, 1982.
- [7] D. Maclay. Simulation gets into the loop. *IEE Review*, 43:109–112, 1997.
- [8] N. Schetinin, N. Moriz, B. Kumar, A. Maier, S. Faltinski, and O. Niggemann. Why do verification approaches in automation rarely use hil-test? *Industrial Technology (ICIT), 2013 IEEE International Conference on*, 1:1428–1433, 2013.
- [9] K. Lamberg. Systematic testing - modern solutions for hardware-in-the-loop-simulations. In *Automotive Electronics*, September 2002.
- [10] IEEE. Ieee 1012 standard for system and software verification and validation. IEEE Standard, 2012.
- [11] L. Pivano and Ø. Smogeli. Independent hil testing of dp systems - a life-cycle perspective. In *First Brazilian Conference on Dynamic Positioning*, April 2013.
- [12] ABS. Guide for systems verification (including hardware-in-the-loop and software-in-the-loop). Guide, 2012.

- [13] DNV. Standard for certification no. 2.24: Hardware in the loop testing. Standard for Certification, 2011.
- [14] DNV. Rules for classification of ships pt. 6 ch. 22: Enhanced system verification. Rules for Classification of Ships, 2013.
- [15] DNV. First ever hardware in the loop test certificate. http://www.dnv.com/resources/publications/dnv_forum/2006/no_2/firsteverhardwareinthelooptestcertificate.asp, August 2006. [visited: 2014-03-19].
- [16] T. I. Fossen. *Handbook of Marine Craft Hydrodynamics and Motion Control*. Wiley, Chichester, UK, 2011.
- [17] T. I. Fossen. *Marine Control Systems - Guidance, Navigation, and Control of Ships, Rigs and Underwater Vehicles*. Marine Cybernetics, Trondheim, Norway, 2002.
- [18] A. J. Sørensen. *Marine Control Systems - Propulsion and Motion Control of Ships and Ocean Structures*. Dept. of Marine Technology, NTNU, Trondheim, Norway, 2013.
- [19] T. A. Johansen, T. I. Fossen, and B. Vik. Hardware-in-the-loop testing of dp systems. In *Dynamic Positioning Conference*, November 2005.
- [20] M. Kirkeby. Comparison of controllers for dynamic positioning and tracking of rov minerva. Master's thesis, NTNU, 2010.
- [21] O. M. Faltinsen. *Sea Loads on Ships and Offshore Structures*. Cambridge University Press, Cambridge, UK, 1990.
- [22] DNV. Dnv-rp-d102 failure mode and effect analysis (fmea) of redundant systems. Recommended Practice, 2012.
- [23] National Instruments. What is ni compactrio - national instruments. <http://sine.ni.com/np/app/main/p/ap/global/lang/no/pg/1/sn/n24:cRIO/fmid/102/>. [visited: 2013-11-27].
- [24] M. Andresen, M. Ludvigsen, and Ø. T. Ødegaard. Sammenfatning av hydrodynamiske forsøk med roven minerva. Report from test, NTNU, April 2006. Summary of previous tests.
- [25] M. Kirkeby. Dynamic positioning of rov minerva. Project Thesis, NTNU, 2010.
- [26] M. Andresen, M. Ludvigsen, and Ø. T. Ødegaard. Slepeforsøk av modell for å bestemme cd -koeffisient. Report from test, NTNU, November 2003. Report from 1:5 scale test of Minerva's drag coefficient.
- [27] M. Ludvigsen and Ø. T. Ødegaard. Slepeforsøk modell cd-koeffisient i alle vinkler. Report from test, NTNU, December 2003. Report from 1:5 scale test of Minerva's drag coefficient.

- [28] Wikipedia. Transmission control protocol. http://en.wikipedia.org/wiki/Transmission_Control_Protocol. [visited: 2014-05-10].
- [29] Kongsberg Maritime. Hipap500 brochure. [http://www.km.kongsberg.com/ks/web/nokbg0397.nsf/AllWeb/1B58E93D7B3A1061C1256C370047D8D7/\\$file/164508ad_HiPAP500_Brochure_lr.pdf?OpenElement](http://www.km.kongsberg.com/ks/web/nokbg0397.nsf/AllWeb/1B58E93D7B3A1061C1256C370047D8D7/$file/164508ad_HiPAP500_Brochure_lr.pdf?OpenElement), October 2003. [visited: 2014-04-16].
- [30] J. Oyen. Gps - nmea sentence information. <http://aprs.gids.nl/nmea/#gga>, July 2001. [visited: 2014-05-03].
- [31] EIVA. The kongsberg nmea format \$psimssb. <http://kb.eiva.dk/Knowledgebase/Article/10223>. [visited: 2014-05-03].
- [32] Valeport. miniips intelligent pressure sensor. <http://www.valeport.co.uk/Products/OceanEngineering/OceanEngineeringProductDetails/ProductID/24>, June 2013. [visited: 2014-04-16].
- [33] Xsens. Mti-100 series. <http://www.xsens.com/products/mti-100-series/>, April 2014. [visited: 2014-04-16].
- [34] Teledyne RDI. Rdi's doppler velocity log. <http://www.rdinstruments.com/navigator.aspx>, July 2013. [visited: 2014-04-16].
- [35] NTNU - Marine Sciences and Technology. Rov minerva spesifications - ntnu. <http://www.ntnu.edu/marine/minerva/spesifications>. [visited: 2013-11-25].

Appendix A

Parameters for NTNU's ROVs

This appendix contains some of the parameters used to model NTNU's ROVs as described in Chapter 3.

A.1 Minerva: Kirkeby

The models are developed and used by Marianne Kirkeby in her Project [25] (spring 2010) and Master [20] (fall 2010) Thesis. There are some small changes such as the weight of the ROV in the two version, and both models will be given here. The Master model is probably the most trustworthy as it is the most developed and tested.

A.1.1 Master model

The following characteristics are used for the ROV Minerva:

- Weight: 460 kg (lowest measured mass - before sea trial - after sea trial weight increases to approx. 475 kg)
- $l = 1.44$ m, $b = 0.82$ m, $h = 0.80$ m
- CoG: $r_G = [0 \ 0 \ 0.12]^\top$, CoB: $r_B = [0 \ 0 \ -0.15]^\top$
- Buoyancy: 5 N

$$\mathbf{M}_{RB} = \begin{bmatrix} 460 & 0 & 0 & 0 & 55.2 & 0 \\ 0 & 460 & 0 & -55.2 & 0 & 0 \\ 0 & 0 & 460 & 0 & 0 & 0 \\ 0 & -55.2 & 0 & 111.9 & 0 & 0 \\ 55.2 & 0 & 0 & 0 & 110.6 & 0 \\ 0 & 0 & 0 & 0 & 0 & 50.3 \end{bmatrix} \quad (\text{A.1})$$

$$\mathbf{M}_A = \begin{bmatrix} 293 & 0 & 0 & 0 & 0 & 0 \\ 0 & 302 & 0 & 0 & 0 & 0 \\ 0 & 0 & 326 & 0 & 0 & 0 \\ 0 & 0 & 0 & 52 & 0 & 0 \\ 0 & 0 & 0 & 0 & 52 & 0 \\ 0 & 0 & 0 & 0 & 0 & 57 \end{bmatrix} \quad (\text{A.2})$$

$$\mathbf{D}_{NL}(\boldsymbol{\nu}_r) = \begin{bmatrix} 292|u_r| & 0 & 0 & 0 & 0 & 0 \\ 0 & 584|v_r| & 0 & 0 & 0 & 0 \\ 0 & 0 & 635|w_r| & 0 & 0 & 0 \\ 0 & 0 & 0 & 84|p| & 0 & 0 \\ 0 & 0 & 0 & 0 & 148|q| & 0 \\ 0 & 0 & 0 & 0 & 0 & 1|r| \end{bmatrix} \quad (\text{A.3})$$

$$\mathbf{D}_L = \begin{bmatrix} 29 & 0 & 0 & 0 & 0 & 0 \\ 0 & 41 & 0 & 0 & 0 & 0 \\ 0 & 0 & 254 & 0 & 0 & 0 \\ 0 & 0 & 0 & 34 & 0 & 0 \\ 0 & 0 & 0 & 0 & 59 & 0 \\ 0 & 0 & 0 & 0 & 0 & 0.2 \end{bmatrix} \quad (\text{A.4})$$

However, some modifications are made in the process plant model in Kirkeby's Master: instead of the standard $\tau_{DL} = \mathbf{D}_L \boldsymbol{\nu}$ she introduces a new model for the linear damping in surge and sway based on the nonlinear damping:

$$\begin{aligned} \tau_{DL,mod}(1) &= 0.8 \mathbf{D}_{NL}(1,1) \cdot e^{-2u_r^2} \cdot u_r, \quad u_r > 0 \\ \tau_{DL,mod}(1) &= 0.8 \mathbf{D}_{NL}(1,1) \cdot e^{-u_r^2} \cdot u_r, \quad u_r < 0 \\ \tau_{DL,mod}(2) &= 0.5 \mathbf{D}_{NL}(2,2) \cdot e^{-8v_r^2} \cdot v_r \end{aligned} \quad (\text{A.5})$$

The drag from the cable is found using Morrison's equation:

$$\boldsymbol{\tau}_{\text{umbilical}} = \begin{bmatrix} -a \int_0^h \frac{1}{2} \rho C_d |u_r| u_r dz \\ -a \int_0^h \frac{1}{2} \rho C_d |v_r| v_r dz \\ 1.2 \cdot w_{\text{cable}} \cdot h \\ x_{\text{arm}} \cdot \tau_{\text{cable}}(1) \\ y_{\text{arm}} \cdot \tau_{\text{cable}}(2) \\ 0 \end{bmatrix} \quad (\text{A.6})$$

With $a = 0.5$ (if current not dependent on depth), $w_{\text{cable}} = -2.83 \cdot 10^{-3}$ kg/m, and $C_d = 1.2$, $x_{\text{arm}} = y_{\text{arm}} = 0$ and $z_{\text{arm}} = 0.52$ m. z_{arm} is the distance from the center to the attachment of the arm. The diameter of the umbilical is 0.022 m (or 0.019 m according to [35]).

The umbilical is assumed to be neutral in heave: $w_{\text{cable}} \approx 0$ (at 500 meter depth it provides a lift of less than 2 N - much less than the buoyancy uncertainty).

A.1.2 Project model

- Weight: 475 kg
- $l = 1.44$ m, $b = 0.82$ m, $h = 0.80$ m
- CoG: $r_G = [0 \ 0 \ 0.12]^\top$, CoB: $r_B = [0 \ 0 \ -0.15]^\top$
- Buoyancy: 50 N (disputed: Minerva might sink when thrusters are off after sea trials)

$$\boldsymbol{M}_{RB} = \begin{bmatrix} 475 & 0 & 0 & 0 & 5700 & 0 \\ 0 & 475 & 0 & -5700 & 0 & 0 \\ 0 & 0 & 475 & 0 & 0 & 0 \\ 0 & -5700 & 0 & 68509 & 0 & 0 \\ 5700 & 0 & 0 & 0 & 68507 & 0 \\ 0 & 0 & 0 & 0 & 0 & 52 \end{bmatrix} \quad (\text{A.7})$$

$$\boldsymbol{M}_A = \begin{bmatrix} 293 & 0 & 0 & 0 & 0 & 0 \\ 0 & 302 & 0 & 0 & 0 & 0 \\ 0 & 0 & 326 & 0 & 0 & 0 \\ 0 & 0 & 0 & 52 & 0 & 0 \\ 0 & 0 & 0 & 0 & 52 & 0 \\ 0 & 0 & 0 & 0 & 0 & 57 \end{bmatrix} \quad (\text{A.8})$$

$$\mathbf{D}_{NL}(\boldsymbol{\nu}_r) = 0.3 \begin{bmatrix} 292|u_r| & 0 & 0 & 0 & 0 & 0 \\ 0 & 584|v_r| & 0 & 0 & 0 & 0 \\ 0 & 0 & 635|w_r| & 0 & 0 & 0 \\ 0 & 0 & 0 & 84|p| & 0 & 0 \\ 0 & 0 & 0 & 0 & 148|q| & 0 \\ 0 & 0 & 0 & 0 & 0 & 1|r| \end{bmatrix} \quad (\text{A.9})$$

$$\mathbf{D}_L = 0.3 \begin{bmatrix} 300 & 0 & 0 & 0 & 0 & 0 \\ 0 & 600 & 0 & 0 & 0 & 0 \\ 0 & 0 & 600 & 0 & 0 & 0 \\ 0 & 0 & 0 & 100 & 0 & 0 \\ 0 & 0 & 0 & 0 & 100 & 0 \\ 0 & 0 & 0 & 0 & 0 & 1 \end{bmatrix} \quad (\text{A.10})$$

0.3 is due to an assumed reduction of 70% to get better consistency with measurements from full scale tests.

The umbilical forces are given in the same way as a mooring line in position mooring (PM):

$$\boldsymbol{\tau}_{cd} = -\mathbf{K}_{cd}(\boldsymbol{\eta} - \boldsymbol{\eta}_{cd}) \quad (\text{A.11})$$

Where $\boldsymbol{\eta}_{cd}$ is the umbilical end point (typically the surface vessel), and \mathbf{K}_{cd} is the cable drag matrix:

$$\mathbf{K}_{cd} = \begin{bmatrix} 0.3 & 0 & 0 & 0 & 0 & 0 \\ 0 & 0.3 & 0 & 0 & 0 & 0 \\ 0 & 0 & 0.12 & 0 & 0 & 0 \\ 0 & 0 & 0 & 0.12 & 0 & 0 \\ 0 & 0 & 0 & 0 & 0 & 0 \\ 0 & 0 & 0 & 0 & 0 & 0 \end{bmatrix} \quad (\text{A.12})$$

A.2 Minerva: Daniel de Almeida Fernandes

The models used in the current control systems are based on the same number material used by Kirkeby in her Master. These numbers have been used by PhD student Daniel de Almeida Fernandes to develop some models for his control needs.

Overall dimensions=[height=0.80m, width=0.82m, length=1.44m]

Buoyancy: 5N

Center of buoyancy = [0m, 0m, -0.12m]

Center of gravity = [0m, 0m, 0.15m]

A.2.1 Data set 1

This data set is very closely related to Kirkeby's Master, except the rigid body mass matrix is diagonal and a rather different Linear damping matrix.

$$M_{RB} = \begin{bmatrix} 460 & 0 & 0 & 0 & 0 & 0 \\ 0 & 460 & 0 & 0 & 0 & 0 \\ 0 & 0 & 460 & 0 & 0 & 0 \\ 0 & 0 & 0 & 105.26 & 0 & 0 \\ 0 & 0 & 0 & 0 & 104.02 & 0 \\ 0 & 0 & 0 & 0 & 0 & 50.31 \end{bmatrix} \quad (\text{A.13})$$

$$M_A = \begin{bmatrix} 293 & 0 & 0 & 0 & 0 & 0 \\ 0 & 302 & 0 & 0 & 0 & 0 \\ 0 & 0 & 326 & 0 & 0 & 0 \\ 0 & 0 & 0 & 52 & 0 & 0 \\ 0 & 0 & 0 & 0 & 52 & 0 \\ 0 & 0 & 0 & 0 & 0 & 57 \end{bmatrix} \quad (\text{A.14})$$

$$D_{NL}(\nu_r) = \begin{bmatrix} 292|u_r| & 0 & 0 & 0 & 0 & 0 \\ 0 & 584|v_r| & 0 & 0 & 0 & 0 \\ 0 & 0 & 635|w_r| & 0 & 0 & 0 \\ 0 & 0 & 0 & 84|p| & 0 & 0 \\ 0 & 0 & 0 & 0 & 148|q| & 0 \\ 0 & 0 & 0 & 0 & 0 & 100|r| \end{bmatrix} \quad (\text{A.15})$$

$$D_L = \begin{bmatrix} 233.6 & 0 & 0 & 0 & 0 & 0 \\ 0 & 292 & 0 & 0 & 0 & 0 \\ 0 & 0 & 64 & 0 & 0 & 0 \\ 0 & 0 & 0 & 16 & 0 & 0 \\ 0 & 0 & 0 & 0 & 30 & 0 \\ 0 & 0 & 0 & 0 & 0 & 25 \end{bmatrix} \quad (\text{A.16})$$

A.2.2 Data set 2

These numbers are very similar to both Data set 1 and Kirkeby's master (only last element of linear damping and rigid body mass matrix being different).

$$\mathbf{M}_{RB} = \begin{bmatrix} 460 & 0 & 0 & 0 & 0 & 0 \\ 0 & 460 & 0 & 0 & 0 & 0 \\ 0 & 0 & 460 & 0 & 0 & 0 \\ 0 & 0 & 0 & 105.26 & 0 & 0 \\ 0 & 0 & 0 & 0 & 104.02 & 0 \\ 0 & 0 & 0 & 0 & 0 & 50.31 \end{bmatrix} \quad (\text{A.17})$$

$$\mathbf{M}_A = \begin{bmatrix} 293 & 0 & 0 & 0 & 0 & 0 \\ 0 & 302 & 0 & 0 & 0 & 0 \\ 0 & 0 & 326 & 0 & 0 & 0 \\ 0 & 0 & 0 & 52 & 0 & 0 \\ 0 & 0 & 0 & 0 & 52 & 0 \\ 0 & 0 & 0 & 0 & 0 & 57 \end{bmatrix} \quad (\text{A.18})$$

$$\mathbf{D}_{NL}(\boldsymbol{\nu}_r) = \begin{bmatrix} 292|u_r| & 0 & 0 & 0 & 0 & 0 \\ 0 & 584|v_r| & 0 & 0 & 0 & 0 \\ 0 & 0 & 635|w_r| & 0 & 0 & 0 \\ 0 & 0 & 0 & 84|p| & 0 & 0 \\ 0 & 0 & 0 & 0 & 148|q| & 0 \\ 0 & 0 & 0 & 0 & 0 & 100|r| \end{bmatrix} \quad (\text{A.19})$$

$$\mathbf{D}_L = \begin{bmatrix} 29 & 0 & 0 & 0 & 0 & 0 \\ 0 & 41 & 0 & 0 & 0 & 0 \\ 0 & 0 & 254 & 0 & 0 & 0 \\ 0 & 0 & 0 & 34 & 0 & 0 \\ 0 & 0 & 0 & 0 & 59 & 0 \\ 0 & 0 & 0 & 0 & 0 & 45 \end{bmatrix} \quad (\text{A.20})$$

A.3 SF 30k: Berg

The models presented here has been developed and used by Victor Berg in his Master Thesis during spring 2012 [3]. These models are also the basis of the original control system Njord for the SF 30k developed in cooperation between Berg and Tolpinrud [2], which is still in use at NTNU.

- Weight: 1862.9 kg
- $l = 2.50$ m, $b = 1.50$ m, $h = 1.60$ m

- CoG: $r_G = [0 \ 0 \ 0]^\top$, CoB: $r_B = [0.0822 \ -0.0077 \ 0.3872]^\top$ (Found from computer modeling/CAD).
- Buoyancy: 209.4 N (disputed: A bit too large, found from CAD with simplified model)

The mass-matrices are computed from models of the ROV in WAMIT and Matlab (to get symmetric values).

$$M_{RB} = \begin{bmatrix} 1862.9 & 0 & 0 & 0 & 0 & 0 \\ 0 & 1862.9 & 0 & 0 & 0 & 0 \\ 0 & 0 & 1862.9 & 0 & 0 & 0 \\ 0 & 0 & 0 & 525.4 & 1.4 & 33.4 \\ 0 & 0 & 0 & 1.4 & 794.2 & 2.6 \\ 0 & 0 & 0 & 33.4 & 2.6 & 691.2 \end{bmatrix} \quad (\text{A.21})$$

$$M_A = \begin{bmatrix} 779.8 & -68.8 & -103.3 & 8.5 & -165.5 & -7.8 \\ -68.8 & 1222.0 & 51.3 & 409.4 & -5.8 & 62.7 \\ -103.3 & 51.3 & 3659.9 & 6.1 & -386.4 & 10.8 \\ 8.5 & 409.4 & 6.1 & 534.9 & -10.0 & 21.0 \\ -165.5 & -5.8 & -386.4 & -10.0 & 842.7 & -1.1 \\ -7.8 & 62.7 & 10.8 & 21.0 & -1.1 & 224.3 \end{bmatrix} \quad (\text{A.22})$$

The damping-matrices are based on numbers from Minerva. Damping is usually found through experiments, and no towing tests have been performed on the SF 30k. The nonlinear damping is based on model towing tests of Minerva, while the linear damping is found from bollard pull tests of Minerva and taken as a percentage of the nonlinear damping.

$$D_{NL}(\nu_r) = \begin{bmatrix} 748.2|u_r| & 0 & 0 & 0 & 0 & 0 \\ 0 & 992.5|v_r| & 0 & 0 & 0 & 0 \\ 0 & 0 & 1821.0|w_r| & 0 & 0 & 0 \\ 0 & 0 & 0 & 672|p| & 0 & 0 \\ 0 & 0 & 0 & 0 & 774.4|q| & 0 \\ 0 & 0 & 0 & 0 & 0 & 523.3|r| \end{bmatrix} \quad (\text{A.23})$$

$$D_L = \begin{bmatrix} 74.8 & 0 & 0 & 0 & 0 & 0 \\ 0 & 69.5 & 0 & 0 & 0 & 0 \\ 0 & 0 & 728.4 & 0 & 0 & 0 \\ 0 & 0 & 0 & 268.8 & 0 & 0 \\ 0 & 0 & 0 & 0 & 309.8 & 0 \\ 0 & 0 & 0 & 0 & 0 & 105.0 \end{bmatrix} \quad (\text{A.24})$$

The forces on the umbilical is found using Morison's Equation and $C_d = 1.2$ and $x_{\text{arm}} = y_{\text{arm}} = 0$, $z_{\text{arm}} = 0.93$ m. The weight of the cable in water is assumed zero. The diameter of the umbilical is 0.027 m.

$$\tau_{\text{umbilical}} = \begin{bmatrix} -8.30 \int_0^h |u_r| u_r \\ -8.30 \int_0^h |v_r| v_r \\ 0 \\ 7.74 \int_0^h |u_r| u_r \\ 7.74 \int_0^h |v_r| v_r \\ 0 \end{bmatrix} \quad (\text{A.25})$$

The SF 30k models used by Fernandes and in current control applications are the same as the ones given by Berg.

Appendix B

System Changes

This appendix contains information on the changes done to the HIL and control system in order to improve communication or output.

B.1 Control System Njord

Some changes were made in order to allow the TCP communication, as well as enabling direct feedback from GPS and HiPAP/APOS without the Navipac through UDP.

The UDP connections are added to the system and can be read in the READ TCP FIFO block if desired, but the \$GPGGA and \$PSIMSSB strings are not used as the system is now.

B.1.1 Opening and Closing connection

Methods for opening TCP and UDP connections are added at the very start of the system. They are inside an if-structure and will only be run if the user decides so on the front panel.

B.1.2 Private Data

The communication is set up through the Vessel.lvclass, which is a class in the object oriented control system. In order to save and utilize the connection IDs 5 new entities have been added to the Vessel.ctl (Private Data for Vessel.lvclass):

- TCP 1 - Telebuf [TCP Network Connection Refnum]

- TCP 2 - ROV String [TCP Network Connection Refnum]
- TCP 3 - Navipac [TCP Network Connection Refnum]
- UDP GPGGA [UDP Network Connection Refnum]
- UDP PSIMSSB [UDP Network Connection Refnum]

B.1.3 Getters and Setters Blocks

To ensure proper encapsulation methods to get and set the values for all the added private elements are implemented:

- TCP Telebuf Connection Refs
 - Write TCP Tebuf Port
 - Read TCP Telebuf port
- TCP ROV Connection Refs
 - Write TCP ROV Port
 - Read TCP ROV port
- TCP Navipac Connection Refs
 - Write TCP Navipac Port
 - Read TCP Navipac port
- UDP PSIMSSB Connection Refs
 - Write UDP PSIMSSB Port
 - Read UDP PSIMSSB port
- UDP GPGGA Connection Refs
 - Write UDP GPGGA Port
 - Read UDP GPGGA port

All these blocks are based on existing cRIO/FPGA reference blocks and are only used to read and write connection reference numbers.

B.1.4 Read and Write Communication Blocks

Several blocks have been changed or remade to fit the TCP rather than the cRIO communication. All the original cRIO blocks still exist and are used if the system is in cRIO/FPGA-mode.

The following blocks are added as direct copies with TCP instead of FPGA communication:

- Vessel(TCPrefs)
- Read TCP FIFO
- Write to TCP
- Read TCP FIFO MTi

B.2 HIL System

Unlike the CS the HIL system does not rely on object oriented design and implementation, and it is much easier to just change certain parts of it. It is also a much smaller implementation.

B.2.1 Communication

The changes made to the HIL system is replacing predefined LabVIEW-blocks inside if-structures to provide an opportunity to switch between cRIO and TCP-mode.

- Open TCP communication added (instead of VISA configure serial port)
- Write TCP added for ROV and Navipac strings (instead of VISA write)
- TCP Read is added (instead of VISA Read)
- Communication is closed after communication loop is done

It is worth noting that each TCP connection must have to senders/receivers: The first will send/receive the length of the actual string to be written, while the other sends/receives the string itself.

UDP Connections, a new queue and methods to generate \$GPGGA and \$PSIMSSB strings are also added to be able to transmit raw data to the control system if it is desired to bypass the Navipac software.

B.2.2 Sensors

Several blocks have been included to properly simulate the sensor behavior. Most attention has been given to the HiPAP as the position is the most important state in the feedback control

To simulate HiPAP and GPS without Navipac there are also methods for generating \$GPGGA and \$PSIMSSB strings.

Blocks included are:

- GPS_Coords

- HiPAP sim PSIMSSB
- HiPAP sim
- Make_PSIMSSB_HIL

B.2.3 Umbilical Forces and Plots

A block to simulate the umbilical forces in surge and sway and moments in roll and pitch working on the ROV is included:

- UmbilicalForce (subVI)

In addition a block to plot the different forces acting on the ROV in real time as the simulations run is implemented:

- GraphForces

B.2.4 Models and User Interface

The main user interface has been improved with a new tab “Vessel Parameters” which allows users to easily change the modeling parameters, as well as adding modeling errors. This must be done before the system is run as the values are only loaded once, at the start of the run.

In addition several minor fixes and changes have been made to make the system more user friendly, such as adding the initial positions to the “States”-tab and the different standard deviations and sample periods for the sensors.

Appendix C

Code Listing

There are two folders of code included. One contains mostly MATLAB code used for processing and plotting different sets of data, while the other contains the complete HIL system, control system Njord and graphical user interface Frigg.

C.1 LabVIEW

The LabVIEW code contains the improved HIL system and control system, as well as the user interface to be able to run them. These are the main contributions to the thesis.

To be able to run the code one must have NI's LabVIEW installed and need to change the path where logfiles are saved (needs to be done every time the directory of the code is changed).

To run the code the following steps are necessary:

1. Open the "AURLab ROV Control System.lvproj" LabVIEW project
 - (a) Open the "Njord Control System.vi"
 - (b) Make choices regarding what kind of communication, what ports etc. is desirable
2. In the folder "HIL simulator 0413", open "HIL pro.lvproj" LabVIEW project
 - (a) Open the "HIL sim sys.vi"
 - (b) Adjust the desired settings in the different tabs
3. In the folder "Graphical User Interface", open "Graphical User Interface for Control System.lvproj" LabVIEW project
 - (a) Open the "Graphical User Interface - Frigg.vi"

4. Run the “Njord Control System.vi”
5. Run the “HIL sim sys.vi”
6. Run the “Graphical User Interface - Frigg.vi”
 - (a) Connect the GUI and CS using “Connect” button

The rest of the operations can be performed in the GUI in the same way as in sea trials. Any desired environmental forces can be adjusted in the HIL system’s tabs.

It is worth noting that if the SIL simulator is to be used, the “Njord Control System.vi” must be run before “HIL sim sys.vi” to ensure proper connection.

C.2 MATLAB

The MATLAB files are used to process and plot graphs from already logged data, either from a sea trial or a simulation. Code is also included to compute Centripetal and Coriolis matrices and restoration forces based on input, as well as computing drag and mass forces for varying velocities.

The following folders are included:

C and g Matrix computations

Contains code to generate the Centripetal and Coriolis matrices and restoration force given the mass matrix and other parameters.

Drag and Mass forces

Contains files to plot the different drag and mass forces in different DOFs and for different vessels. A file contains all parameters given in Appendix A.

Processing Sensor data - raw GPS and HiPAP

Contains files to process GPGGA and PSIMSSB string directly from the GPA and HiPAP. Some raw logfiles are attached.

Processing Sensor data - mat files

Contains files process data from the CS already transformed into .mat-files. Some logfiles are attached.

In order to run the files to process raw GPS and HiPAP data the two files “ReadA-POS.m” and “ReadGPS.m” should be run first to load the data from the files into MATLAB. The “PlottingROVPos.m” should then be able to plot the movements of the vessel.